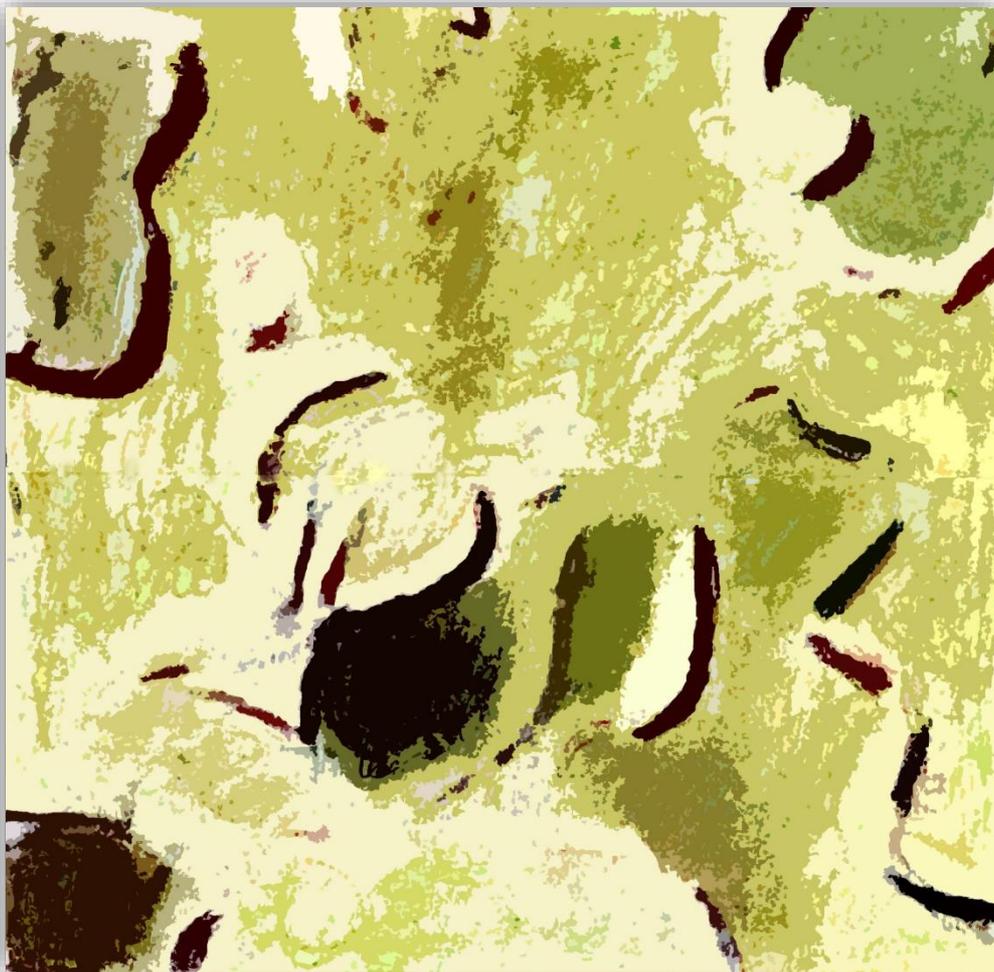UiT The Arctic University of Norway

Faculty of Science and Technology
Department of Geosciences

Kortejärvi Veiki moraine plateau – a key to the glacial history of northern Sweden

Mimmi Adina Lindqvist

Master's thesis in Geology - GEO-3900 - March 2020

Abstract

In many parts of Scandinavia, the glacial history is more well established than in northern Sweden. The Veiki moraines in northeastern Sweden presumably store information about the Weichselian glaciations. The moraines were formed when stagnant ice was slowly melting under a thick debris cover, forming water filled sinkholes, that were left as elevated ice-walled lake plains when the ice finally melted. The latest age estimations of the Veiki moraines suggest that the landscape was formed during a Middle Weichselian interstadial. The late Weichselian ice sheet that covered much of northern Europe was presumably partially cold based and left the Veiki moraines nearly untouched. However, the age of the moraines had previously been suggested to be Early Weichselian and therefore possibly overridden by two consequent ice sheets. To this day, the ages of the moraines have been disputed. The highly irregular shapes of the moraines have caused some obscurity in the genesis of the Veiki moraines and in this report, subsequent processes are suggested as contributory factors in the formation of the landscape.

The obtained OSL ages reinforce that the Veiki moraines were formed during a Middle Weichselian interstadial. The most prominent moraine plateaus were formed in well insulated parts of the ice where the debris cover was thick, while the less prominent moraine plateaus were in poorly insulated parts of the ice. The poorly insulated lakes were affected by faster melting rates and consequently they merged with surrounding lakes, forming a landscape of highly irregular merged ice-walled lake plains once the ice melted. A faster melting rate likely caused differences in the ice surface gradient and led to collapsing lakes in the downslopes. The landscape was later only slightly reworked by the Late Weichselian ice. Reworking by later fluvial processes makes the reconstruction of the original ice-walled lakes somewhat challenging.

A geomorphologically unique Veiki moraine plateau has been studied using sedimentological and stratigraphical data, ground penetrating radar (GPR) and high-resolution LiDAR data. Two dating techniques have been applied including optically stimulated luminescence (OSL) and radiocarbon. To improve the chronostratigraphical correlations of the sediments, samples have been scanned and checked for most common pollen taxa.

Keywords: Veiki moraines, ice-walled lake plain, stagnant ice, Weichselian glaciation, interstadial, Fennoscandian ice sheets.

Foreword

It has been an inspiring journey to write this thesis and I am ending it with a "suitcase" full of new knowledge, and it has certainly been worth the efforts made. I would like to start by designating a few words to everyone who has helped me in different ways along the way

I would like to thank my parents for always pushing me forward in my studies as well as friends who have made sure to fill life with laughter and relatable memes. An extra thanks to my mum for designing the front-page illustration.

Marcus, you have been my rock throughout the process, and I will not forget your irreplaceable support and your astonishing patience during this time.

Lastly, I would like to dedicate the thesis to my grandmother Maija, the source of my curiosity for nature. I believe she is the main reason I stand here with a thesis fresh out the oven.

Maija planning an expedition to South East Asia in the 1950's.

Tromsø, March 2020

Mimmi Lindqvist

Table of Contents

1 Introduction

1.1 Studying the Quaternary

1.1.1 Stratigraphical divisions of the Quaternary

At around 2.6 Ma years ago, worldwide cooling events mark the start of the Quaternary period, the most recent major subdivision of the geological records. The Quaternary is known as a period of frequent and extensive climatic fluctuations and repeated glaciations. It consists of two epochs out of which the first one is the Pleistocene and lasted until 11.7 ka. 11.7 ka marks the start of the Holocene, the second epoch (Cohen and Gibbard, 2019). The Quaternary is characterized by periodic cold phases, during which continental ice sheets have grown and mountain glaciers expanded around the world (Pillans and Naish, 2004). Temperature fluctuations during the Quaternary have been segmented into glacial- and interglacial periods; glacials are extensive cold phases with major ice sheet expansions; interglacials are warm periods during which the temperatures were as high as or higher than during the Holocene. Several stadials and interstadials characterizes each glacial period; stadials are shorter cold periods with local ice advances; interstadials are relatively short-lived periods with warmer temperatures. The last interglacial period, the Eemian, began at ~130 ka (Mangerud, 1991) and about 10 000 years later, the temperatures dropped, and the most recent glacial period started, in northwestern Europe referred to as the Weichselian (Cohen and Gibbard, 2019). The Weichselian lasted until our current interglacial stage started. Changes in the Earth's orbit and axes might be the primary driving mechanism behind Quaternary climatic changes (Imbrie *et al.*, 1993).

1.1.2 Why should we study past climates?

Since 1860, most regions in the world show a temperature increase (Oerlemans, 2005) and it has become increasingly important to gather data from the Earth's climate system in order to predict how it will react to the ongoing rapid global warming (IPCC, 2001). In fact, it has become one of the biggest challenges for humans in modern time. A warming climate has led to glacier recession all over the world (IPCC, 2001) and assessing the possible outcomes of the ongoing glacier decay requires a deeper understanding of past deglaciations (Schomacker, 2008). Glaciers, ice sheets and ice caps store important information that can be used to reconstruct past climates, as well as landforms left behind by ancient glaciers, as they are sensitive to climatic changes. The way a glacier responds to climate change depends on its geometry and its climatic setting (Oerlemans *et al.*, 1998; 2005). Glaciers in different

geographical settings will react in different ways but in general, a warming climate will lead to surface melt and runoff, mass balance variations and an overall decrease of the ice area and volume (Oerlemans *et al.*, 1998). On a continental scale, ice fluctuations over decades and centuries are predominantly driven by temperature (Oerlemans, 2005). Apart from this, the climate sensitivity of glaciers also depends on the annual mean precipitation (Oerlemans *et al.*, 1998; 2005). Continental glaciers are in general less sensitive and maritime glaciers more sensitive (Oerlemans *et al.*, 1998).

Studying paleoclimates becomes harder as we go further back in time. Consequently, the most detailed paleoclimatic data can be extracted from the Weichselian stadials and interstadials (Hättestrand, 2007a). Since much of the pre-late Weichselian records are eroded and reworked especially in terrestrial environments, Late Weichselian records provide the best opportunities for reconstructions (Svendsen *et al.,* 2004). When reconstructing terrestrial environments, inter-regional correlations are often made. Interregional correlations are attempts to determine the ages of the deposits, but such attempts can be somewhat speculative, and inferences which are themselves based on inferences are made, which raises the possible errors (Lowe and Walker, 2015). Reconstructing past ice sheets has therefore been proven challenging, and has been compared to an attempt to construct a three or four dimensional puzzle (Mangerud, 1991). In some areas, up to a million years or more of sedimentary history might be missing (Lowe and Walker, 2015).

Likewise, we can obtain analogue models for formerly glaciated areas by studying present day glacial environments (Schomacker, 2008). Not all features from past glaciations have a modern analogue however, and some supraglacial landforms are among them (Johnson and Clayton, 2003). The focus of this report lies on presumably supraglacial landforms, which are believed to have been left behind by stagnant ice that covered the study area during the Weichselian, as will be introduced in subchapter 1.3. Modern supraglacial features, such as sinkholes and supraglacial lakes, lack similarities with ice-walled lake plains that have been described from earlier glaciations. Therefore, studies on past dead ice should not be based on models developed entirely on modern glaciers (Johnson and Clayton, 2003). It has been concluded that identical processes happen in different climates (Schomacker, 2008), and therefore dead-ice deposits left behind by past ice sheets and glaciers provide little information about the past climates. Future challenges therefore include quantifying the ongoing dead-ice melting under changing climate conditions (Schomacker, 2008).

Following the ongoing rapid melting, retreat and stagnation of many glaciers, dead-ice areas are likely to become more common in the future (D'Agata and Zanutta, 2007; Schomacker, 2008). Consequently, there will be more possibilities to study them in order to predict potential geohazards caused by them (Schomacker, 2008). Locally, debris-covered glaciers already make up large proportions of glaciated areas, as an example in many alpine landscapes. Here, melt-out of ice-cored moraines and debris covered glaciers lead to high magnitude floods and landslides, which negatively affects the local communities (Schomacker, 2008).

As a short summary, deposits from past deglaciations contribute in varying amounts with information that can be useful when studying present day glacier decay, while the present-day processes can be important when studying past deglaciations. Not all past glaciations have present day analogues, however. Therefore, a study should not solely rely on information from one or the other, but instead combine data from both to gain the best reconstructions and predictions.

1.2 Proxies

The methods that are used to study past environments have advanced much during the 1900's. While we are still waiting for the invention of the time machine, which would allow us to travel back in time and carry out direct measurements, we use proxies. Proxies are indirect evidence preserved from the past, used instead of direct meteorological measurements. Proxies come in many different forms.

Landforms, sediments and fossils that prevail from growing and decaying ice sheets are among many other variables that can be used as proxies. Sedimentological analysis of cores yields information about structures and textures, which in order can be correlated to a depositional environment. Geomorphological landforms also function as proxies, as specific glacial landforms are characteristic of different states of an ice sheet, which in order yields information about the climate during which it prevailed. Relationships between primary sedimentary structures in the subsurface, retrieved by ground-penetrating radar, can reveal relative chronologies and might help determine the order of processes related to climate fluctuations. Fossils have been used as proxies, as knowledge of their habitat reveals information about the environment in which they lived. Dating techniques, such as radiocarbon dating, allows us to know at what time these environmental conditions prevailed. In addition, the development of other dating techniques, such as luminescence dating, have enabled the use of buried quartz and feldspar as proxies.

Proxies from terrestrial stratigraphic records are often fragmented; therefore, attempts to correlate them to marine isotope stages is common (Lowe and Walker, 2015). Marine isotope stages (MIS) are chronostratigraphical units based on proxy data. The proxy that has been used to establish the units are oxygen isotope composition variations constructed from deep-sea sediments. The variations reflect alterations in the global ice volume and therefore provide a long and continuous record on global climate variations, including glacial/interglacial cycles (Lowe and Walker, 2015).

1.3 Veiki moraines

Northern Sweden is a core area of former ice sheets. The area is important for reconstructing the Fennoscandian ice sheets that advanced over the area during the Weichselian glacial period. The palimpsest landscape left behind as evidence from these reoccurring ice sheets consist of a well-preserved pre-Late Weichselian landscape referred to

Figure 1.1. Veiki moraine plateau in the front, 15 NW of Nattavaara. Lagerbäck (1980) (from Lagerbäck, 1988).

as the Veiki moraines (Lagerbäck, 1988; Hättestrand, 1998). The Veiki moraine landscape constitutes irregularly shaped moraine plateaus surrounded by wetlands and lakes (Figure 1.1.). Their most prominent occurrence is in Norrbotten in northeastern Sweden.

Gunnar Hoppe suggested the Veiki moraine concept in 1952 and named them after a hummocky moraine locality ~20 kilometers north of Malmberget. The "Veiki district" had been well known before that, and preceding research had been done by several authors (Lagerbäck, 1988). Before the term Veiki moraine was introduced, the formations were referred to as "dead-ice moraines" (Magnusson *et al.,* 1949). This interpretive term implies that the early researchers accepted the importance of stagnant ice in the genesis. Hoppe however, questioned the importance of the dead-ice concept and referred to them in a more descriptive manner as "hummocky moraine terrain" (Hoppe, 1952).

A few reoccurring elements that characterize the Veiki moraine landscape can be noted. The most prominent features are perhaps the rounded, irregularly shaped moraine plateaus with shapes that can resemble a cat or a fish among other things, together with the rim ridges that

often surround them. Whilst in between the Veiki moraine plateaus there are hollows with ponds and peat bogs. Ponds and peat bogs are also reoccurring on top of the moraine plateaus. Not all Veiki moraine plateaus constitute a prominent plateau in the center, and some have an outer rim ridge surrounding the inner ridge. Another important stratigraphic feature in the Veiki moraine landscape is a thin layer of reworked sediment or till that lies below the post-glacial peat. It has been suggested that partially cold-based ice covered the landscape and draped it with till but apart from that, left the landscape nearly undisturbed (Lagerbäck, 1988).

Interpreting the formation process remains difficult to this day, as the moraines vary in shape, composition, length and height. The formation process presumably varied among the moraines, and they have undergone post-depositional disturbance to various extents (Lagerbäck, 1988).

1.3.1 From a Late-Weichselian subglacial- to a Middle Weichselian supraglacial formation theory

Hoppe (1952) suggested a subglacial formation process for several reasons. Firstly, the moraines were found in close connection with drumlins, and drumlinoid features occurred superimposed on some of the plateaus. Secondly, because the till in the moraines was solidly packed and thirdly, because the pebbles and cobbles in the moraine ridges had reoccurring orientation parallel to, and at right angles to, the main motional direction. He suggested that they were formed subglacially, as basal water-soaked debris was squeezed into subglacial cavities such as crevasses. The plateaus were mainly regarded as primary formations; elevations of moraine material below the ice (Hoppe, 1952). Lagerbäck (1988) questioned both the genesis and the suggested age of the moraines. He reintroduced the dead ice-concept, suggesting that areal downwasting of a stagnant ice was the main mechanism behind the landforms. The ice was covered by thick accumulations of supraglacial debris and to some extent of subarctic vegetation. The surface of the ice was covered in hollows, into which debris was transported by sliding and flowing events and running water. The plateaus he investigated revealed fine-grained organic bearing sediments, which he interpreted as lacustrine deposits. Hereby, the concept of ice-walled lake plains was introduced. The rim ridges formed when the walls of the ice-walled lakes collapsed when the ice melted. The lakes probably formed on top of the ice and settled on the ground during a later phase of the deglaciation. Lagerbäck also pointed out that the theory of ice-walled lake plains does not fit all the moraines plateaus (Lagerbäck, 1988).

Lagerbäck suggested an Early Weichselian age partly because the results from the radiocarbon dates, obtained from the organic bearing lacustrine sediments, had pre-Late Weichselian ages,

but also because he found evidence indicating that the Veiki moraines were formed simultaneously with the eskers and drumlins that cover much of the landscape eastward, as some of these eskers integrated with the Veiki moraine landscape. The eskers and drumlins are known to have been formed during the Early Weichselian and hence only very weakly affected by later ice sheets (Lagerbäck, 1988). Clas Hättestrand (1998), argued that from a morphological point of view these landforms might not be related to each other. Martina Hättestrand applied the discipline of palynology to the Veiki moraine studies, agreeing with the genesis suggested by Lagerbäck but not completely convinced by the Early Weichselian age. After comprehensive palynological studies, and a chronostratigraphic correlation of the results with a succession from Sokli in Finland, a Middle Weichselian age was proposed in 2007 (Hättestrand, 2007b) and again in 2010 (Hättestrand and Robertsson, 2010).

In 2013, attention was brought to the sedimentology of the moraines. Sigfúsdóttir (2013), examined two Veiki moraines through excavations, with emphasis on stratigraphy and more specifically clast fabrics. The findings support the genesis suggested by Lagerbäck (1988) and the age suggested by Hättestrand (2007b). The findings imply that much of the diamict is emplaced by debris flows and that not all Veiki moraines comprise lacustrine sediments (Sigfúsdóttir, 2013).

1.3.2 Distribution

The largest display of Veiki moraine lies in the northern Swedish lowlands between Lainioälven (Lainio river) and Piteälven (Pite River). In the eastern parts of the distribution area, the landscape is regularly demarcated by terminal moraines or moraine ridges that are often lobate formed. Such moraine ridges occur sporadically also within the landscape. Towards south, north and west, the landforms disappear gradually (Hättestrand, 1998). Veiki moraine plateaus have not been identified east of these terminal moraine zones (Lagerbäck, 1988).

One of the most distinct terminal moraine zones is the Lainio arc, which constitutes the northernmost Veiki moraine occurrence in Sweden. The Lainio arc is demarcated with a terminal moraine towards east and constitutes the northernmost out of 3-4 lobate formed terminal moraine zones, which demarcate Veiki moraine towards east (Figure 1.2). The location of the lobes seems to be controlled by the bedrock topography and therefore it has been suggested that the ice flow followed river valleys to the lowlands where the terminal moraines were formed (Hättestrand, 1998).

Landforms interpreted as Veiki moraine occur also in other parts of Sweden. There are patchy findings until lakes Vänern and Vättern in the south and significant occurrences also in the central parts of Västerbotten (Hättestrand, 1998). In other countries, such as Finland, Norway and northern America, landforms resembling Veiki moraines have been described (Lagerbäck, 1988). Landforms resembling Veiki moraines have also been described on Mars (Figure 1.3), which presumably is indicative of ancient glaciation on the planet (Johnsson *et al*. 2017).
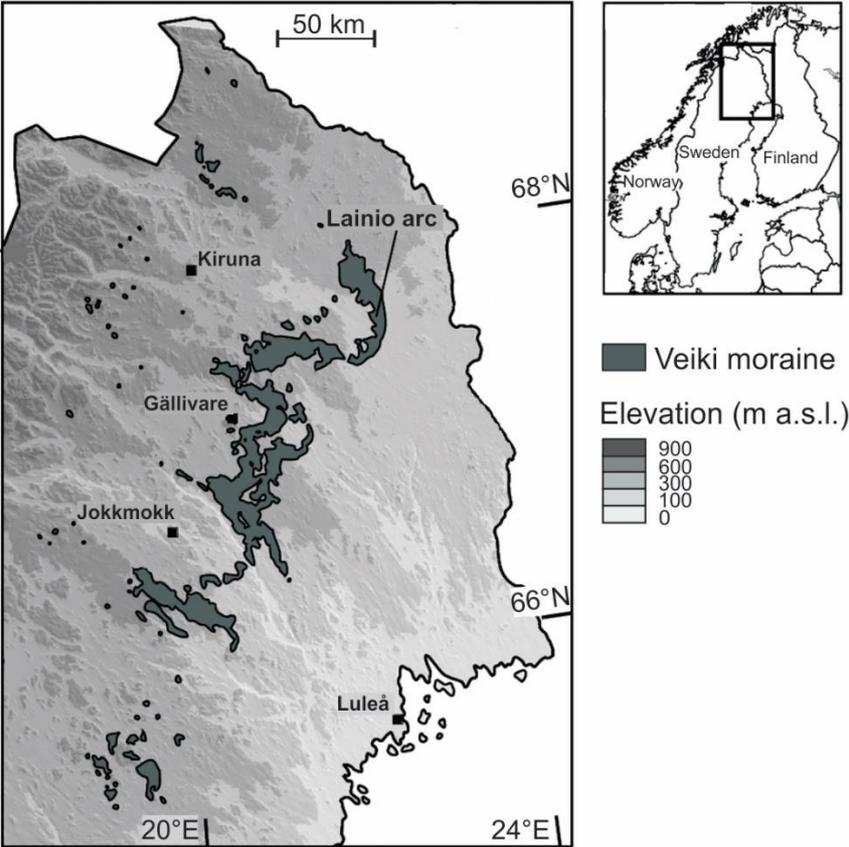
Figure 1.2. *The distribution of the Veiki moraines in northern Sweden. Modified from Hättestrand and Robertsson (2010).*
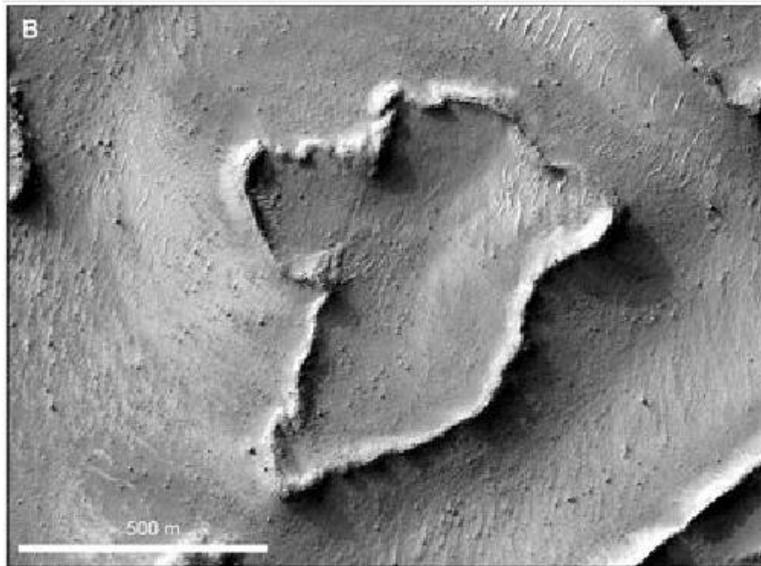
Figure 1.3. *Image of a Veiki moraine like landforms observed on Mars. Modified from Johnsson et al. (2016).*

1.4 Weichselian chronology

The Weichselian glacial period consist of Early-, Middle- and Late Weichselian. The stadials and interstadials during these periods have been correlated with the worldwide marine isotope stages (MIS).

During the Early Weichselian, two warm interstadials occurred in northern Europe; *Brørup* (MIS 5c) and *Odderade* (MIS 5a). Two interstadials have likewise been recognized in northeastern Sweden; Tärendö 1 and Tärendö 2. Two correlation alternatives have been suggested (Figure 1.4). Alternative 1;

Figure 1.4. *Marine isotope stages correlated with northern European interstadials and the periods of the last glacial-interglacial cycle. The blue boxes show correlation alternative 1 and the yellow boxes show correlation alternative 2. Modified from Hättestrand (2007a).*

Tärendö 1 correlates with *Brørup* interstadial and Tärendö 2 with *Odderade* interstadial (Lagerbäck, 1988); Alternative 2; Tärendö 1 correlates with *Odderade* while Tärendö 2 corresponds with the Middle Weichselian interstadial (Hättestrand, 2007b; Hättestrand and Robertsson, 2010). Earlier it was assumed that an ice sheet prevailed in the central areas of

Scandinavia between MIS 4/5 transition and the final Weichselian deglaciation (Mangerud, 1991), but this has later been proven false and an ice retreat during MIS 3 has been constructed at few localities (Mangerud *et al*. 2011). The Veiki moraines may be the evidence that ice sheets diminished during the Middle Weichselian interstadial in the northern parts of Sweden (Hättestrand, 2007a).

The Late Weichselian include the last glacial stage (MIS 2), also called the last glacial maximum (LGM), as it marks the period with the largest ice coverage during the Weichselian. LGM occurred ~ 20 - 15 ka years ago, after which the ice sheet started to disappear (Figure 1.5) (Svendsen *et al*., 2004). Reconstructions of the ice recession by Stroeven *et al*., (2016) suggests that Fennoscandia was deglaciated sometime after 9.7 ka, and according to Hughes *et al*., (2015) the deglaciation was complete at 9 ka or slightly earlier. MIS 1 refers to the Holocene.
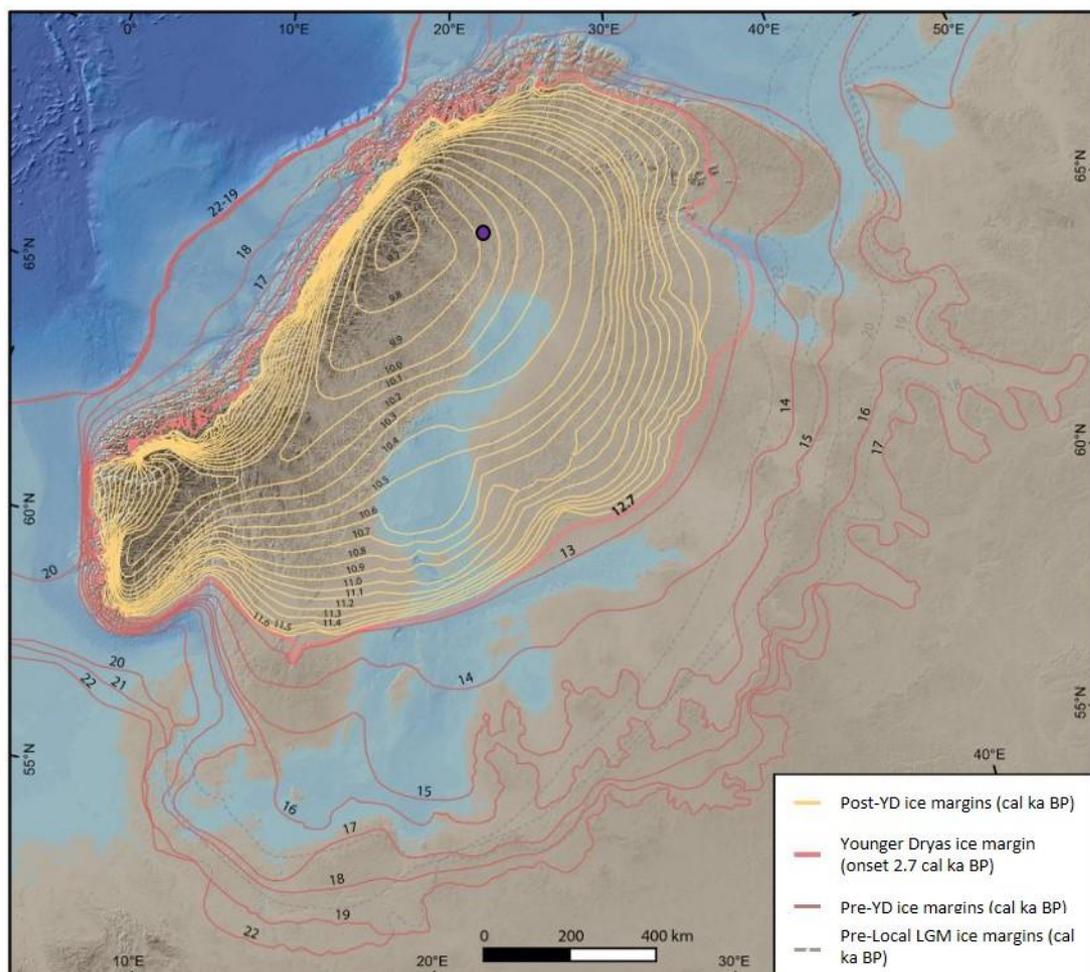
Figure 1.5. *Reconstruction of ice recessional lines for the last Fennoscandian Ice Sheet. The study area Kortejärvi is marked with a violet circle. Modified from Stroeven et al. (2016).*

1.5 Remaining questions regarding the Veiki moraines

So far, a well-established explanation behind the landscape is that it was formed during the downwasting of a debris rich stagnant ice lobe. Several publications that were mentioned above, support the theory and similar landforms identified in other countries support this genesis, as an example Ham and Attig (1996) and Clayton *et al*. (2008). The time of formation has been proven pre-Late Weichselian. There are, however, several parameters that remain uncertain and some of them will be presented here.

Which other processes had an impact on the shapes?

As Lagerbäck (1988) mentions, no simple mechanism could have resulted in the diverse and irregular shapes of the moraine plateaus. Along with the ice-walled lake phase, other processes have likely contributed in the formation of the landscape, but contributory factors have previously not been discussed in detail. Reworking by the Late Weichselian ice sheet, in various degrees, has been mentioned (Lagerbäck, 1988; Sigfúsdóttir, 2013). In this report, I present processes that likely have contributed to the shapes of the moraine plateaus after the ice-walled lakes formed, but prior to the reworking by the last ice sheet and the deglaciation.

Does the gradual diminishment of Veiki moraines towards west signal of change in the ice sheet properties?

As mentioned earlier, the occurrence of Veiki moraine plateaus in northern Sweden is clearly demarcated towards east and no plateaus occur east of the terminal moraines, while they gradually diminish towards west, south and north. This gradual diminishing has not been discussed further, but reasons to their demarcated occurrence in lowland areas west of the area of distribution has been discussed briefly. It has been suggested that either the conditions changed during the decay of the ice, the climate changed, or the supply of supraglacial debris ceased (Lagerbäck, 1988). In this report, I suggest that the gradual diminishment of Veiki moraines within the area of occurrence, likely signal of a change in the debris cover properties, which affected the melting rate of the ice.

A surge implies a change in the thermal regime within the ice; was the surge triggered by a climatic change?

Extensive thrusting that brought debris to the ice surface perhaps implies that a part of the ice margin surged before it got stagnated (Lagerbäck, 1988; Hättestrand, 1998; Sigfúsdóttir, 2013). A surge implies a change in the thermal regime within the ice and could have been triggered by a climatic change. The wide extent of the Veiki moraine landscape is believed to reflect a regional warming climate, which resulted in areal downwasting of the former ice sheet

(Lagerbäck, 1988). The question will be discussed in the final chapter but will not be addressed directly through own data.

In which ways have alluvial processes imprint the landscape?

Lagerbäck (1988) states that glaciofluvial transport is one of the mechanisms that likely contributed to the concentration of material in certain areas resulting in ice-walled lake plains. He also points that the landscape likely is built up of water laid sediments to a much higher degree than is visible from the surface. Hoppe (1952) mentions that there are traces of glaciofluvial erosion almost everywhere in the terrain and that the Lainio arc contains considerable amounts of glaciofluvial elements such as eskers. Glaciofluvial processes and meltwater channels have been mentioned in previous Veiki moraine studies, but without much emphasis on their contribution to the development of the area or more detailed descriptions of the fluvial sediments. In this report I present a sedimentological analysis of alluvial sediments within a Veiki moraine plateau.

What is the absolute age of the landforms and how do they correlate to local interstadials?

It is important to establish a good chronology of the Weichselian interstadials in Sweden if we are to understand the climatic fluctuations in Fennoscandia during the Weichselian glaciations. For parts of northern Fennoscandia, as an example the coasts of Norway and Sokli in northern Finland, ice-free conditions have been suggested during the Middle Weichselian (Helmens *et al.*, 2007; Mangerud *et al.,* 2011), but the extent of ice coverage in northern Sweden is still unclear (Hättestrand, 2007a). Veiki moraines are one of the key landforms that presumably hide information about the Weichselian interstadials (Hättestrand, 2007b). Some absolute dating have been done at a few sites in the Veiki moraine landscape (eg. Lagerbäck, 1988), mainly radiocarbon, optically stimulated luminescence (OSL) and thermoluminescence (TL), but they are in general of poor quality (Mangerud, 1991). Consequently, a firm chronology has not been established and the absolute age of the landforms remains uncertain, and the correlation of the local interstadials is problematic. Two possible correlations have been discussed, as mentioned earlier. Alternative 1; Tärendö 1 correlates with *Brørup* interstadial and Tärendö 2 with *Odderade* interstadial (Lagerbäck, 1988); Alternative 2; Tärendö 1 correlates with *Odderade* while Tärendö 2 corresponds with the Middle Weichselian interstadial (Hättestrand, 2007b; Hättestrand and Robertsson, 2010). I have obtained new dates, which support correlation alternative 2. Additionally, I have obtained dates belonging to a younger generation, which presumably originate from the last deglaciation.

1.6 The focus and approach of this study

Following Hättestrand (2007b), who suggested that more interstadial sequences within the Veiki moraines could be analyzed to find out if more than one interstadial warm phase could be identified at other sites, the aim of this study was to date a sediment sequence within a Veiki moraine plateau and reconstruct its genesis. Being supportive of the ice-walled lake plain theory suggested by Lagerbäck (1988), I expected to find lacustrine sediments in the chosen moraine plateau Kortejärvi (Figure 1.6), but instead we obtained mostly coarse gravelly sediments, which are characteristics commonly not associated with lacustrine deposits. The lack of lacustrine sediments empowered me to consider alternative and contributory theories for the formation of the moraine plateaus. Whilst still supporting the ice-walled lake plain theory suggested by Lagerbäck (1988), I will in this report present subsequent processes that have contributed to the diverse shapes of the moraine plateaus at the time of formation as well as post depositional processes. The studied moraine plateau Kortejärvi is located close to the "transition zone" between the prominent moraines towards east and the less prominent and finally diminishing moraines towards west (Figure 1.6.).

I will also present the results of the obtained ages from the radiocarbon- and OSL dating. The obtained ages are further applied to the history of the Fennoscandian ice sheets and hereby contribute with some new information about the glacial history of northern Sweden. The discussion will focus on a few parameters including the irregular shapes-, the age-, the variations in prominence of the moraines, and the alluvial deposits. In the end, I evaluate if it is possible to extract information about the ice thickness of ice sheet that formed the Veiki moraines and return to the remaining questions which were presented in the previous subchapter.

The results of this study are based on a combination of different techniques. Geomorphological data has been gathered from the high-resolution airborne LiDAR (Light Detection and Ranging) data set of Sweden, while lithological evidence was obtained by analyzing sedimentary textures and structures from a core and several hand-dug outcrops. Knowledge on the stratigraphical continuity of the sediments was retrieved through analyzing ground-penetrating radar profiles. Dating techniques including radiocarbon and optically stimulated luminescence (OSL) contributed with a time frame for the processes. Additionally, three pollen samples were scanned for most common pollen taxa from the retrieved core, and an X-ray fluorescence

scanning was performed. Literature about Veiki moraines, stagnant ice environments, supraglacial environments and ice-walled lake plains has been reviewed.
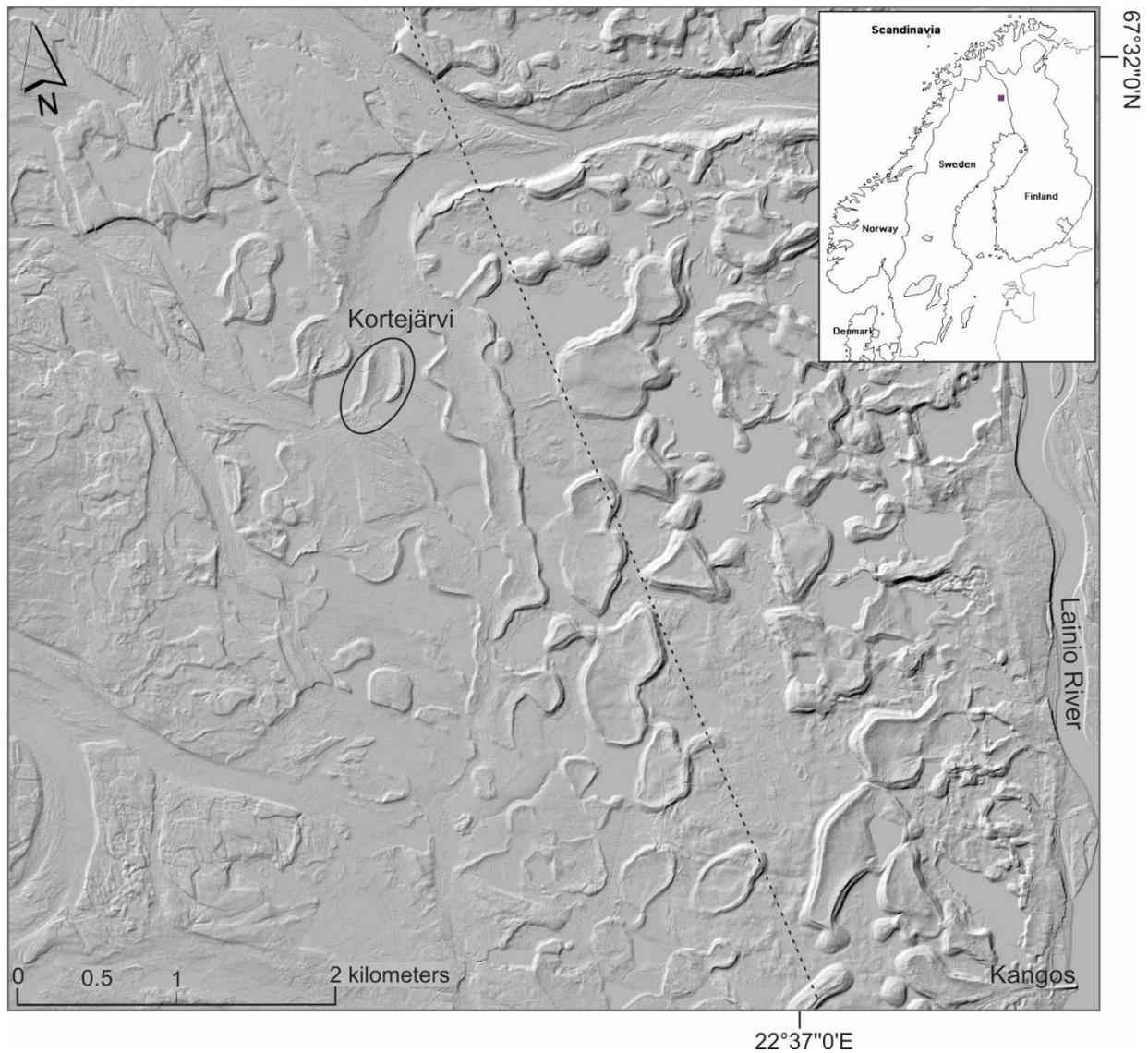
Figure 1.6. *Elevation model of Kortejärvi and its surrounding. See Figure 2.2. for a simple terrain map. Kortejärvi moraine is located close to the transition zone between the more prominent moraines towards east and the less prominent moraines towards west. The most prominent moraines in the image are between 10 and 20 meters high and the ridges on each side of Kortejärvi morain plateau are ~six meters high. Background map: Nationell höjdmodell, 1:100 000 © Lantmäteriet I2018/00104 (2011b).*

2 Geological background and theoretical framework

2.1 Glacial geomorphology of northern Sweden

Much of the Quaternary deposits in northern Sweden are landforms formed during the growth and decay of the Late Weichselian Fennoscandian ice sheet. Hummocky moraine, drumlins, flutes, eskers and De Geer moraines are among widely occurring landforms. In areas above the highest post-glacial shoreline, glacial meltwater channels are found increasingly towards the position of the last ice remnants (Hättestrand, 1998). However, a nearly undisturbed pre-Late Weichselian landscape is found in northeastern Sweden. This landscape includes the Veiki moraines and other glacial landforms such as drumlins, end moraines, eskers and meltwater channels. The well-preserved landforms indicate that the Late Weichselian ice sheet that covered the landscape did not remold the landscape to a large extent and was probably cold based at its central parts (Lagerbäck, 1988; Hättestrand, 1998).

In Northeastern Sweden, at least three different glacial flow systems have been identified from directional glacial landforms (Hättestrand, 1998). Landforms from the first Weichselian stadial, including drumlins, crag-and-tails, large meltwater channels and eskers, trend NW-SE and indicate an ice flow from NW. The second directional trend, in form of faint fluting and small drumlins, together with till fabrics and striations, indicate ice flow from south to north. These landforms have been associated with the LGM. The youngest set, mostly meltwater channels, overprints all the other glacial features. It is associated with the deglaciation of the last Weichselian ice sheet. Eskers in this set are rare, and those that occur are small and discontinuous. This set trends SW-NE and W-E in the central parts (Hättestrand, 1998).

2.2 Study area

The study area is in the Lainio arc, which is the northernmost lobe with Veiki moraines between the Lainio river and Pite river (Figure 2.1). Kortejärvi lies about six kilometers northwest from a small village called Kangos (Figure 2.2) and the name refers to a nearby lake with the same name. It is located at the edge of the westward occurrence of the prominent Veiki moraines at this locality (Figure 1.6). The studied Veiki moraine plateau is geomorphologically different from most of the plateaus further east as it does not constitute an elevated plateau in
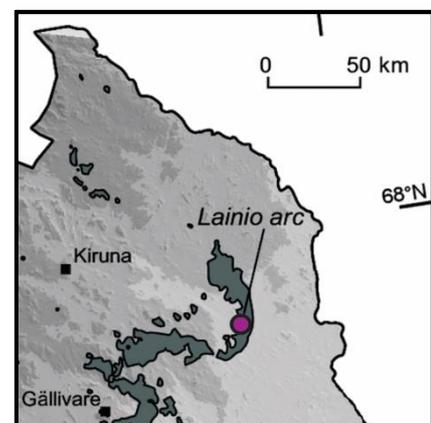
Figure 2.1. The studied moraine (marked with a violet dot) is in the Lainio arc. Modified from Hättestrand (2007b).

the center. Wetlands, lakes and forest surround the area. The lowered center between the ridges is composed of wetland and marshy vegetation, while spruce, pine tree, birch and shrubs cover the ridges. The depth to the bedrock is between 5 and 20 meters in the area and the surroundings (SGU, 2020c). The Quaternary deposits consist of glacifluvial sediment, peat and till (Figure 2.3) (SGU, 2020a). The time of deglaciation in Kangos has been studied in an archaeological context by Östlund (2004), who suggests that the deglaciation occurred between 10.11 – 9.54 ka cal BP (calibrated by Möller *et al.*, 2013). Among others, Stroeven *et al.* (2016) has reconstructed the deglaciation of Fennoscandia and suggests deglaciation in the areas around Kangos between 10- and 9. 9 ka cal BP (Figure 1.5). Hughes *et al.*, (2015) suggest a maximum ice margin at the area around Kangos at 10 ka cal BP but emphasizes that the area likely was deglaciated at that time.

The study area is in the Norrbotten lithotectonic unit, and the surrounding bedrock consists of gabbro, diorite, diabase, gneiss, granite and amphibolite. The age of the local bedrock ranges between ~ 2800 and 1700 million years (SGU, 2020b).
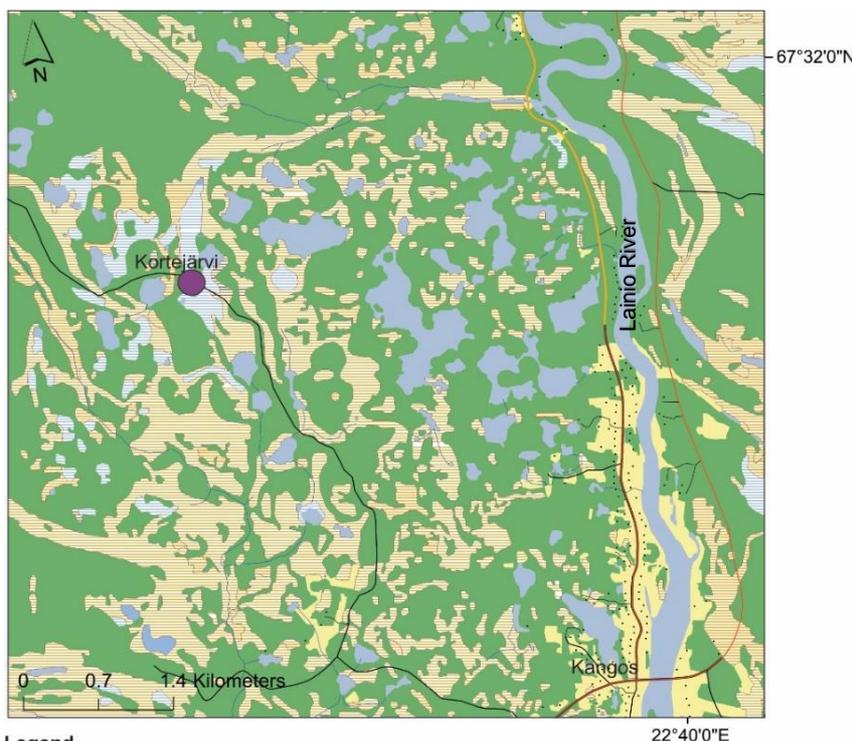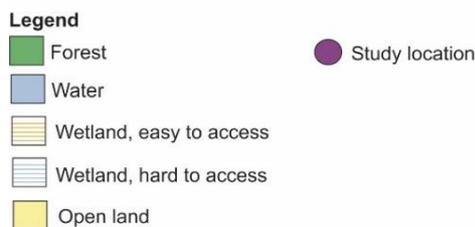
Figure 2.2. Study area Kortejärvi lies ~6 kilometers northwest of the village Kangos. The area is covered in lakes, forest and wetland. GSD-Vägkartan, 1:100 000 © Lantmäteriet I2018/00104 (2015).

Figure 2.3. *The Quaternary deposits in the study area and surrounding consist of glacifluvial sediments, peat and till. Modified from © Sveriges Geologiska Undersökning (SGU); Quaternary Deposits, 1:250 000 (2020a).*

2.3 Scientific approach

Paleoenvironmental interpretations often require several different approaches due to the complicated nature of formerly glaciated landscapes. By combining geomorphological, sedimentological and biological evidence, we can obtain results that are more reliable. The scientific approach and the methods in my study were chosen regarding the aim and time frame.

All available techniques that could enhance the outcome were used. In the following subchapters, the theory behind the methods is presented to support the outcomes of the study, as well as a short description on stagnant ice environments and ice-walled lake plains, which is the presumed environment in which the Veiki moraines formed and the landform that the moraine plateaus represent (Lagerbäck, 1988).

2.3.1 Stagnant ice environments

Ice fronts can become stagnant when the movement of the ice ceases, the mass balance is negative and large amounts of debris accumulate at the terminal zone. Temperatures and climate, geothermal heat flow, meltwater drainage and en- and supraglacial debris content, control the melting rate (Krüger *et al*., 2010; Ham and Attig, 1996; Johnson and Clayton, 2003) and out of these factors, climate and debris-cover properties are the dominant factors (Ham and Attig, 1996; Schomacker, 2008). Without a thick supraglacial debris, warm temperatures would lead to rapid ablation. When the supraglacial debris cover becomes thicker, the remaining ice becomes more deeply buried and the melting rates decrease (Kjær and Kjær, 2000). The melting can become so slow that vegetation is established on the surface (Johnson and Clayton, 2003). Stagnant ice can prevail for long times and especially in continental settings the melting might persist for thousands of years (Ham and Attig, 1996; Krüger *et al*., 2010).

Johnson and Clayton (2003) described a "stagnant-ice landsystem in lowland terrains" which well describes the terrain in which the Veiki moraines presumably were formed. Lowland terrains refer to places with a low relief at the margin of the ice sheet. The glacial debris in such regions commonly has a subglacial origin and is transported to the margin subglacially or englacially (Johnson and Clayton, 2003). The development from a fully ice-cored dead-ice field to a partially ice-cored dead-ice field and finally to the post-melt landscape has been studied and illustrated (Figure 2.4) by Krüger *et al*., (2010) at the modern day glacier Kötlujökull in Iceland. Although it is likely that these processes are somewhat different in terms of scale, when comparing a glacier with an ice sheet, we may assume that designated depositional processes dominate in each phase.
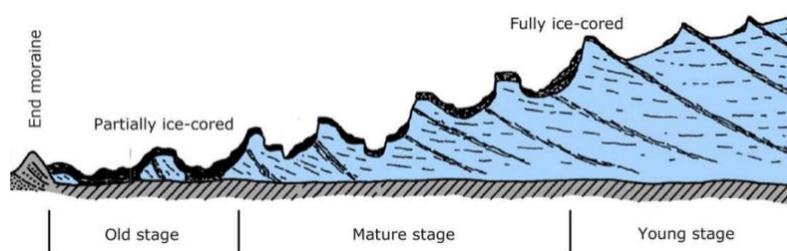
Figure 2.4. Different stages of a stagnant ice margin. Modified from Kruger et al. (2010).

The debris covered stagnant ice surface is typically hummocky and irregular (Krüger *et al.*, 2010). Resedimentation of debris occurs due to uneven downwasting and backwasting of the underlying ice, which eventually leads to frequent topographic inversion (Ham and Attig, 1996; Benn and Evans, 2010). As a result, the debris typically consists of mixed material (Kjær and Kjær, 2000). Only the deeply buried parts of the supraglacial debris may avoid extensive reworking and produce melt out till (Johnson *et al.*, 1995).

Hummocks in stagnant margins of modern glaciers commonly contain interbedded till and stratified sediments with normal faults (Johnson and Clayton, 2003). Such structures can form when supraglacial "flow till" or melt out till and stream and /or lake sediments are interbedded and collapse due to melting of underlying ice. The downwasting of the underlying ice results in faults and disruptions in the sediments (Johnson and Clayton, 2003). Hereby, the most important depositing processes are slumping, sliding and flowing of sediments. Gravity flows are strongly influenced by water content as it determines the flow velocity. Referring to a modern glacier, much of the sediment flows have a low velocity since the supraglacial debris is predominantly coarse-grained and drains water easily. Supposedly, precipitation and temperature control much of the supraglacial sedimentary processes at present day (Krüger *et al.*, 2010).

Widely occurring landforms in the stagnant-ice landsystem are hummocks, ring forms, ice-walled lake plains, dump moraines, outwash fans and disintegration ridges (Johnson and Clayton, 2003). Elevated landforms that hold fluvial and lacustrine sediments indicate a relief inversion as they represent former depressions that grounded when the underlying ice melted. As mentioned earlier, identical landforms and sediments, as an example mass-flow deposits in hummocky moraines, can form in many different climatic settings (Schomacker, 2008). Therefore, it is doubtful how much these landforms can tell us about the climate during their formation.

The thickness of stagnant ice at a glacier snout may vary widely, ranging from a few meters to tens of meters (Winters, 1961). As a modern example, the fully ice cored terminal dead-ice terrain at Kötlujökull in Iceland, measure between 10-40 meters in thickness. The lateral extent of stagnant ice fronts can be very large, indicated by landscapes left behind by ancient stagnant ice fronts, which cover areas bigger than 2000 km^2 in north America (Winters, 1961; Ham and Attig, 1996). Such landscapes document stagnant ice environments that lack modern analogues.

2.3.2 Ice-walled lake plains

Ice-walled lake plains are remnants of water filled sinkholes in stagnant ice (Johnson and Clayton, 2003). The surrounding rim ridges can rise to tens of meters above the central part of the landforms (Clayton *et al*., 2008). The slope towards the plateau is in general gentler than the outer slope, while some compose an even plateau in the middle. Ice-walled lake plains typically appear in clusters. According to Johnson and Clayton (2003) the terraces or second rim ridges that surround the landforms, indicate progressive widening of the ice-walled lake. Because of the high heat capacity of water, most ice-walled lakes melt through the ice and ground before the surrounding ice melts (Ham and Attig 1996; Clayton *et al*., 2008; Johnson and Clayton, 2003).

The rim ridges often reveal sorted sand and gravel interbedded with "flow till", which dip towards the center of the plains (Johnson and Clayton, 2003). The centers of ice-walled lake plains are typically composed of bedded or varved clayey and silty sediments to fine sand (Clayton *et al*., 2008). The lake sediments can be several tens of meters thick. Not all ice-walled lake plains match perfectly into these descriptions. Some are composed solely of till, and differences might occur even within one region of occurrence.

2.3.3 Geomorphology

Geomorphological evidence can be used to establish former glacier extent and direction of ice movement. Designated glacial landforms can also indicate the state of the ice sheet, as an example, ice-walled lake plains characterize a stagnant ice environment. Geomorphology can be studied by field mapping or with different remote sensing techniques like aerial photography, satellite imagery, LiDAR and seismic sensing (Lowe and Walker, 2015).

2.3.4 Sedimentary analysis

By analyzing sediments from glacial landforms, important evidence from the depositional setting can be obtained. Yet the sediment sequences in glacial environments are often highly complex (Benn and Evans, 2010), including intercalating tills, flow deposits and stratified sediments (Lowe and Walker 2015).

The nature and composition of glacial deposits depends on the thickness of the ice, the rate of melting, the topography, the concentration and type of clasts contained within the ice and the part in which the sediments were initially entrained and how they finally were deposited (Benn and Evans, 2010). Simply explained, glacial debris may be of subglacial, englacial or

supraglacial position. A wide range of laboratory methods are now available to determine the origin and depositional environment for glacial sediments. The methods used in this study are described in chapter 3. The principles behind sedimentary structures and how they can be interpreted are described below.

2.3.4.1 Lithofacies

The sedimentary structures formed during deposition of sediments, can give us information about the depositional environment. To understand the processes behind sedimentary structures, knowledge of the physical properties of the agent that eroded, transported and deposited the sediment is needed. Many of these processes result from movement of water, but air and ice are also important agents, while some sediments are directly emplaced by gravity. The general rule is that sediments settle down when the physical conditions and the sediment supply change over time at a given place. The physical variations in grains including size, shape and density, influence their response to the flows that transport them, and vice versa (Collinson *et al.*, 2006). Therefore, grain-size can be an indication of the relative amount of energy incorporated when emplacing the grains (Miall, 2016). Syn- and post-depositional disturbances will affect the final sedimentary structures of a succession (Collinson *et al.*, 2006).

The basal contacts between layers can be sharp or gradational, depending on the way in which processes or sediment supply changes and on the textural characteristics of the sediments (Collinson *et al.*, 2006). Gradational contacts reflect gradual changes in the conditions. Sharp changes may be non-erosional or erosional. Erosional bed contacts are often marked by crosscutting relationships. Erosion happens when the critical erosion velocity for a given grain size has been reached. Erosional periods can be long and result in big unconformities in the sequence. It is impossible to know what type and thickness of sediments are missing due to erosion, but as a rule, sediments deposited in the topographical highs are more likely to be eroded than those in the topographical lows (Collinson *et al.*, 2006).

When collecting data in field, a detailed description of the sediment successions is essential. Lithostratigraphical logging is a widely used approach where it is up to the researcher to define the level of details required for the study. A lithofacies is a rock unit (lithified or not) defined by its distinctive lithologic features such as composition, grain size, type of bedding and sedimentary structures. A lithostratigraphic unit represents one episode of sedimentation and the physical nature of the units reflects depositional environments. Boundaries of lithostratigraphic units are defined as surfaces of lithologic change.

Sedimentary textures include three properties; grain size, grain shape and fabric (Boggs, 2009). The techniques used to determine the first two, will be presented briefly. The grain size distribution can be determined with a particle size analysis. The size distribution of a sediment yields information about the distance the grains have travelled before deposition and the textural maturity of the sediment. Poorly sorted sediments have often been deposited close to the source while well sorted sediments have undergone a longer transport (Boggs, 2009).

To determine the size distribution for unconsolidated sandy sediments, sieving is a likely choice (Lowe and Walker, 2015). Sieving implies series of stacked meshes that divide the sample into decreasing size fractions. The sediment fractions retained in each mesh are weighed to obtain the percentage relative to the whole sample. Sieving is a relatively low-resolution technique (Boggs, 2009) but can be appropriate depending on the required resolution of the study. Prior to sieving, removal of non - clastic material from the sediments, such as organic material, should be done if the material includes > 2-4% organic material (Stål, 1972), or when an exact estimate of particles <20 μm is needed (Jensen *et al*., 2017) since organic material can influence the clay and silt content measurements. The LOI should be measured in advance to calculate the percentage organic matter in the sample and determine if organic material should be removed. The sample should be dispersed prior to sieving to avoid flocculation.

Mathematically calculating the roundness of clasts, as defined by Wadell (1932), is a time-consuming approach and hence visual estimations are often the method of choice. The general trend in the roundness distribution of a sediment can yield information about the transport distance and transporting agent of the particles. Particles become more rounded when they have been transported in water but will remain angular if the transport distance is short, as an example in a gravity flow.

Particle shape has been effective in the analysis of glacial, glaciofluvial and fluvial sediments. Krumbein (1941) defined the shape of a particle as a "measure of the surface area to its volume". For a sphere, the ratio is at minimum and for all other forms, the ratio is larger. The shapes of natural sedimentary particles are, however, very irregular and diverse. The sphericity (ψ) can be determined by measuring the three orthogonal axes of a particle and the calculations are based on relative lengths of the three axes; longest axis d_L, intermediate axis d_I and shortest axis d_s. According to Sneed & Folk (1958) a maximum projection sphericity can be calculated with the following formula:

$$\psi = \frac{\sqrt[3]{dS^2}}{dL \times dI} \quad \text{[Eq. 1]}$$

As described above, a wide range of sedimentary analysis techniques are available, and the method of choice depends on the characteristics of the sediments and the study in question. The texture of sediments affects porosity, permeability, bulk density and electrical conductivity, which can be important parameters when, for example, evaluating the sediments ability to transmit and store fluids.

2.3.5 Ground penetrating radar

One of the methods used in the study was interpreting GPR profiles. The principles behind the method are explained here.

A ground-penetrating radar (GPR) device transmits high frequency electromagnetic energy to the ground and detects electrical discontinuities in the shallow subsurface down to ~50 meters (Neal, 2004). Propagating electromagnetic waves loose energy in the ground and hence the depth to which they propagate is limited. The higher the antenna´s frequency, the shallower is the depth it can penetrate and the higher is generally the resolution of the resulting profile (Gehrig *et al*., 2004). When the waves propagate downwards, they encounter materials of different electrical properties/ dielectric constant (K) which is observed as changes in the velocity of the ground. Factors influencing the velocity are the mineralogy and the water content, which reflect porosity and grain size. The reflection coefficient R can be calculated as:

$$R = \frac{\sqrt{K_2} - \sqrt{K_1}}{\sqrt{K_2} + \sqrt{K_1}} \qquad \text{[Eq. 2]}$$

Where K_1 stands for the dielectric constant of upper layer 1 and K_2 for the dielectric constant of lower layer 2. The reflection coefficient is the amount of energy reflected from an interface of two layers. The bigger the contrast between two horizons, the more GPR energy reflects and the higher is the reflection coefficient and the stronger is the reflection seen on the GPR profile.

The energy that is reflected back to the surface and recorded by a receiving antenna on a GPR device, helps determining the depth of that horizon. The time between transmission, reflection and reception is called the two-way travel time and is measured in nanoseconds. The two-way travel time can be converted into more easily interpretable depth values if the average velocity of the ground profile is known, as:

$$Depth = \frac{Speed \ x \ time}{2} \qquad \text{[Eq. 3]}$$

where speed stands for the mean velocity (m/ns).

A GPR commonly consists of a transmitting antenna and a receiving antenna, a control unit, display and a recorder (Figure 2.5a). Common offset survey systems consist of either a single transmitting and receiving antenna or two separate transmitting and receiving antennas (Figure 2.5b) (Neal 2004; Kovin 2016).
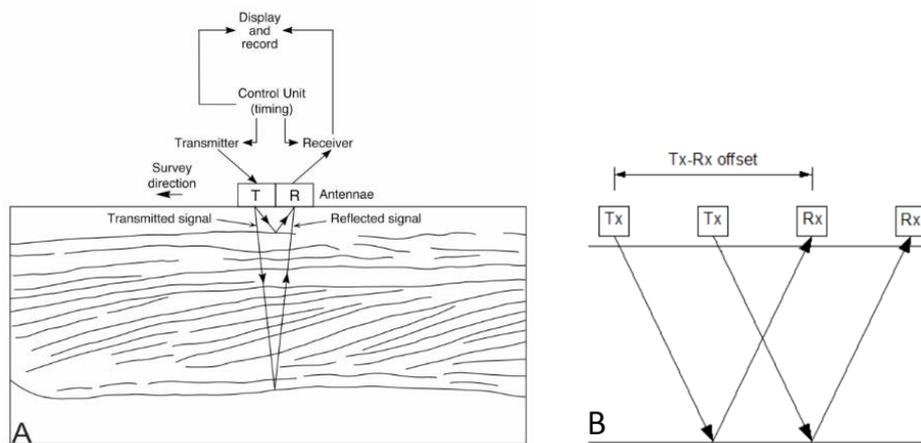
Figure 2.5a. A GPR device commonly consist of a transmitting antenna and a receiving antenna, a control unit, display and a recorder (Neal, 2004). Figure 2.5b. The principle of a common offset survey. (Kovin, 2016).

It is assumed that primary reflections parallel depositional structures in the subsurface, as the shape and orientation of bedding and sedimentary structures are more or less well represented by the recorded reflections. The degree of accuracy depends on the nature of the sediment body, the water table and type of terrain, type of data processing and the interpreter (Neal, 2004).

2.3.5.1 Processing functions

GPR comes with a few inherent limitations and overcoming them in order to get a realistic picture of the subsurface, often requires the data to be processed. Simple data processing should not radically modify the data but rather enhance the basic aspects of it. The nature and order of any processing applied on a GPR set is different for all GPR data sets. In sedimentological studies, form and orientation of primary reflections is normally of high importance and basic processing should enhance these features. Some of the common processing functions are normal-moveout corrections, signal saturation correction or dewow, gains and filters, velocity

profile estimates, topographical corrections and migration algorithms (Neal, 2004). A few of these functions are presented below briefly.

Velocity profile estimates

A good mean velocity estimate is needed to convert two-way travel time to a depth estimation. The velocity can be estimated in several different ways including hyperbola fitting, common-midpoint survey and correlation of a reflection to a known depth. Velocity can vary both vertically and laterally. Lateral velocity variations can lead to lateral distortion of the resulting GPR profile (Neal, 2004).

Topographic correction

Recording the topography of a GPR profile requires a device that can collect data rapidly with the required vertical accuracy such as a differential GPS (Neal, 2004).

Gains and filters

As the radar signal decreases with increasing depth, it might be necessary to strengthen the weaker signals. By applying the right gain to a GPR data set, one can obtain relevant information without introducing false reflections to the data. In sedimentological studies, where continuity of stratigraphic horizons is essential, it is important to show all recorded information. That is why in many sedimentological studies, the data is plotted and interpreted with an automatic gain control (AGC). AGC attempts to equalize all signals, which means that information regarding relative amplitude is lost (Neal, 2004).

Filters enhance and/or eliminate certain features through mathematical manipulation and often ease the process of interpreting the radar profiles. Typical features that one wants to delete from GPR data include the low-frequency wow and ambient and systematic noise (Neal, 2004).

2.3.5.2 Interpreting GPR data

All GPR reflections do not parallel bedding. Some reflections result from features unrelated to primary sedimentary structures, such as utilities and the water table. The "GPR community" is still lacking a common methodology, and hence misinterpretations are common. When describing GPR profiles terms that are both descriptive and interpretive should be avoided (Neal, 2004).

Knowing the relationships between facies is essential when reconstructing the development of the environment (Neal, 2004) and subsurface reflections reveal information that cannot be seen

from the surface. Basic geological rules such as the principle of cross-cutting relationships should logically also be followed when interpreting GPR data. Information from historical aerial images, the geological context, data from ground truthing, field observations, laboratory analyses and literature about similar deposits can be used together with the GPR profile interpretation to reach the best sedimentological analysis (Neal, 2004).

An objective method of choice, to help interpret GPR data in a sedimentological context, is the principle of radar stratigraphy defined by Neal (2004). This method was developed to avoid terms that are both descriptive and interpretive. Radar stratigraphy is designed to describe GPR profiles as radar surfaces and radar facies; a systematic description of reflections generated by primary depositional structure. The radar surfaces and radar facies can then be described by using objective radar-stratigraphy terminology including; shape, dip, relationship between the reflections and the continuity of the reflections.

All in all, interpreting a GPR profile involves much evaluation, and a full understanding of the technique will help to obtain a more realistic picture of the subsurface.

2.3.6 Luminescence dating

Dating techniques allow us to emplace past depositional events into a time context and helps determining the order of events. In this subchapter, the theory behind luminescence dating will be presented.

Luminescence dating refers to light-based luminescence dating (OSL and IRSL), thermoluminescence dating (TL) and other related techniques. In optical dating (Huntley *et al.,* 1985) the sample is exposed to an intense light, after which the luminescence signal is measured. The signal originates from electrons in the mineral, which are accumulated after the grain has been buried by overlying sediments and therefore been out of daylight. The surrounding sediments, and to some extent the grain itself, expose the buried grain to gamma-, beta- and alfa radiation in varying amounts, while cosmic radiation contributes with a smaller amount of radiation. The amount of radiation that reach the grains depends on factors such as the water content, locality and the local mineralogy. Irradiation originating from the decay of radioisotopes (mainly thorium, uranium and potassium) in the surrounding sediments, produces free electrons in the mineral grains that become trapped in the crystal (Raymond, 2015). The longer the minerals have been buried and therefore exposed to radiation, the higher the number of trapped electrons and the greater the luminescence signal (Huntley *et al*., 1985). Various methods are applied in the laboratory to release the trapped electrons. Illumination in form of

blue LEDs, which the sample is exposed to during an OSL measurement, forces the charge from light-sensitive traps in the minerals to be emptied. In the thermoluminescence technique, the traps are emptied by heating the sample. OSL uses the luminescence signal of quartz or feldspar. The infrared-stimulated luminescence (IRSL) uses signals of only feldspar (Rhodes, 2011). The accumulated signal is zeroed through exposure to daylight during transportation (OSL and IRSL) and therefore it is possible to determine the amount of time that has elapsed since the time of deposition of the quartz and feldspar grains in a sample (Thrasher *et al*., 2009). The TL signal is fastest emptied when subjected to high temperatures between 200-400 °C (Raymond, 2015).

2.3.6.1 Calculating the OSL age

The dose of the sample can be determined in a luminescence lab with an OSL reader. First, the natural luminescence signal of the sample is measured by exposing a subset, or aliquot, to a light source. In a single aliquot regeneration protocol, the same aliquot will then be given laboratory doses of radiation and exposed to a light source. The resulting luminescence signal from the subsequent measurements will result in a growth curve, which will help determine how much radiation the sample has accumulated in nature. The amount of laboratory irradiation needed to produce the same luminescence signal as that from the natural irradiation is called the equivalent dose (D_e). When the D_e is known, information about the dose rate is needed in order to calculate the age. The dose rate is the amount of radiation that the sample has been exposed to each year. The age can be calculated with the following formula:

$$Age \ (a) = \frac{Equivalent \ dose \ (D_e)(Gy)}{Dose \ rate \ (Gy a^{-1})} \quad [\text{Eq. 4}]$$

where Gy stands for Gray (1 Gy equals SI units 1J/kg) and a for annum (year). If a successful age calculation is to be done the sample must be completely bleached at the time to be dated. If that is not the case, any remaining signal must be quantifiable because a luminescence clock that has not been zeroed will lead to an age overestimation.

Equivalent dose

Choosing the grain size fraction for which the luminescence signal will be measured, depends on the sample and what is available in it. The degree of bleaching and potential post depositional mixing of the sediments should be considered. The interpretation of the geological history of the study site can help determine how trustworthy the results from the grains in that area are for age calculations by OSL (Rhodes, 2011). Different transport processes effect the grains

differently and hence, sizes that more likely have been exposed to enough daylight should be preferred. It has been debated whether silt- or sand sized fractions are better for OSL dating, when accounting their typical degree of bleaching (Alexanderson, 2007). For glaciofluvial and fluvial sediments, coarse size fractions might be better bleached than fine grains (Alexanderson, 2007; Truelsen and Wallinga, 2003). OSL laboratories commonly have a standard grain size used for measurements. The standard size depends on the available equipment in the laboratory, but also on what likely gives the best results. Lund Luminescence Laboratory routinely uses size fraction 180-250 µm. The sample preparations start with drying and weighing and after that sieving the sample. Before going into the OSL reader, the samples are mechanically and chemically treated to extract pure quartz (or feldspar) grains of a certain size.

In the OSL reader, the sample is placed on a heater plate with raised temperature, and illuminated by stimulation wave lengths from either blue or IR- light emitting diodes (LEDs) (Rhodes, 2011). The blue LEDs generate an OSL signal from both quartz and feldspar, while IR-light produce an IRSL signal from feldspar only. IRSL can therefore be a method for determining how successful the separation of quartz from feldspar has been (Duller, 2008). A photomultiplier tube detects the signal through a glass filter. The Risø automated luminescence reader (Figure 2.6), which was used for this study, has 48 sample aliquots.

The single aliquot regenerative-dose (SAR) protocol (Murray and Roberts, 1998; Murray and Wintle, 2000) has significantly improved the reliability of OSL dating due to its accuracy and reliability (Rhodes, 2011). The SAR protocol aims to determine the equivalent dose by a sensitivity corrected

Figure 2.6. A schematic picture of the Risø automated luminescence reader (Rhodes, 2011).

measurements and hence accounts for any changes that may have happened in the minerals during the measurement (Duller, 2008). A SAR cycle/run is composed of two parts. In the first half, the natural and regenerated luminescence signals are measured, and in the second half the luminescence sensitivity is measured. Typically, six or seven cycles are performed (Rhodes, 2011).

Before each OSL measurement, the sample is preheated up to between 160°C and 300°C for ~10 seconds (Duller, 2008). The preheating removes unstable electrons from shallow traps so that the OSL signal comes only from electrons that have been stored safely when buried. As individual samples are different, different preheat temperatures may be necessary (Rhodes 2011). The appropriate preheat temperature is determined by using a range of different temperatures while making D_e measurements. When the same D_e value is reached by a specific temperature range, a temperature within that range can be used (Duller, 2008).

The first OSL signal is received from the natural radiation dose termed L_N (luminescence nature). In the second cycle, the aliquot is exposed to a laboratory dose of radiation and the OSL signal (L_1) is measured. The following cycles measure the OSL signals (L_2, L_3) as the aliquot is exposed to varying regeneration doses. The amount of laboratory radiation is commonly increased for every regeneration dose.

The luminescence sensitivity of the aliquot may change depending on the undertaken procedures, such as temperature and length of preheat, but also depending on conditions during burial time (Duller, 2008). These changes are accounted for in the second half of the cycle by measuring the luminescence sensitivity, which is done by exposing the aliquot to a test dose. The given test dose is the same throughout all the SAR cycles. If there is no sensitivity change, the resulting luminescence signals (test signals T_X), should be identical to the first test signal (T_N). The ratio L_X/T_X is visualized in a dose response curve (Figure 2.7) and the D_e for that

aliquot can be determined. The maximum test dose error is commonly 10%, but depending on the amounts of accepted and not accepted aliquots, the error can be increased to 15% or to maximum 20% (Helena Alexanderson, pers. comm.) Accepting a higher test dose error will rise the uncertainty in the obtained age but may still verify the age range.
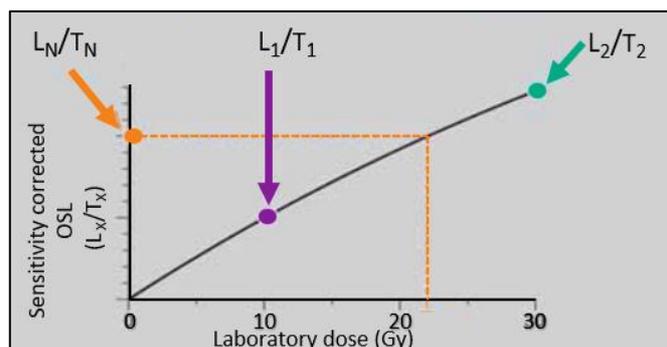
Figure 2.7. Sensitivity corrected OSL visualized in a dose response curve. Each arrow represents the L_X/T_X ratio of one SAR cycle. Modified from Duller (2008).

The suitability of the SAR protocol can be evaluated through quality controls; the recuperation test and the recycling ratio. The recuperation effect signal is measured after giving the sample a zero dose, and if it results in a signal, the sample might not be suitable for OSL. Commonly

a maximum of 5% of the natural signal in the recouperation test is accepted. The recycling ratio implies that the measurement is repeated with one of the regenerative laboratory doses, commonly the first. If the SAR protocol has corrected the changes in the sensitivity of the sample, the luminescence signals of the repeated dose should be the same. The ratio between the two sensitivity corrected luminescence signals is the recycling ratio. The ratio should lie between 0.9 and 1.1 to qualify (maximum error 10%), but the ideal ratio is 1 (Rhodes, 2011). Values greater or less, suggests that the sample is more complex or the procedures undertaken are inappropriate and therefore that the results of the aliquot should not be considered true (Duller, 2008).

Additionally, a dose recovery test can be applied to determine the suitability of the SAR protocol. During the dose recovery test, the natural signal is zeroed after which the sample is exposed to a dose. This dose is considered as the natural dose in the SAR protocol and will be treated and measured as unknown. The SAR procedure is then applied. If the calculated dose and the given known dose are same, the protocol and the selected settings during the SAR protocol can be assumed to give the correct results. If a sample fails a dose recovery test, it is likely that the calculated D_e value is false due to unsuitable protocol settings (Duller, 2008).

If repeated D_e measurements give different results, the sample may be incompletely bleached or alternatively the quartz is dim (of poor quality) and therefore less suitable for OSL measurements. It is, however, rare to get the exact same D_e value from all measurements (Helena Alexanderson pers. comm.), but if the D_e values are scattered and the dose distribution skewed, more investigations are needed (Helena Alexanderson pers. comm.). The most common cause of poor precision is incomplete bleaching and post depositional mixing of grains (Rhodes, 2011). Another cause of large variations in D_e can be due to different parts of the sample having received different radiation doses during its burial time.

Dose rate and water content

A major problem in luminescence dating is understanding how the environmental dose rate (Gy/a) has varied over time. A good estimate of the mean dose rate is, however, necessary for all OSL samples in order to determine the age. Most of the radiation comes from the surrounding grains. Sediment dose rate can be determined by measuring radioactive emissions directly or by analyzing concentrations of K, U, and Th in the laboratory. If the dose rate is measured in the laboratory, material from homogeneous sediments surrounding the OSL sample must be collected.

Water in the sediments constricts radiation, which means that a grain in a saturated sediment sample receives less radiation if compared with a grain in a dry area. The luminescence will be lower in grains in saturated sediments and lead to an incorrect age if the water content is not accounted for. Wallinga (2002) has calculated that an error of 1% in water content results in an error of 1% in the age estimate. The water content at the time of sampling and at saturation should be calculated and the mean water content during its burial time should be estimated. Knowing how the mean water content has varied over a period requires knowledge of the geological history of that period in the area.

Other factors influencing the dose rate are sediment composition, porosity and pore fill, the amount of organic material and the bulk density. The altitude of the sampling site, depth of the sample in the ground and the latitudinal position will influence the amount of cosmic radiation. Cosmic dose contributes with less than 10%, while at least 90% comes from gamma, beta and alpha radiation (Rhodes, 2011).

2.3.6.2 Accuracy of OSL dating

The obtained OSL age of a sample is the time of the last event that involved exposure to day light. There is a great probability of quartz and feldspar to be bleached or zeroed during the transportation, but the degree is highly dependent on the transport path. The electron traps for both quartz and feldspar are very light-sensitive and an exposure from a few tens of seconds to a few minutes, will be enough to 'zero the clock' (Raymond, 2015). A big advance in luminescence dating has been the ability to make replicate measurements on the same aliquot of a sample (SAR protocol). This gives the possibility to evaluate if the mineral grains were exposed to enough daylight for the OSL signal to be zeroed at deposition, by accounting for the sensitivity changes during the measurement (Duller, 2008).

The accuracy of luminescence dates depends on several parameters and the datable timeframe ranges from a few years up to 200ka or more (Duller, 2008; Raymond, 2015; Rhodes, 2011) depending on the luminescence characteristics of the minerals. Hence, OSL dating of quartz grains covers at least the last glacial-interglacial cycle, making it a useful tool in especially Quaternary climate reconstruction. The expected errors in luminescence dating range between ± 5 and 10% of the samples actual age (Duller, 2008; Rhodes, 2011).

2.3.7 Radiocarbon dating

Radiocarbon (^{14}C) dating (Libby, 1946) is the most widely applied dating method for organic material less than 45 000 years (Alexanderson *et al*., 2014) and within the study of Late Quaternary climate fluctuations (Raymond, 2015). A brief description of the method follows below.

^{14}C can be used globally, and it can be used for a wide range of organic materials such as peat, wood, bone, shell, paleosols, seawater, marine, and lacustrine sediments and carbonaceous particles trapped in ice. It is assumed that plants and animals assimilate radiocarbon and other carbon isotopes in the same proportions as they exist in the atmosphere, and hence the radiocarbon can be used as a proxy of climatic conditions in the past (Bowman, 1990).

Radiocarbon is produced in the upper atmosphere by neutron bombardment of atmospheric nitrogen atoms (Bowman, 1990). The neutrons are produced by cosmic radiation entering the upper atmosphere with a maximum concentration at an altitude of ~15 kilometer (Raymond, 2015). The ^{14}C atoms oxidize rapidly to $^{14}CO_2$, which then mixes with the rest of the atmospheric carbon dioxide and enters the biosphere. In theory, an equilibrium between the rate of new ^{14}C production and the rate of ^{14}C decay should exist, since it is assumed that the total mass of global ^{14}C remains constant (Bowman, 1990). Moreover, fractionation occurs in plants and hence the ^{14}C depletion in organisms may be up to 5% below atmospheric levels, the amount varying for individual plants (Raymond, 2015). Moreover, since the 1950s, the amount of artificially produced ^{14}C has increased due to atomic bomb explosions in the atmosphere (Aitken, 1974). It is also widely accepted among scientists today, that human activity has altered the CO_2 balance of the atmosphere by burning fossil fuels. The dating techniques have however, developed so that the raised radiocarbon emissions are being taken into account and relatively reliable results can be obtained (Povinec *et al*., 2009). However, the effects of industrial activity and atomic explosions makes modern organic samples unsuitable as reference samples for radiocarbon activity (Lowe and Walker, 2015).

The tissues of plants and animals are in constant exchange with the atmosphere as old cells die and are replaced. As soon as an organism dies the exchange of ^{14}C ceases and the radiocarbon clock is activated. The radiocarbon within the organism decays to nitrogen. One half-life for radiocarbon is 5730 years (Bowman, 1990). After ten half-lives (57 300 years) the sample contains less than 0,01% of the original ^{14}C content of the organism (Raymond, 2015).

Today a widely used method for radiocarbon dating is accelerator mass spectrometry (AMS). The equipment used in AMS in highly sensitive and allows dating of very small sample sizes, as only 1 mg of carbon is required (Raymond, 2015). AMS measures the concentration of individual ions; ^{12}C, ^{13}C, and ^{14}C (Bowman, 1990).

2.3.7.1 Radiocarbon disadvantages

Radiocarbon dates are radiometric measurements and hence the ages are statements of probability (Raymond, 2015). A statistical uncertainty in the radioactivity should be accounted for all samples and therefore a single absolute age cannot be obtained. ^{14}C dates older than 45 000 years should always be viewed with caution (Raymond, 2015).

Even if a sample age is precisely determined, it can be false if for instance, it is contaminated. Contamination vary in significance; modern carbon is highly active, and a relatively small amount of contaminant can result in large errors in the obtained dates (Lowe and Walker, 2015). Natural contamination can occur in the depositional- or post-depositional environment and can be difficult to detect. Contamination by recent rootlets is a common modern carbon contaminator, as well as other kind of bioturbation. Permafrost can also result in both modern and old carbon contamination, as it might cause reworking of sediments. Reworking of the sediments can also occur, for instance, through anthropogenic activities such as forestry. Accidental mistakes by the scientist during sampling can also be the cause of contamination. Chemical reactions that may exchange carbon with the sample can also cause contamination, as an example mobile humic remains. Rain- and groundwater can cause chemical reactions with carbonates, which complicates the detection of contamination for samples that contain carbonates (Raymond, 2015).

2.3.8 Pollen

An important field in paleoclimate reconstructions is palynology or pollen analysis. A central aim of the method is to trace the local and regional vegetation development by looking into fossil pollen records (Lowe and Walker, 2015). A brief description of the method follows below.

Pollen are spread to the atmosphere by flowering plants and cryptogams and can be distributed far from their sources. Fossil pollen are extremely resistant especially when stored in lakes and wetlands (Lowe and Walker, 2015), and they are good archives of information about past vegetation changes, which in turn largely are controlled by climate. The species-specific

morphological characteristics of pollen help identify which plant species were growing at the time of deposition. In some areas pollen records span over the whole Quaternary, but a more common time frame is Holocene to late-glacial (Raymond, 2015). Pollen data can be used as a basis for correlating Quaternary stratigraphic units.

Not all vegetation changes are due to change in climate, however. Other reasons can be fire, insect infestation, plant successional changes, anthropogenic activity and changes in factors leading to the accumulation and preservation of the fossil material itself (Raymond, 2015). Knowing the relationship between plant frequency in an area and the total pollen rain from that plant species is important in order to calculate the actual composition of the surrounding vegetation (Raymond, 2015).

A sediment core is generally sampled at intervals of a few centimeters and slides of pollen and spores of each level are prepared. When isolating pollen and spores from organic or inorganic sediment samples, the samples are treated with chemicals to remove irrelevant material. The remaining pollen grains and spores are then analyzed by microscope and the number of different grains in each sample is noted. The total number of grains counted depends on the purpose of the study and the source material. Usually at least 200 grains are counted (Raymond, 2015).

2.3.9 X-ray fluorescence scanning

XRF data provides information in down core variations in element abundance. An XRF scanner can perform rapid qualitative measurements of all elements from Magnesium to Uranium, the range depending on the scanner (Brouwer, 2010). The results of the measurements are commonly studied in characteristic element ratios, which are used as proxies for, as an example, variations in the depositional environment and sediment source. Therefore, the depositional setting controls the choice of element ratio /proxy (Croudace and Rothwell, 2015). XRF scanning has been widely used within Quaternary marine and lacustrine studies because unlike fluvial deposits, their records are commonly more continuous and undisturbed. River systems are sensitive to environmental change and typically respond fast to small changes and thus their records are often fragmented (Croudace and Rothwell, 2015).

An XRF scanner is based on the principle that electromagnetic waves (X-rays) collide with matter leading to the elements emitting fluorescent x-ray radiation. Each element has characteristic fluorescence energies, and this allows the identification of elements in the sample (Brouwer, 2010). The measurements are performed in multiple runs using different currents,

voltages and filters. Standardized settings are available for different types of measurements. Filters are placed between the source and the sample to reduce the intensity of background noise, and thereby improve the signal to noise ratio (Brouwer, 2010). Moreover, when measuring XRF the surface of the sediment should be homogeneous and dry with a flat and smooth surface (Richter *et al*., 2006) and the core should be covered with a thin film preventing it from contamination. Large grain size differences result in a rough surface, which negatively affects the quality of the measurements. The resulting element ratios can be correlated with other data such as a lithological descriptions (Richter *et al*., 2006).

3 Methods

The study location was chosen by Helena Alexanderson and Martina Hättestrand. Kortejärvi was chosen based on promising GPR reflections of the moraine, which showed a prominent deepening in the central part of the moraine and could potentially contain a good sediment record. The aim was also to gain a more widespread distribution of investigated Veiki moraines. Collecting data from geomorphologically different Veiki moraines was also one ambition. In this chapter, the methods that were used in this study are presented.

3.1 Field work

My field work was carried out 27th September to 2nd October 2018. Four people participated in the field work; Mimmi Lindqvist (UiT), Helena Alexanderson (LU/UiT), Martina Hättestrand (SU) and Petra Zahajská (LU). The site was revisited in October 2019 together with Amanda Karlsen.

3.1.1 Coring site, Kortejärvi 2

The coring location lies 236 meters above sea level at the coordinates 67.520 °N, 22.571 °E. The equipment used for drilling was a Russian peat corer and a cobra vibration corer (Atlas Copco Pionjär). The Russian peat corer did not penetrate more than a maximum depth of 40 centimeter and the vibration corer was therefore the preferred equipment together with a 1-meter long corer in metal. The drill was held on hammering mode to avoid much disturbance of the sediment layers. Two cores were retrieved from this site, the second one, Kortejärvi 2 (K2), is used in this study. The cores were collected one meter at a time in plastic tubes (33-millimeter diameter), wrapped in dark plastic and stored out of daylight in a cool room. The coring site was described and documented with photos (Figure 3.1).

Figure 3.1. Petra Zahajská, Martina Hättestrand and Mimmi Lindqvist operating the cobra vibration corer. Photo by Helena Alexanderson (2018).

3.1.2 Outcrops, Kortejärvi 3 and 4

Two ridges, which lie on both sides of the lowered center of the moraine, were exposed by clearing six outcrops (A-E) on the western ridge and two outcrops (F-G) and one hand-dug hole on the eastern ridge (H). Section drawings and lithostratigraphical descriptions were made following Krüger & Kjær (1999) and Miall (1996). Bulk samples for grain size analyses and samples for luminescence dating were collected. Clast samples were extracted to determine roundness and the dominant lithologies.

Figure 3.2. An overview image of the crest of the western ridge. Photo by Helena Alexanderson (2018).

3.2 Laboratory analyses

3.2.1 Core opening and visual logging

The core K2 was opened with a vibrating multitool under darkroom conditions at the Department of Geosciences, UiT. Lithostratigraphical logging and facies classification was done visually by systematically describing the sediments and defining boundaries, following Krüger and Kjær (1999) and Miall (1996). The core was documented with photos.

3.2.2 Sedimentary texture

Grain size samples were collected from the core and from the outcrops. Sampling spots were selected to demonstrate representative lithofacies, such as diamict, medium sand, coarse sand and gravelly sand. The scale of grading was also of interest when choosing samples. The sample size for the outcrop samples was determined according to Hoare and Gale (1992). For the core samples, the size of the plastic tubes in which the core was collected, limited the size of the sample and hence the recommended minimum amount of sediments to determine specific sediment types (Hoare and Gale, 1992) could not be used. The grain size distribution diagrams (4.6b and 4.6c) should therefore be considered indicative rather than definitive.

The dry weight of all the samples was measured after being dried for 24 hours in 105 °C. The total organic matter (LOI) was calculated for several parts of the core and resulted to be less than 2%, no removal with H_2O_2 was therefore done prior to analysis. The carbonate concentration was also insignificant or non-existent when applying a small amount of HCl to the samples. Chemical dispersion was done with 0.0133% sodium pyrophosphate ($Na_4P_2O_7$) to remove flocculating sediments (Stål, 1972). All samples, both from the core and the outcrops, were wet sieved through 8 mm, 4 mm, 2 mm, 1 mm, 500 µm, 250 µm, 124 µm and 63 µm stacked sieves. The retrieved fractions were dried, and the percentage of each fraction was calculated as:

$$fraction\% = \frac{w_d \; of \; the \; fraction}{w_d \; of \; the \; total \; sample} \qquad [Eq. 5]$$

where w stands for weight (g) and d for dry.

The visualization of the grain size distributions and the cumulative weight percent was plotted with RStudio (RStudio Team, 2015).

The roundness was determined visually by following Powers (1953), and the resulting roundness distribution was visualized with Microsoft Excel. The shape of the particles was determined by measuring the three orthogonal axes of the clasts, after which they were plotted with Tri-Plot v1.4.2 (Graham and Midgley, 2000).

3.2.3 Optically stimulated luminescence

OSL samples were collected from five sections of the core with fine to medium grain sizes, to have a higher likelihood of suitable grains for luminescence measurements. Additionally, four OSL samples were collected from the outcrops with opaque grey plastic tubes; two from outcrop A, one from outcrop B and one from E. OSL samples from both locations were prepared and analyzed at the Lund Luminescence laboratory. I have participated in all preparation steps and carried out the age calculations, but Helena Alexanderson did the measurements and analyses of the equivalent dose. The environmental dose rate and the final OSL ages were calculated with the online calculator DRAC v1.2 – **D**ose **R**ate and **A**ge Calculator *(Durcan et al.*, 2015). See all the input data in Appendix 1.

3.2.3.1 Equivalent dose

The samples from the outcrops (K3) were sieved with stacked meshes; 355µm 250µm, 180µm, 90µm, 63µm and then treated with 10% HCl to remove carbonates and 10% H_2O_2 to remove

organic material. The samples from the core (K2) were not sieved before the first chemical treatment due the small amount of material. All the OSL samples were dried after the chemical treatment and after that quartz was separated from feldspar with a heavy liquid (LST Fastfloat) with the density 2.62 g/cm^3. After that, the quartz grains were treated with 40% HF to etch the grains and after that with HCl one more time and then dried. The samples from the core were sieved with the stacked meshes 250µm, 180µm, 90µm, while the outcrop samples were re-sieved with a 180µm sieve. A magnet was used to remove magnetic heavy mineral grains from the sediments. A small amount of each sample was attached on a disc (Figure 3.3a) and the discs were placed in the OSL reader.

The D$_e$ measurements were done in a Risø automated TL/OSL reader model DA-20 at the Lund Luminescence Laboratory (Figure 3.3b). Several aliquots where measured for each sample, the amount depending on the quality of the obtained results from each aliquot. Preheat and dose recovery tests were carried out to determine suitable analytical protocols for each sample. OSL stimulation was by blue (470 ± 30 nm) light sources and detection by a 7 mm U340 glass filter. The luminescence signal is dominated by a fast component and the first 0.48 seconds were integrated for the peak and the following 0.48 seconds for the background.
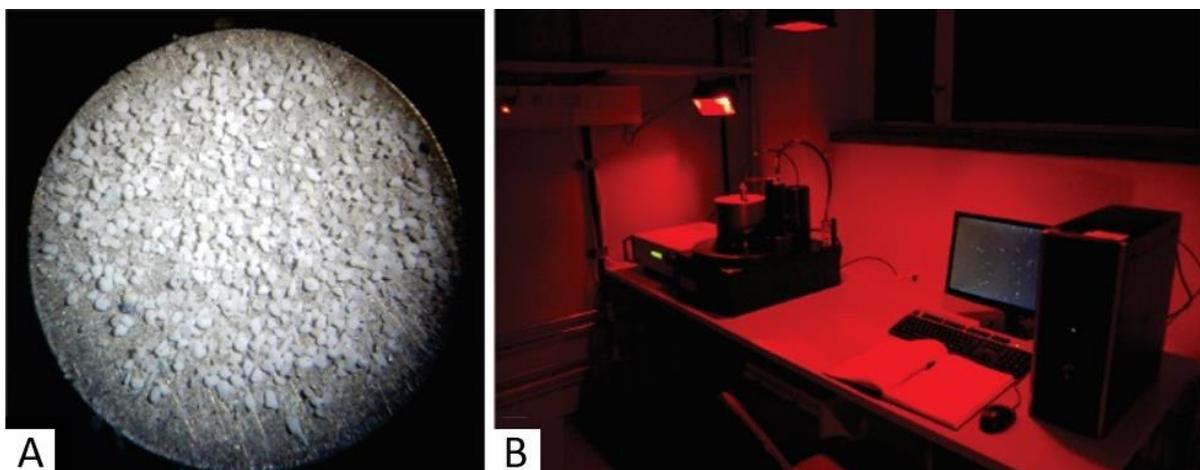
Figure 3.3a. Etched quarts grains under a microscope. *3.3b.* Risø automated TL/OSL reader at Lund luminescence laboratory. Photograph by Helena Alexanderson.

After measuring the natural OSL signal the aliquots were given regenerative laboratory doses and test doses to determine the dose. Recycling ratio and recuperation values were also determined. The test dose error was set to 10% for most of the samples except for three of the samples for which 15% error was used. The recuperation error limit was 5% and the recycling ratio limit 10%. The results were analyzed by Helena Alexanderson with the software Analyst

v4.31.9 and 4.57, which enables to view, edit and analyze luminescence data collected with a Risø automated TL/OSL reader.

Once the equivalent doses from all the aliquots were obtained, the dose was calculated from the accepted aliquots for each sample by using statistically elaborated values. Statistically elaborated dose values were obtained by using the central age model CAM (Galibraith *et al*., 1999). CAM is a statistical model that calculates the weighted average doses including all dose estimates (Medialdea *et al*., 2014). CAM was considered the best option compared to the mean dose estimate and minimum dose estimate, because the number of accepted aliquots was low (between 15/63 and 29/45) and the doses were somewhat scattered. CAM accounts for precision and puts more weight on the values with smaller errors, and therefore it was more applicable than the mean dose estimation. The mean dose can be used when ages are not so scattered (Rodnight, 2008). The minimum age model will not give good results on samples with a small number of accepted aliquots (Rodnight, 2008). The required number of accepted aliquots depends, as an example, on how well the samples are bleached. The appropriate number of D_e values is not currently specified, but it is known that well bleached samples requires less aliquots while poorly bleached samples naturally requires more (Rodnight, 2008). In some occasions, the amount of material available for analysis can be a limiting factor (Rodnight, 2008).

3.2.3.2 Dose rate

Samples for calculating the background radiation were collected just below and above each OSL sample from the core. From the outcrops, the background samples were collected in the same opaque grey plastic tubes as the OSL samples (Figure 3.4), while the water content and density were calculated from samples collected in cylinder volumeters right next to the OSL sample. The samples were weighed, and the weight percentage of water was calculated as:

$$W.c.\% = \frac{W_{wet} - W_{dry}}{W_{dry}} \times 100 \quad [Eq. 6]$$

Figure 3.4*. The OSL samples and the background samples from the western ridge were collected in opaque grey plastic tubes (black lid). The water content and density were measured from material collected in cylinder volumeters (white lid). Photo by Helena Alexanderson (2018).*

where W_{wet} is weight of sediment and water and W_{dry} is weight of dry sediment. The samples were water saturated and weighed, after which the samples were dried for 24 hours in 105 °C respectively 24 hours in 450 °C, being weighed in between and after. Then saturated water content (Φ) was calculated as:

$$\Phi = \frac{V_{pore}}{V_{pore} + m_{dry}} \ x \ 100 \quad \text{[Eq. 7]}$$

where V_{pore} stands for pore volume.

The water content which was used in the dose rate estimations was estimated by using the field water content and the saturated water content. The geological setting of the site was then accounted for in order to make an estimate of the time that the grains had been saturated contra drier (present day conditions in the end of a dry summer). The error in water content was considered 4% for each sample as a certain uncertainty is required for all paleo water content estimations and 4% is the default error.

The LOI percentage was calculated as:

$$LOI\% = \frac{W_{dry} - W_{LOI}}{W_{dry}} \times 100 \ \text{[Eq. 8]}$$

The sediments were crushed in a mechanical grinder into particles of even size (silt size) and sent to the Nordic Laboratory for Luminescence dating in Denmark. Here, dose rate measurements using gamma spectrometry were made, meaning that the environmental concentration of natural radionuclides in the sediments was measured (Murray *et al*., 1987).

3.2.4 Radiocarbon dating and pollen

Three peat layers were identified in the core, out of which the deepest one was mixed with silt. Radiocarbon samples were collected from the top two organic layers and several samples were collected from organic pieces of unidentified species, scattered throughout 410 centimeters of the core. The organic material was wet sieved through 250 µm sieve with distilled water and examined with an optical microscope. Three of the samples which were considered suitable for radiocarbon dating were dried in 50 °C then weighed and sent to the Radiocarbon laboratory at Lund University, where the age was determined by using AMS.

The three organic layers, which remained in the archive half of the core, were split into 1-centimeter pieces, stored in a cool room in separate bags and sent to Stockholm University for pollen identification, which was carried out by Martina Hättestrand.

3.2.5 Ground-penetrating radar

Prior to my fieldwork, GPR data were collected by Helena Alexanderson (Lund University, LU), Leif Vidar Jakobsen (Norwegian University of Life Sciences, NMBU), Martina Hättestrand (Stockholm University, SU) and Clas Hättestrand (SU) in 2012. The 520 meters long radar profiles at Kortejärvi were recorded using GPR common-offset measurements, along the road crossing the moraine from E-SE to W-NW (Figure 3.5), using a pulseEKKO PRO GPR (Sensors and Software). Only the part crossing Kortejärvi was used, since only scarce field observations outside the Kortejärvi moraine were made and interpretations would have been done with little to no certainty. Three different frequencies were used during data collection in field; 50 MHz, 100 MHz and 200 MHz. The GPR track was positioned using a handheld GPS. Field notes to be used when interpreting GPR profiles, were made simultaneously with the GPR measurements. These data were made available to me for this project.
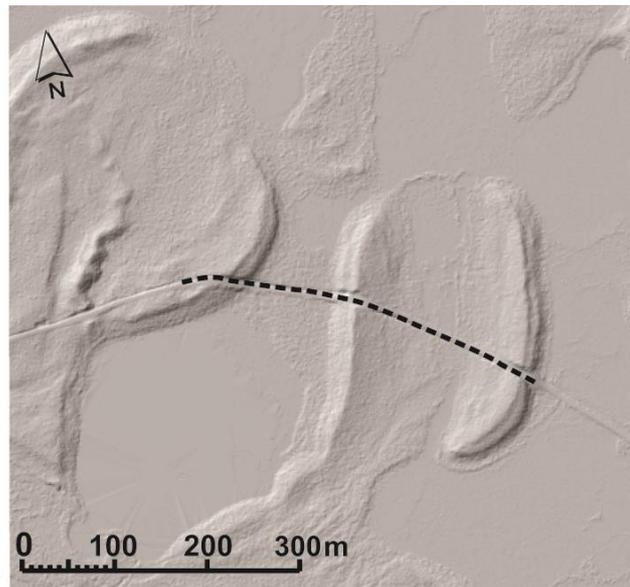
Figure 3.5. The radar profiles from Kortejärvi are 520 meters long. The profiles were collected on the gravel road that crosscuts the moraine. The survey line is marked with a black dashed line. Background map: Nationell höjdmodell © Lantmäteriet I2018/00104 (2011b).

The radar profiles from Kortejärvi were processed and interpreted in EKKO_Project V5 R3 (Sensors & Software). The 100 MHz and 200 MHz GPR profiles were processed with time-zero corrections, dewow filter and F-K migration. For unprocessed profiles see appendix 2. Three different methods were used to determine the mean velocity; hyperbolic fitting, correlation of the depth to a known horizon and a common mid-point survey (CMP). Leif Jakobsen (NMBU) carried out the CMP survey. A topographic correction was made with data retrieved from the GSDHöjddata grid +2 (Lantmäteriet, 2011a). The profiles were described and interpreted following the radar stratigraphy method defined by Neal (2004). To help interpret the profiles, additional information was retrieved from the field observations, the K2

core, from aerial images and literature about deposits in glacial environments (Arcone *et al*. 2014).

3.2.6 X-ray fluorescence scanning

The core was run through an XRF core scanner (AVAATECH) at UiT. The measurements were partly regarded as an experiment to find out if coarse grained sediments are suitable for XRF scanning, but also in order to figure out elemental changes that would signal of environmental changes during deposition. The measurements were made in 1 cm intervals with the following settings; 10 kV, 1000 µA, no filter and 30 kV, 2000 µA, Pd-thick filter. Clasts bigger than 2 centimeters were removed temporary before to measurements to avoid an uneven surface. The element ratios Zr/Rb and Zr/Ti were chosen as proxies (Turner *et al*., 2015). High resolution line scan photographs of the core were also retrieved.

4 Results

4.1 Kortejärvi study locations

The coring location K2 lies in the center of the moraine, and K3 and K4 stands for the field locations on the ridges. Additionally, two holes, K5 and K6, were hand dug in the northern and southern parts of the moraine. The study locations are marked in Figure 4.1a. The ridges are slightly bended and stand ~ six meters over the surroundings and clearly define the western and eastern limits. They measure ~560 respectively ~360 meters in length. Both ridges have a double crest, but the eastern one is more prominent. The outcrops A-G (Figure 4.1b), which were cleared at the ridges K3 and K4 revealed a soil component of varying thickness below the present-day vegetation.
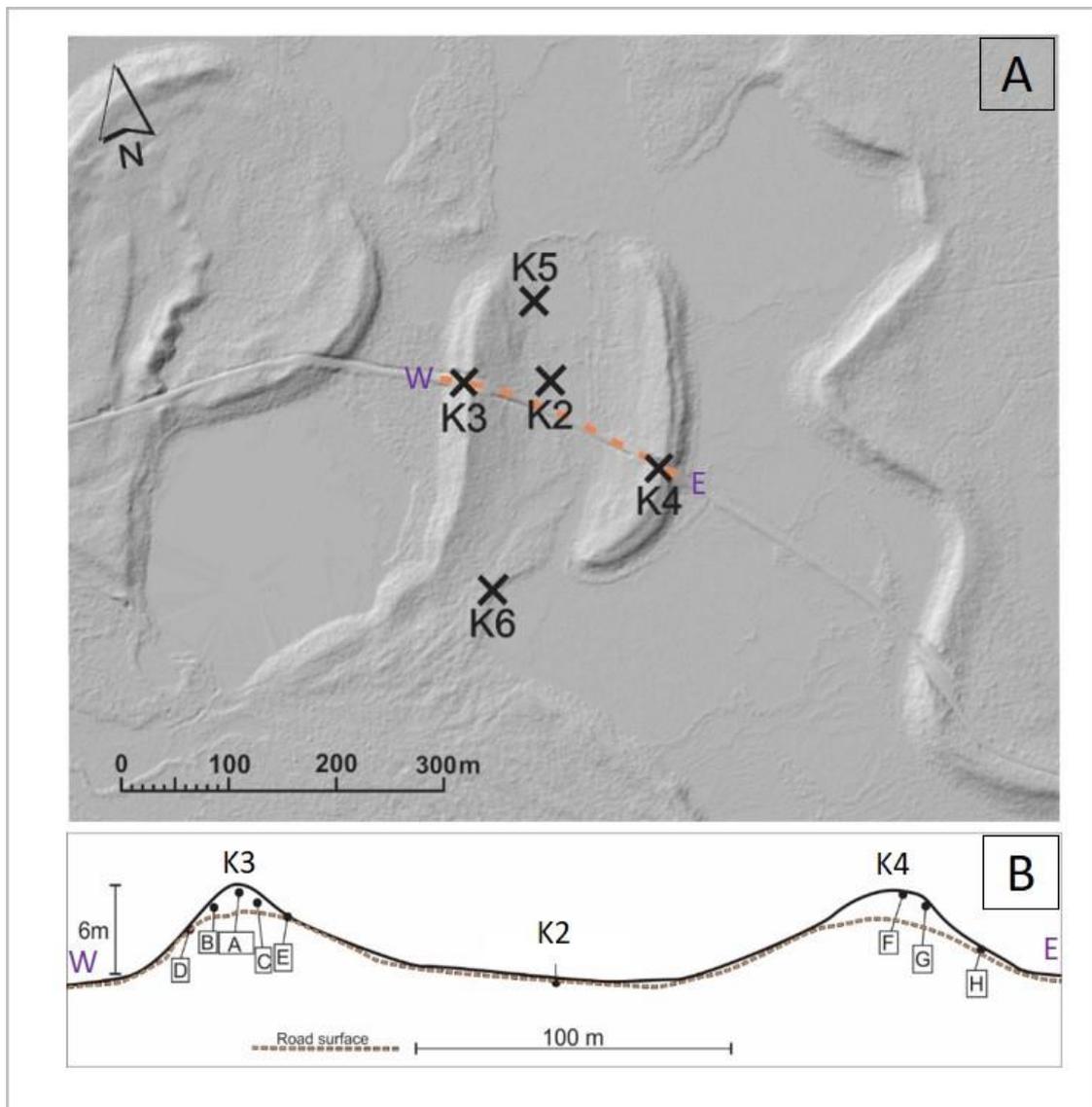
Figure 4.1a. *Sampling locations K2-K6 marked on a hill shaded relief map of Kortejärvi. Background map: Nationell höjdmodell © Lantmäteriet I2018/00104 (2011b).* **4.1b.** *Cross sectional sketch of Kortejärvi moraine and field locations. Note that the height scale is exaggerated 5 x.*

4.2 Lithostratigraphical description

4.2.1 Core K2

The core is in total five meters long, and out of the top 70 centimeters, only the lowest five centimeters were retrieved with the vibrocorer. From the Russian peat corer, we could however see that the top 65 centimeters consisted of peat.

The core is essentially composed of four main sedimentary units; K2-1 to K2-4, separated by both sharp and gradational transitions. K2-1 and -2, represent two lithofacies; massive gravelly diamict (K2-1) and massive silty diamict (K2-2) (Figure 4.2a). K2-3 consists of three different lithofacies: gravelly sand, massive sand and peat. A large part of the unit is composed of well sorted medium to coarse massive sand (Figure 4.2b) and moderately to well sorted coarse to very coarse gravelly sand (Figure 4.2c). The size of the gravel ranges between 2 mm and 60 mm. The shapes of the clasts bigger than 1 centimeter within the unit are mainly sub-rounded or sub-angular, with a few rounded and angular clasts (Figure 4.3). K2-3 composes four distinct upwards fining sequences and on top of two of them, lies a layer of peat (Figure 4.2d). The components in the organic layers are remnants of *Carex*, leaves, seeds and roots from unidentified species. The topmost unit (K2-4) is composed of peat. Small pieces of unidentified organic material are scattered almost throughout the core. A lithostratigraphical log is presented in Figure 4.5a.

The two diamicts in the bottom and the overlying gravelly unit are separated by a sharp contact respectively (Figure 4.2a). Within K2-3 there is a sharp contact on top of each medium sand layer and organic layer (Figure 4.2b and 4.2d). The boundary between the top peat layer and the underlying gravel is sharp.

There is an apparent change in the lithology distribution between the gravelly sand and the diamict layers at the bottom (Figure 4.4).
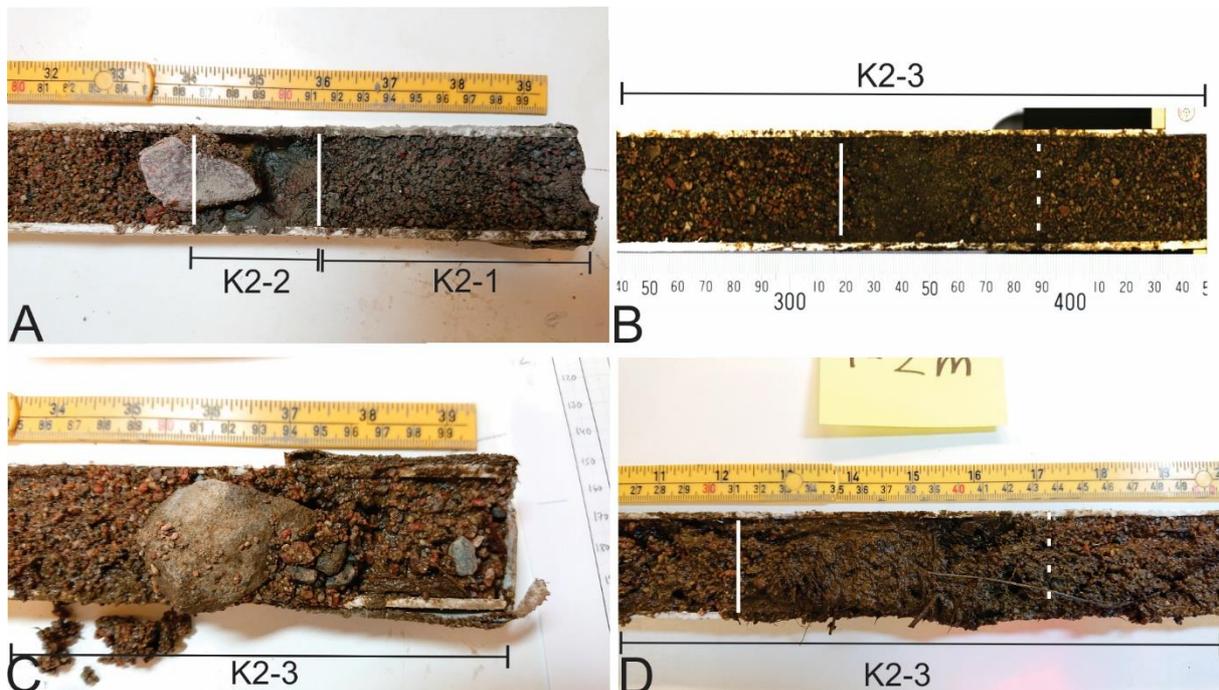
Figure 4.2a. Unit K2-1 and K2-2 separated by sharp contacts. **4.2b.** Unit K2-3 massive medium to coarse sand with a fining upwards sequence. **4.2c.** Poorly sorted coarse gravelly sand or sandy gravel. **4.2d.** A layer of peat lies between coarse gravelly sand layers.
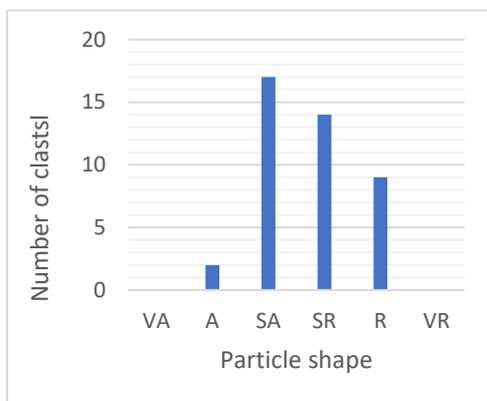
Figure 4.3. The shapes of the clasts >1 cm in diameter within unit K2-3 are predominantly sub angular and sub rounded.
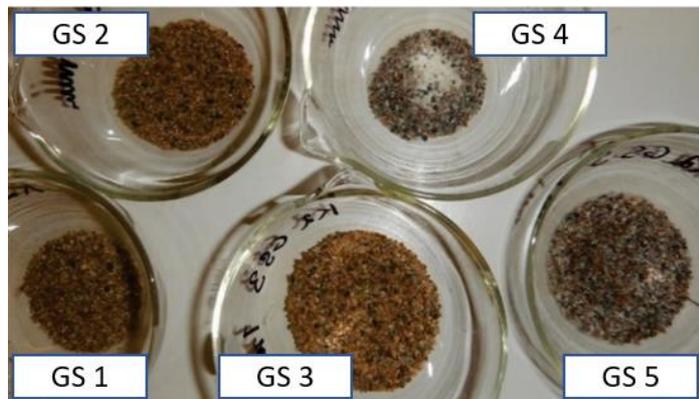
Figure 4.4. The color difference between the sieved fractions (1-2 mm) illustrate the change in lithology between the two bottom units (GS4-5) and the overlying unit K2-3 (GS 1-3). See sampling spots in Figure 4.5a.
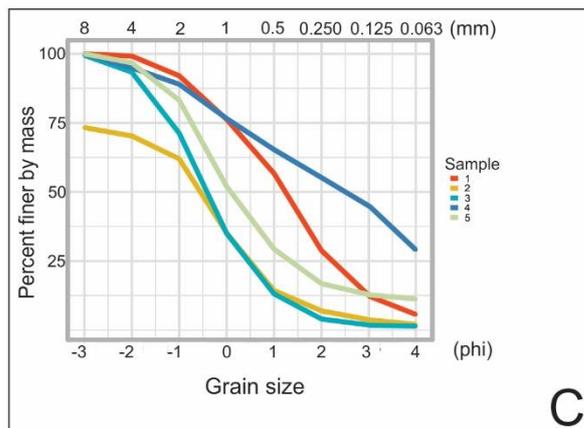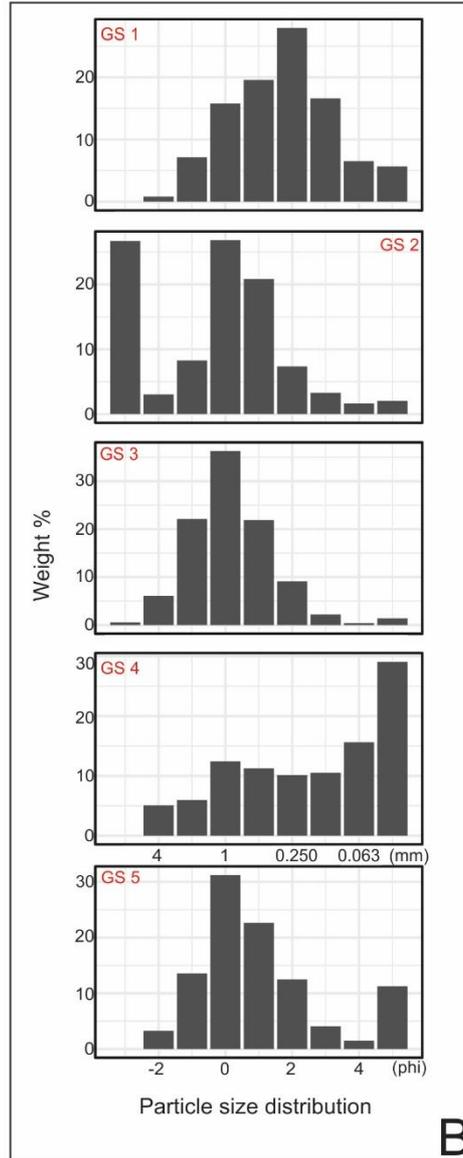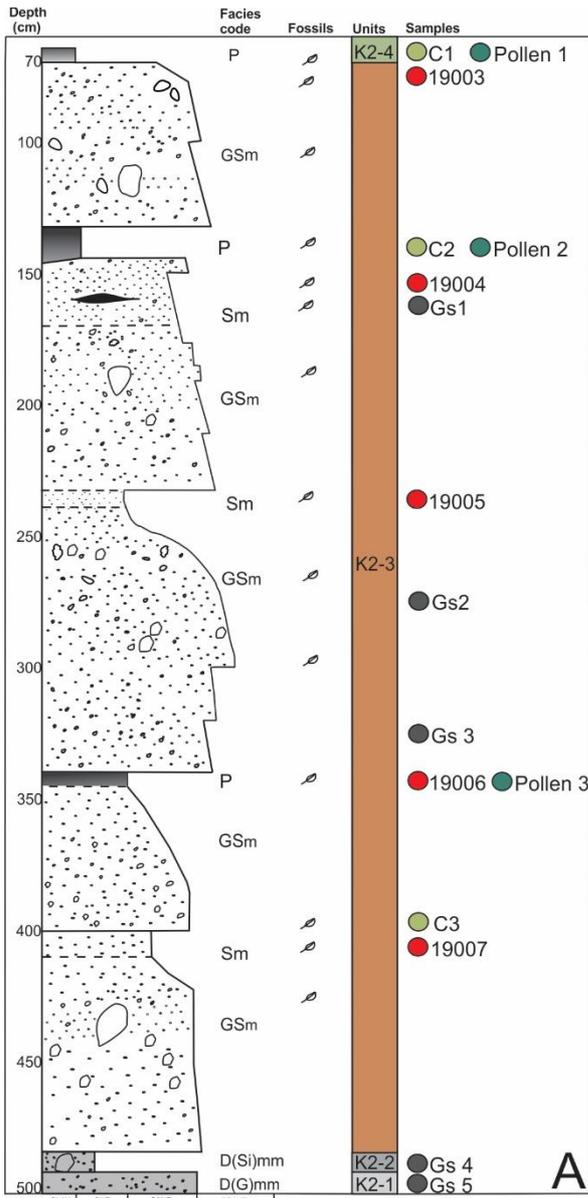
Figure 4.5a. *Lithostratigraphical log of K2 and sampling positions for all OSL- (19xxx), grain size (Gs x)-, radiocarbon C x)- and pollen (Pollen x) samples. For legend see Figure 4.6.* **4.5b.** *Grain size distribution of the grain size samples retrieved from the core.* **4.5c.** *Cumulative weight percent of the grain size samples.*

Units

▢	K2-1	▢	K3-1	▢	K4-1	
▢	K2-2	▢	K3-2			
▢	K2-3	▢	K3-2(def)			
▢	K2-4	⊠	Disturbed, soil, vegetation			

Boundaries

——————	Sharp
- - - - - - - -	Gradational
∿∿∿	Deformed
⌄⌄⌄	Loaded

Structures

▢	Diamict	≋	Faint wavy lamination	▤	Coarse sand lens
▢	Gravelly sand	▨	Normal graded	◤	Silt lens
▢	Massive sand	▧	Trough cross lamination	⬬	Unidentified fossil
▢	Peat	∽	Ripple cross lamination	▢	Soil
		▤	Parallel lamination		

Lithofacies

D(G)mm - massive gravelly diamict	Sm - massive sand
D(Si)mm - massive silty diamict	GSm - gravelly massive sand
D(S)mm - massive sandy diamict	Sr - sand, ripple laminated
D(SiS)mm - massive silty sandy diamict	St - trough cross laminated sand
P - peat	Sl - sand, laminated
	Sl(def) - deformed laminated sand
	Sm - deformed massive sand

Samples

🟢	C14
🟢	Pollen
🔴	OSL
⚫	Grain size

*Figure **4.6**. Legend for all lithostratigraphical logs and overview sketches of the outcrops. The legend includes symbols and colors that are used to present units, boundaries, structures, lithofacies and samples.*

4.2.2 Ridges K3 and K4

The positions of the outcrops are presented in Figure 4.1b. The outcrops A-E on the western ridge were subdivided into two main units, K3-1 and K3-2. They consist of a diamict layer at the bottom (K3-1) underlying a sandy unit (K3-2), containing fine to coarse sand forming various structures. The eastern ridge revealed exclusively diamict material and will be referred to as unit K4-1.

4.2.2.1 Western ridge, outcrop A

Outcrop A consists of units K3-1 and -2, out of which the latter is divided into four subunits (Figure 4.7a). Unit K3-1 composes a massive diamict with a sandy silt matrix. The clasts in this unit are sub-angular to sub-rounded and the main lithologies are red granite and basalt (Figure 4.8). The shapes of the clast are mainly bladed (Figure 4.9). The lowermost layer in unit K3-2 composes two lithofacies; faint wavy laminae at the base and trough cross laminated fine to medium sand on top (Figure 4.7b). In some parts, a discontinuous layer of normal graded gravelly sand and gravel lies above. The second layer in unit 2 is a massive layer of medium to coarse sand and gravel with faint parallel lamination. The third layer consists of parallel horizontal beds at the bottom, which continue as parallel laminae further up. The beds and laminae alter between fine black sand and medium to coarse lighter colored sand. Randomly distributed clasts > 1 cm are widespread together with discontinuous layers of very coarse sand. Towards the top of the layer, the parallel laminae gradually change into faint ripple cross lamination (Figure 4.7c). A disturbed layer with roots and other organic remains lies on top.

The transition between the two main units is sharp (Figure 4.7b) and within unit K3-2, there are both gradational and sharp contacts (Figure 4.7a and Figure 4.10). Two small-scale normal faults lie in the lowermost layer of K3-2 (Figure 4.7d).
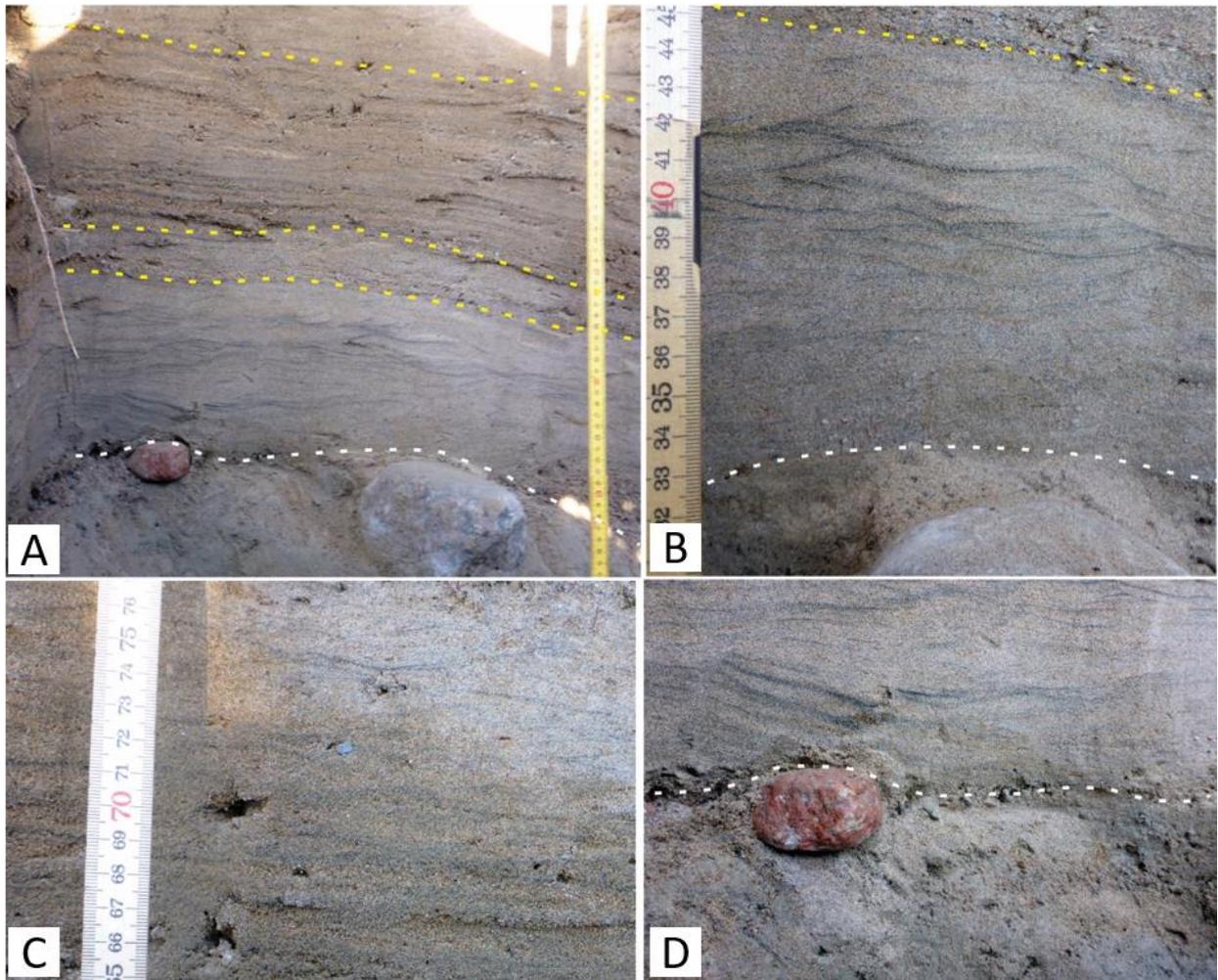
Figure 4.7. *The white dashed line demarcates the boundary between unit K3-1 and K3-2, while the yellow dashed lines demarcates subunits within unit K3-2. 4.7a. Overview image of outcrop A. 4.7b. Trough cross lamination in the lowermost layer of K3-2. Picture by Helena Alexanderson (2018).*
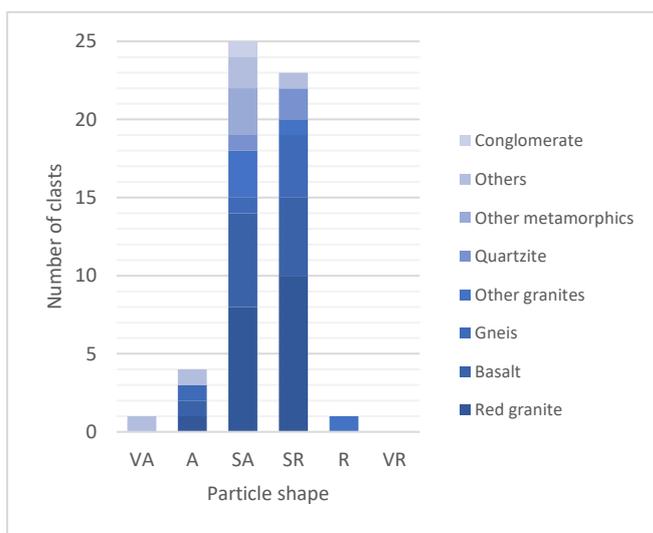
Figure 4.8. *The lithologies and roundness of diamict K3-1. The clasts in the diamict consist predominantly of red granite and basalt and clasts are mainly subangular to subrounded.*
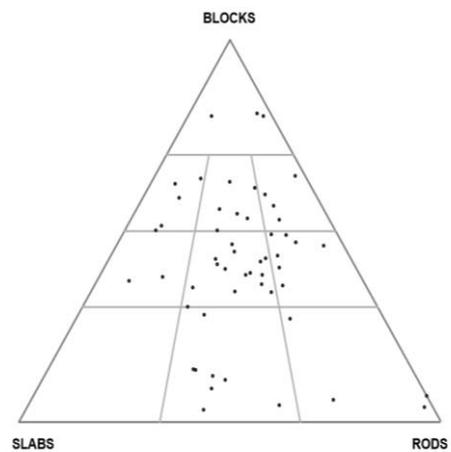
Figure 4.9. *The shapes of the clasts in the diamict layer K3-1 are mainly bladed.*
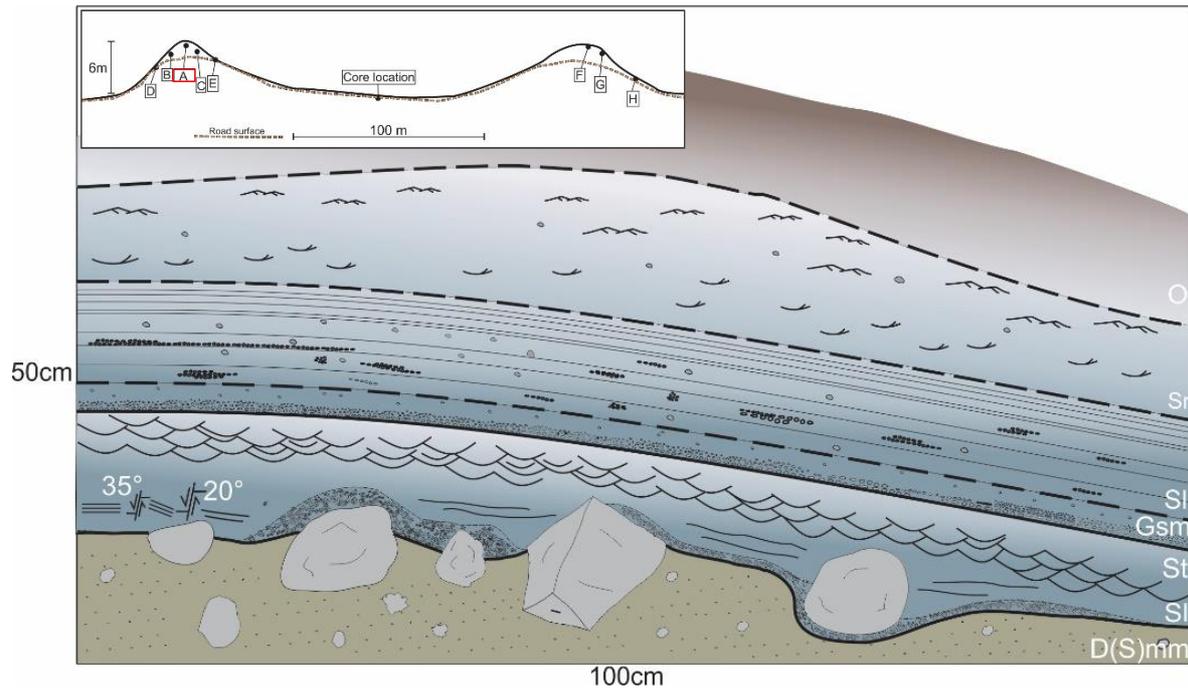
Figure 4.10. An overview sketch of outcrop A. The diamict at the bottom is separated with a sharp boundary while K3-2 composes both gradational and sharp boundaries. The shade of blue indicates changing flow velocities. The lighter the blue the lower is the flow speed. The flow speed is discussed in chapter 6.
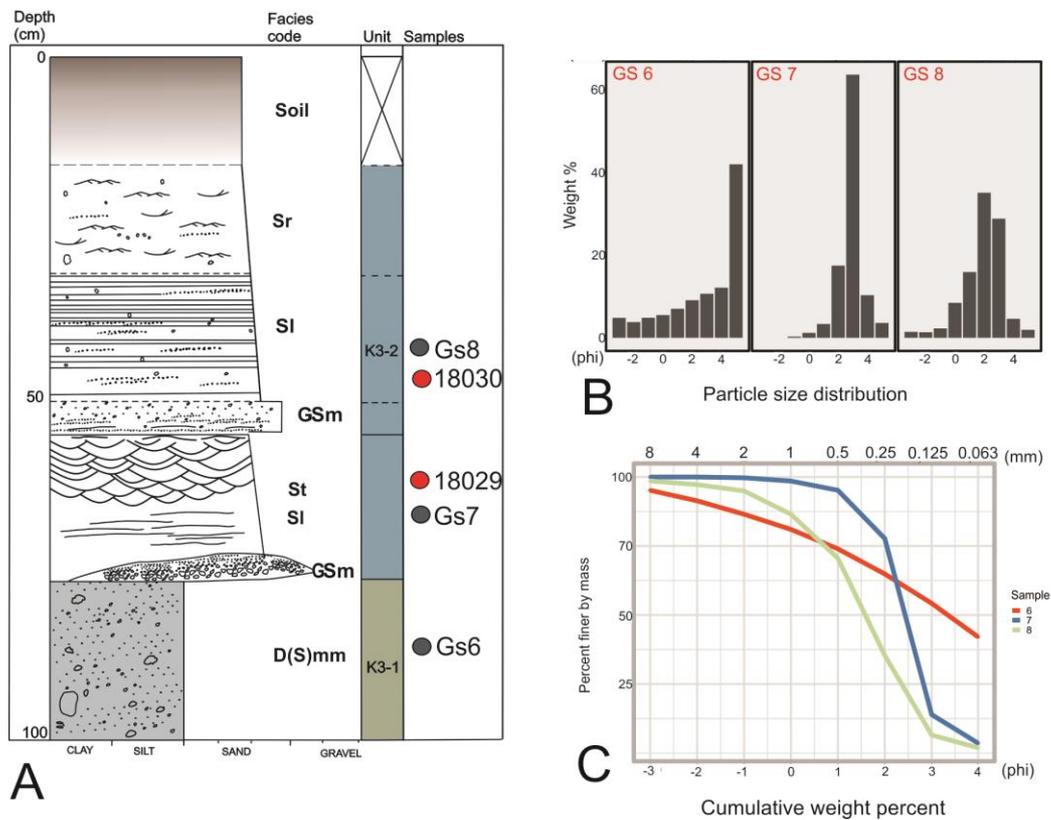
Figure 4.11 a. Lithostratigraphical log of outcrop A. See Figure 4.6 for legend. **4.11b.** Grain size distribution of grain size samples 6-8. **4.11c.** Cumulative weight percent of grain size samples 6-8.

4.2.2.2 Western ridge, outcrop B

Outcrop B likewise consists of the two main units K3-1 and K3-2 (Figure 4.12). The bottom layer of unit K3-1 is a compact diamict with a silty sand matrix. A separate diamict forms a nearly vertical sharp boundary to unit K3-2 across the entire section (Figure 4.13). The first layer of unit K3-2 consists of medium sand altering with fine dark sand in inclined layers, forming ripple cross lamination (Figure 4.14b). The second layer of unit K3-2 is separated by a sharp interbedded boundary and consists of fine to coarse deformed sand (Figure 4.14c). Discontinuous fine black laminated sand layers are widespread in the deformed unit K3-2 (def.).
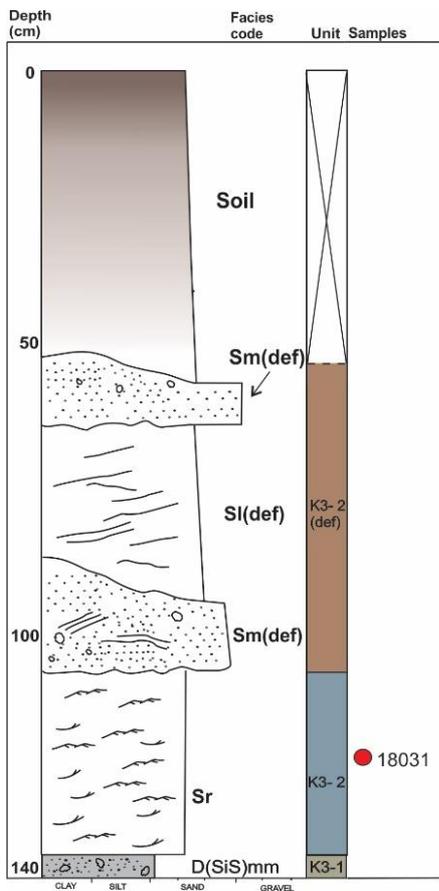
Figure 4.12. Lithostratigraphical log of outcrop B. See figure 4.6 for legend.
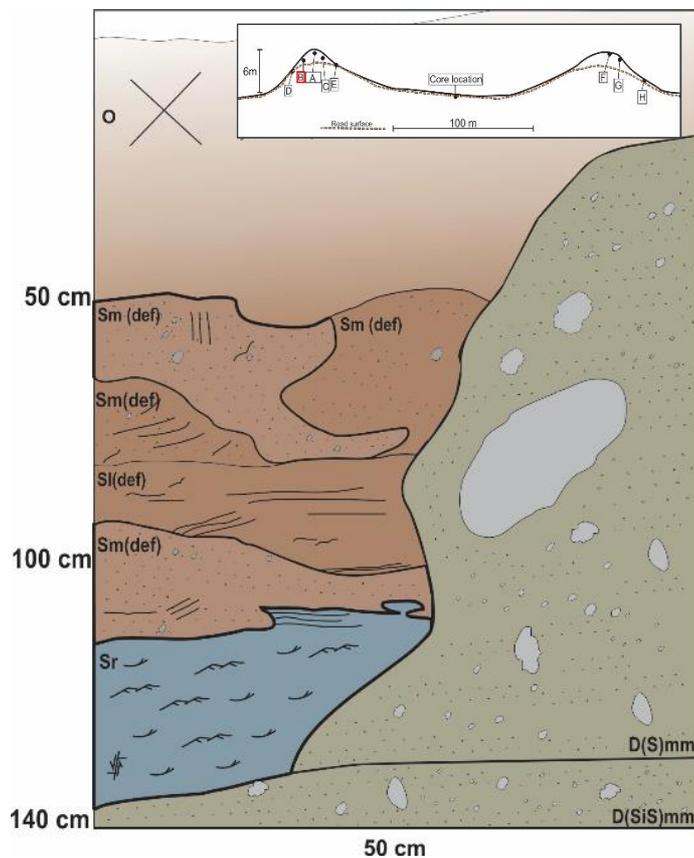
Figure 4.13. Overview sketch of outcrop B. See figure 4.6 for legend.
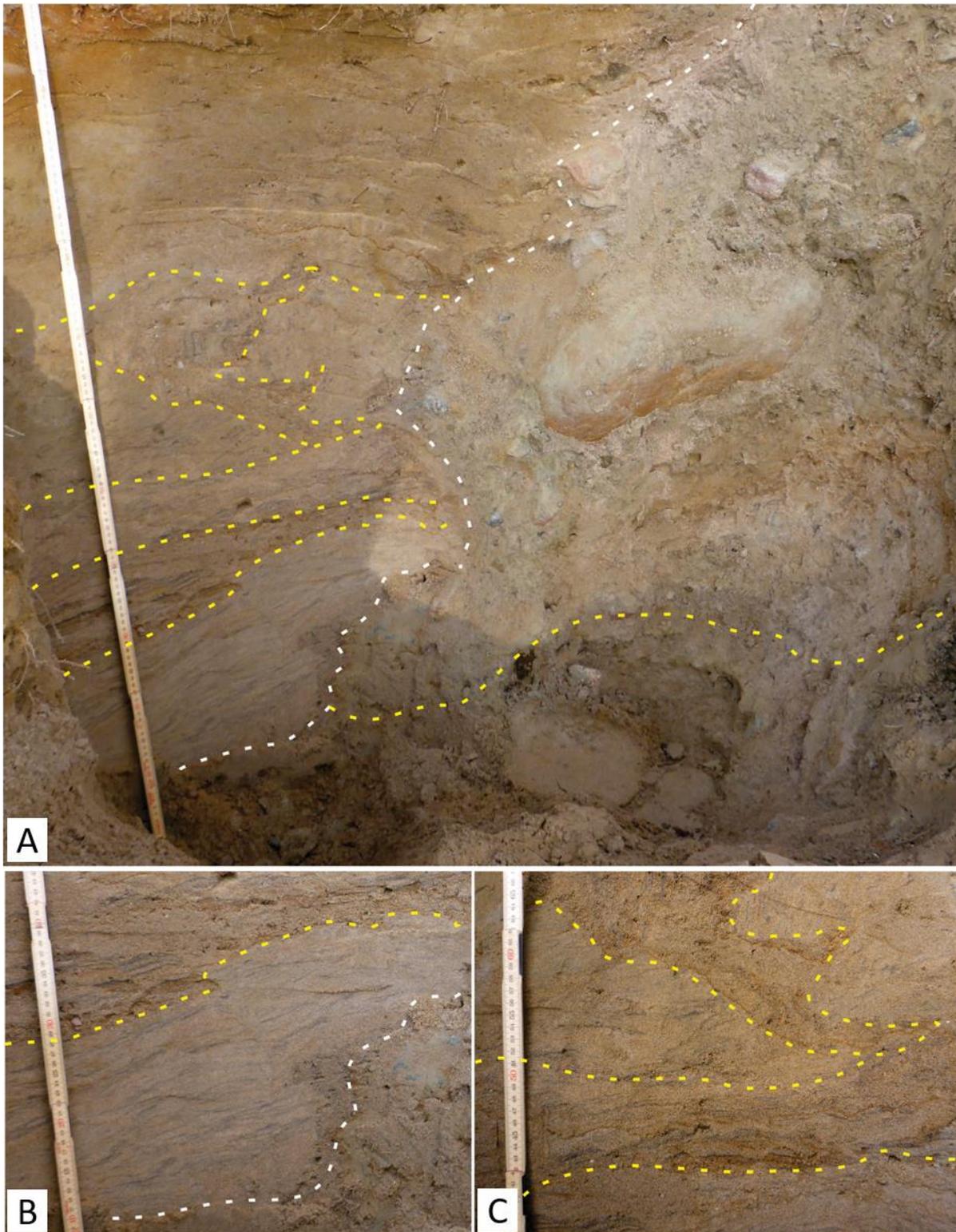
Figure 4.14. The white dashed line demarcates the boundary between unit K3-1 and K3-2, while the yellow dashed lines demarcates subunits within K3-1 and also marks the deformation structures in unit K3-2. **4.14a.** Overview image of outcrop B. A vertical sharp boundary runs through the whole section and separates diamict K3-1 from K3-2 and K3-2 (def). **4.14b.** The first layer in K3- 2 is a ripple cross-laminated sand layer. **4.14c.** The second layer of K3-2 is strongly deformed. Pictures by Helena Alexanderson (2018).

4.2.2.3 Western ridge, outcrops C and D

Outcrops D (Figure 4.15a) and C (Figure 4.15b) have a massive sand unit overlying the diamict (K3-1) in the bottom, respectively. The sand units (K3-2) have faint laminae. The boundaries between the diamict and the sand is sharp. Both sequences dip ~25˚ downwards away from the crest of the ridge, outcrop D in E-W direction and outcrop C in W-E direction. Lithostratigraphical logs are presented in Figure 4.16.
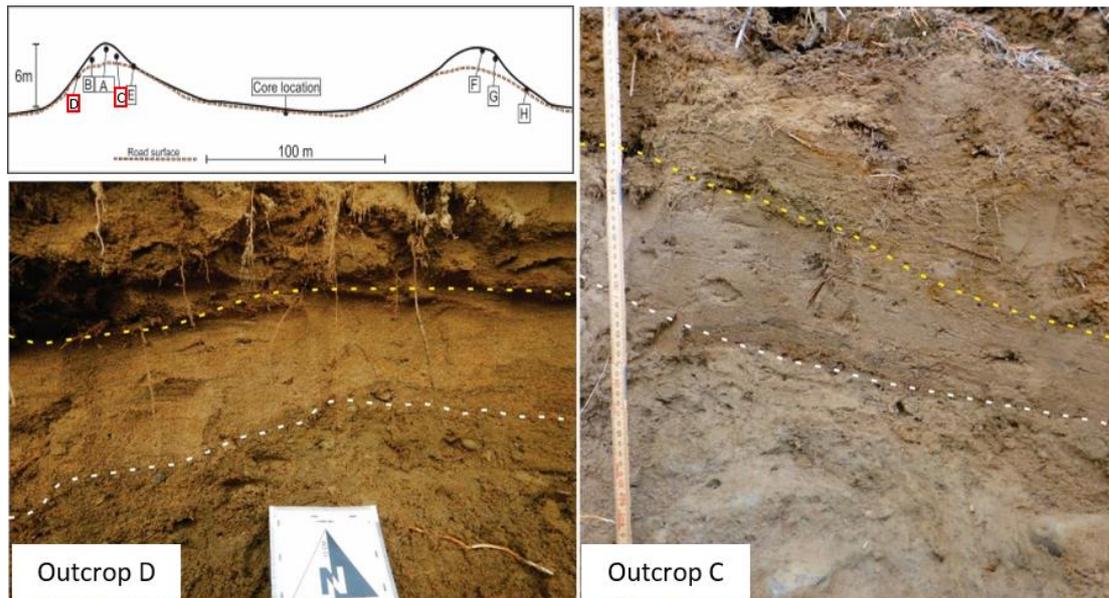
Figure 4.15a. Outcrop D dips outwards from the moraine in E- W direction. A sharp boundary separates the underlying diamict from the overlying sand unit. *4.15b.* Outcrop C dips inwards in W-E direction. A sharp boundary separates the underlying diamict from the sand. The pictures are taken in different lightning and do not demonstrate a difference in color.
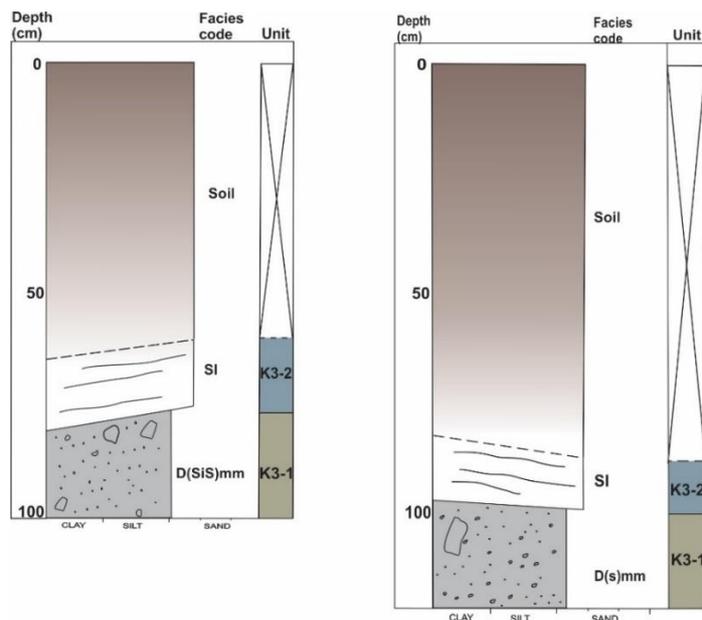
Figure 4.16. Lithostratigraphical logs of outcrops D (left) and C (right).

4.2.2.4 Western ridge, outcrop E

Section E lies on the inwards slope of the ridge, at the level of the road surface (Figure 4.17). A lithostratigraphical log of the section is illustrated in Figure 4.17 and an overview image in Figure 4.18a. The base consists of a compact impenetrable layer of massive sandy diamict (K3-1). On top of the diamict lies a sandy unit composed of fine to medium sand and four different lithofacies can be distinguished, including; faint ripple cross lamination, horizontal parallel lamination (Figure 4.18b), massive sand and trough cross lamination.

The boundaries between the layers are either gradational or sharp. An erosional boundary lies on top of the parallel laminae (Figure 4.18c). The boundary between the faint ripples and the parallel laminae is slightly loaded (Figure 4.18d), but the loads are not continuous throughout the boundary.
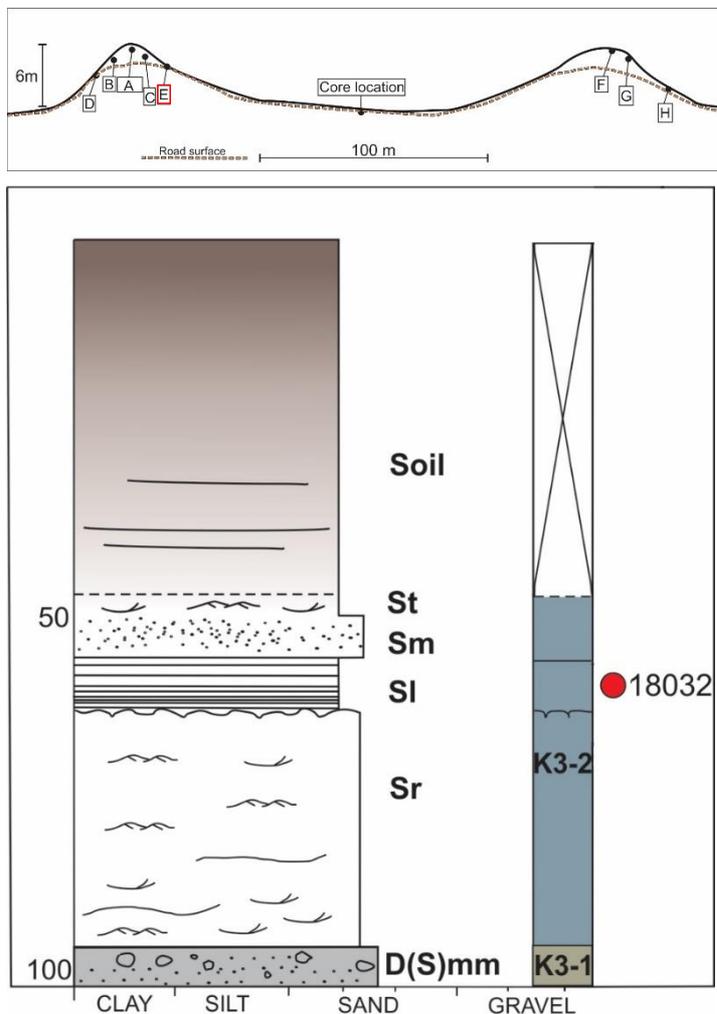
Figure 4.17. Lithostratigraphical log of outcrop E.
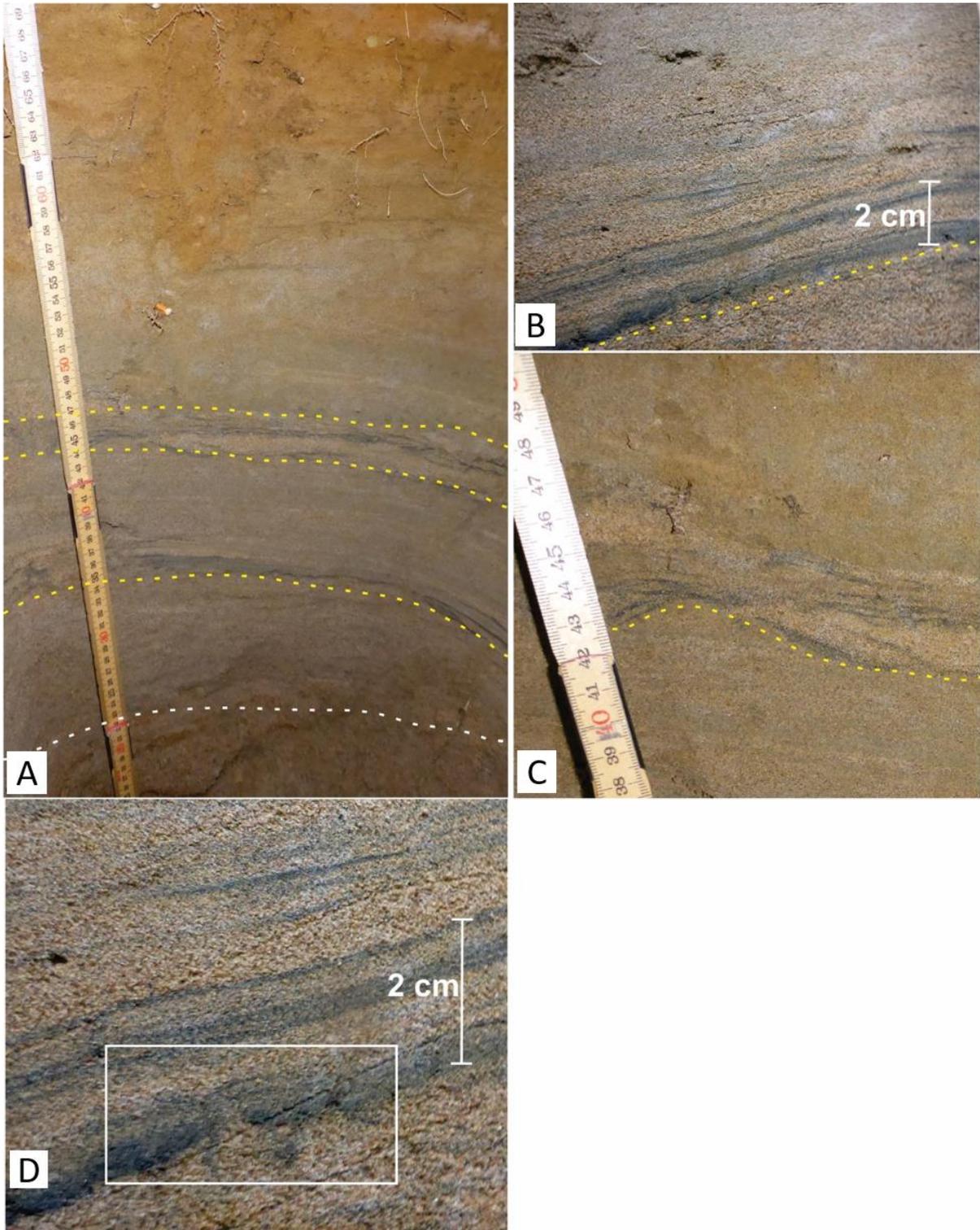
Figure 4.18a. *Overview image of outcrop E. The yellow dashed lines mark subunits while the white dashed line marks unit boundaries.* ***4.18b.*** *Parallel lamination consisting of fine to very fine sand.* ***4.18c.*** *Erosional boundary on top of the parallel lamination.* ***4.18d.*** *Loaded boundary below the parallel lamination. Pictures by Helena Alexanderson (2018).*

4.2.2.5 Eastern ridge, outcrop F, G and H

Outcrop F is located at the top of the crest of the eastern ridge (Figure 4.19) and consists of one unit (Figure 4.19), which is a massive grey diamict with a sandy silty matrix, unit K4-1 (Figure 4.20a). Outcrop G lies closer to the outer slope of the rim ridge and likewise consist of one unit (Figure 4.19), which composes brown massive diamict with a sandy silty matrix at the top and changes color to grey at ~20 cm depth (Figure 4.20b). A lens of well sorted coarse sand is found at 35 cm depth (Figure 4.20c). The matrix of the diamict in section G becomes slightly finer towards the bottom. A small pit (H) was dug into the base of the ridge. It revealed grey massive diamict with a sandy matrix (Figure 4.20d).
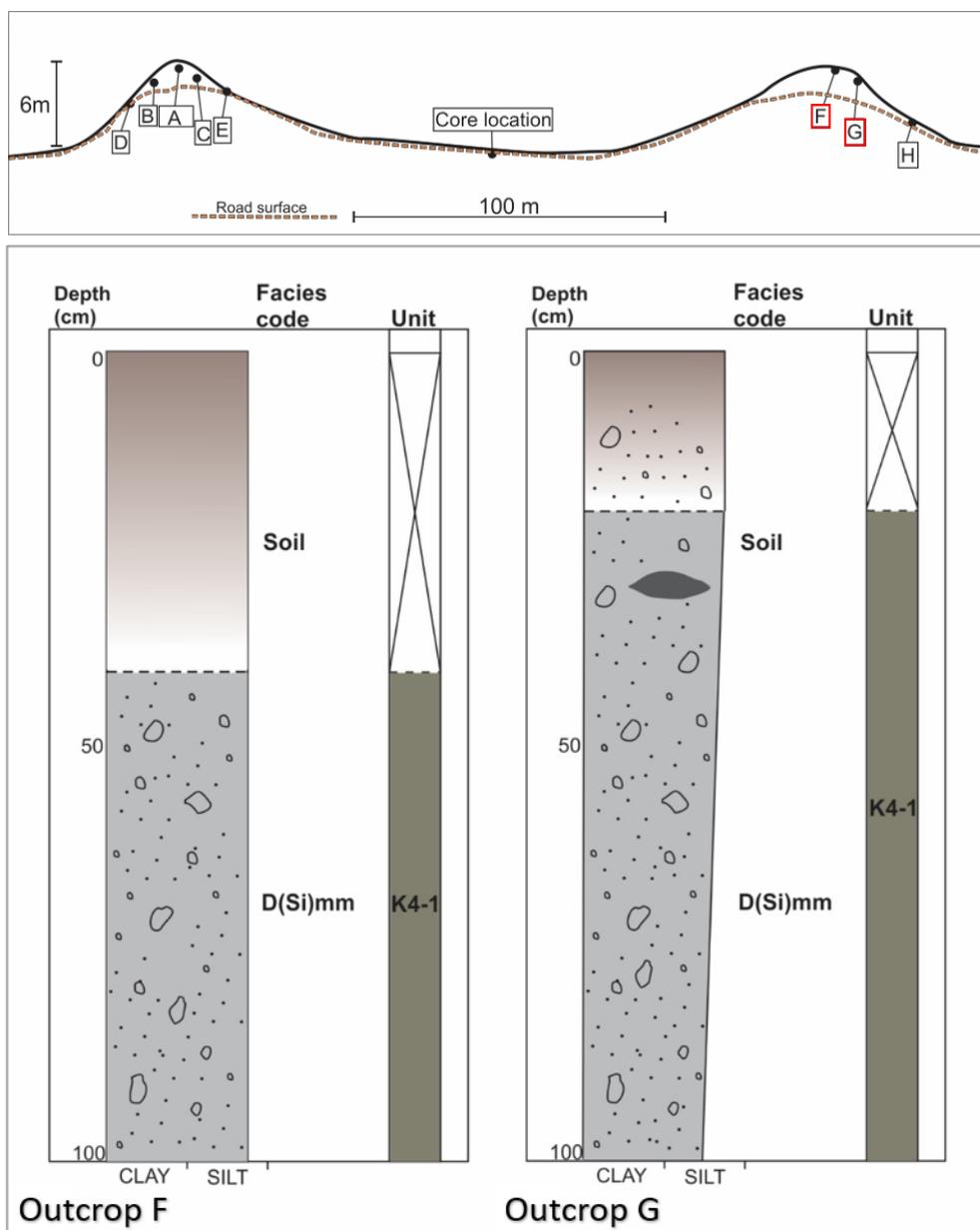
Figure 4.19. Lithostratigraphical log of outcrop F (left). Lithostratigraphical log of outcrop G (right).
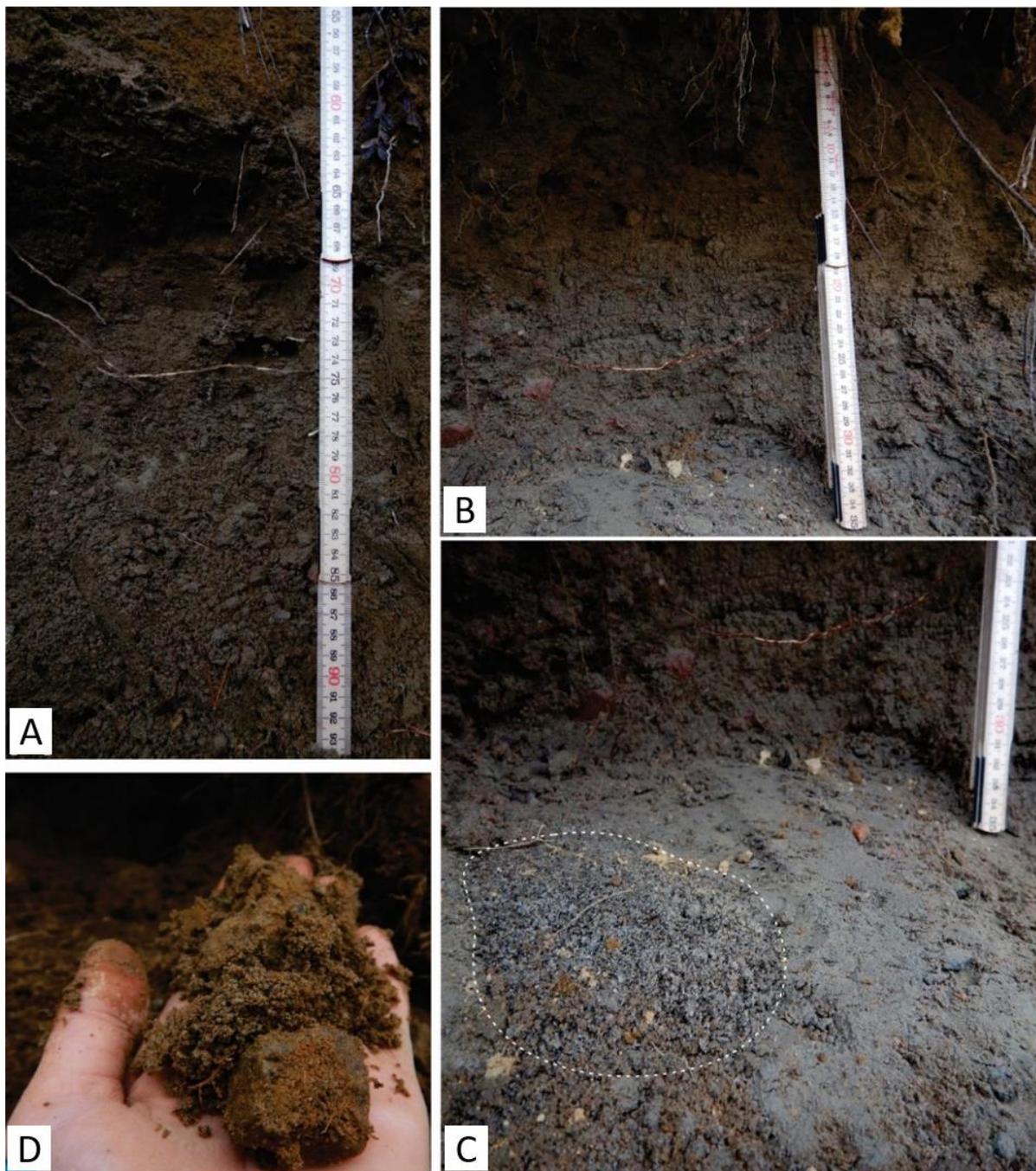
Figure 4.20a. Outcrop F with grey massive diamict (K4-1). 4.20b. Outcrop G with brownish massive diamict at the top and grey massive diamict towards the base of the outcrop. 4.20c. Well sorted sand lens in outcrop H. 4.20d. Diamict with coarser matrix in H.

4.2.3 K5 and K6

In order to verify the continuity of the sediments in the core, two additional holes K5 and K6 were hand dug in two spots in the central part of the moraine (Figure 4.1a), in which we found gravelly sand resembling K2-3 at about 60 centimeters depth.

4.3 Ground-penetrating radar

The GPR profiles were collected on the gravel road constructed on the moraine and much of the investigated outcrops on the ridges lie higher than the GPR profiles as the road cuts through them. The core was retrieved a few meters north from the road. The continuous parallel reflections that lie within approximately one meter or less from the ground surface, were not considered primary depositional structures as the roadwork has affected the top layers. The 200 MHz profile was used for interpretations because of its high resolution. Only the part of the profile that covers Kortejärvi moraine was interpreted in this study.

4.3.1 Velocity ground estimates

The hyperbola measurements resulted in a mean velocity of 0.071 m/ns (Figure 4.21a). The CMP measurements yield a velocity between 0.05 - 0.10 m/ns, being higher towards the surface (Figure 4.21b). Additionally, by assuming that the strong reflection at the center of the moraine corresponds with the base of the core K2, a mean velocity of 0.07 m/ns was chosen.

As can be seen from the different velocities from the hyperbolas, it is apparent that the velocity changes laterally throughout the profile. Some of the reflections can therefore be slightly distorted. The depth of penetration is between 4.5 and 10 meters.
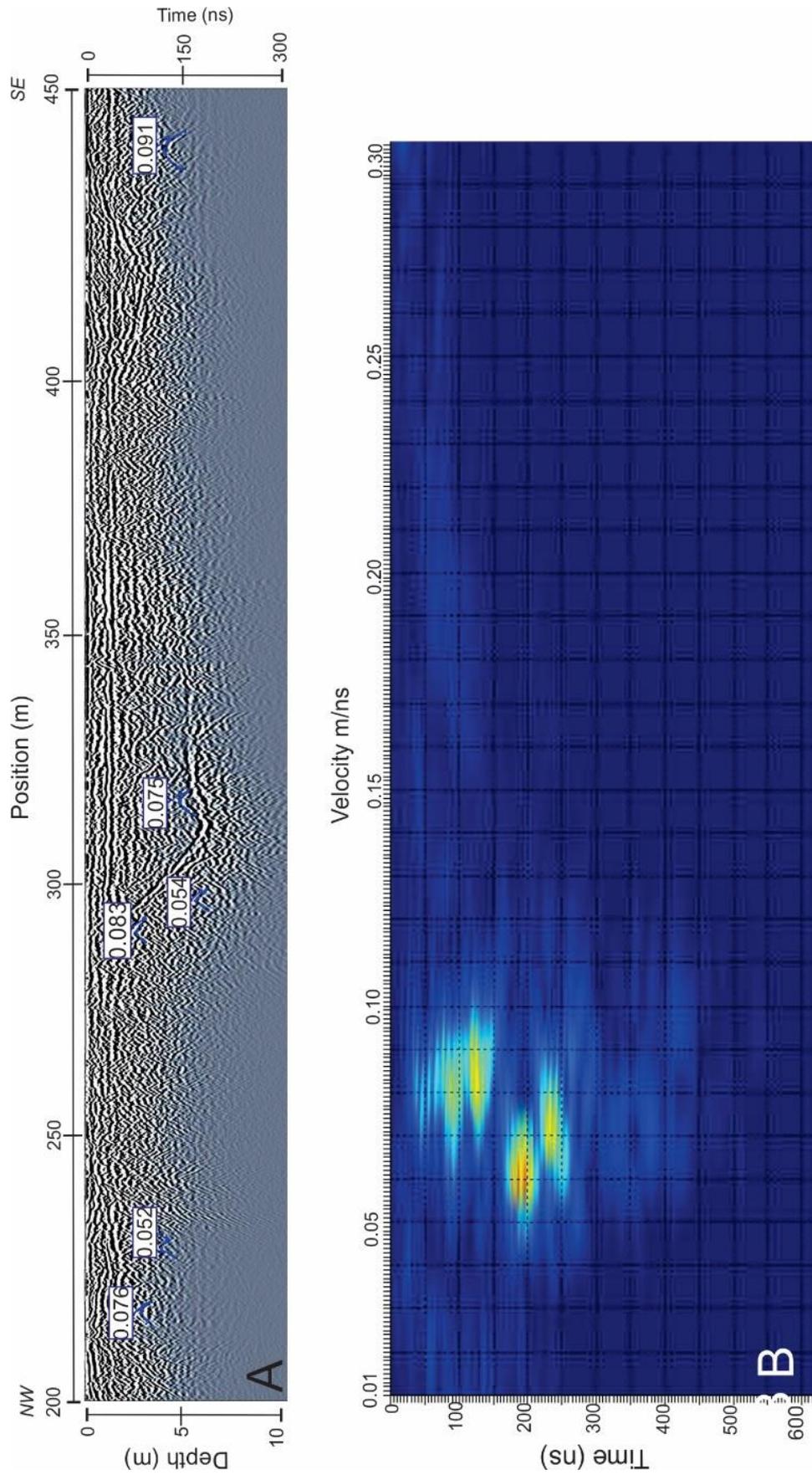
Figure 4.21 a - *The resulting velocities from each measured hyperbola marked with a blue line.* **4.21b.** *The CMP measurement gave a velocity estimate between 0.05 and 0.10 m/ns.*

4.3.2 Radar stratigraphy of Kortejärvi

Two radar surfaces and four radar facies were identified in the GPR profiles of Kortejärvi. The radar facies and surfaces are marked in Figure 4.23a.

Radar surface 1 is an irregular and moderately continuous reflection of medium strength. In many occasions, it separates lower discontinuous and chaotic reflections from overlying continuous or moderately continuous reflections. Radar surface 2 is a trough shaped strong continuous reflection at the center of the moraine, with a ~40˚ westwards dipping slope and a less steep and less prominent slope ~ 25˚, towards east.

Radar facies 1 is at the base of the moraine plateau and consists of strong discontinuous reflections in a chaotic configuration (Figure 4.22). Hyperbolas of different sizes are detected in the facies.

Radar facies 2 lies on top of the western ridge and consists of strong continuous subparallel reflections (Figure 4.22). At the crest, the reflections are wavy and some of them are weaker. At the slope towards the lowered center of the moraine plateau, the continuous lines disappear.

Radar facies 3 lies on top of the eastern ridge. A strong and continuous concave reflection can be detected (Figure 4.22). On top of the concave line, lies a few lobate formed reflections. Moreover, the eastern ridge consists of mostly discontinuous and chaotic reflections.

Radar facies 4 lies comprise all sediments in the lowered center of the moraine with discontinuous reflections. A few strong parallel continuous lines can be identified in between (Figure 4.22).
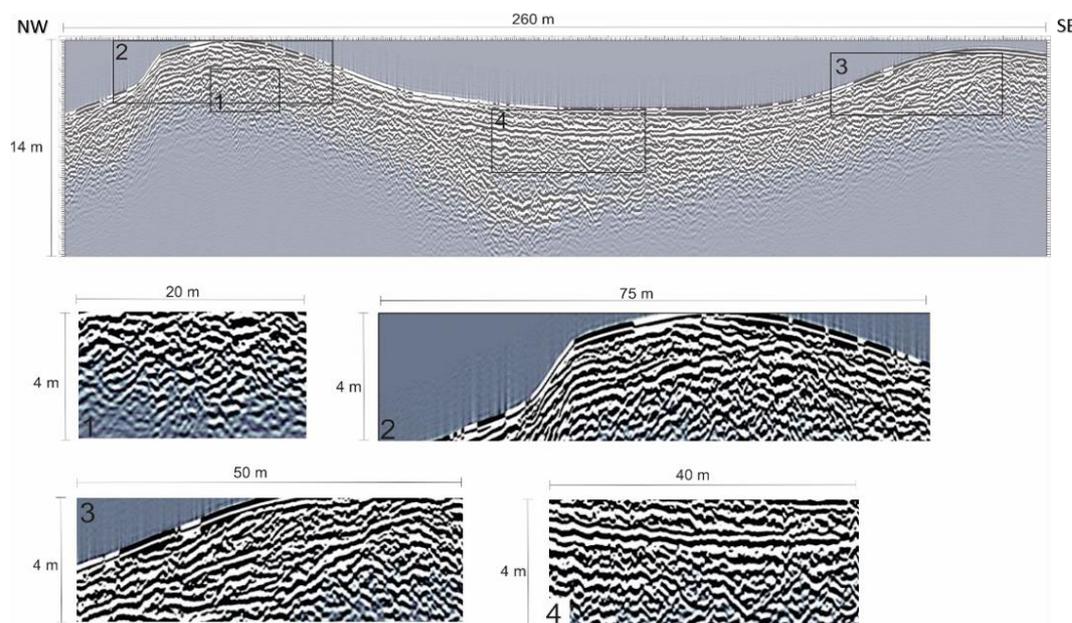
Figure 4.22. 1: Radar facies 1 composing discontinuous chaotic reflections. 2: Radar facies 2 consisting of parallel to subparallel continuous reflections. 3: Radar facies 3 consisting of chaotic reflections, but a clearly visible concave reflection can be distinguished and on top of it a few lobate formed reflections. 4: Radar facies 4 composed of both chaotic reflections and a few prominent strong continuous lines.

4.3.3 Artefacts

Reflections that are not related to primary sedimentary structures were also identified (Figure 4.23b). The water table was identified as a strong continuous reflection; it is especially prominent in the center of the moraine but can also be followed a short distance up the ridges. As it cuts through different reflections, it likely represents liquid. A ditch was noted on the GPS track while collecting the GPR profile and is marked as an artefact in the profile.

4.3.4 Preliminary interpretations

The radar facies and surfaces were identified along with information from the field and the sedimentary analyses. A brief interpretation will be presented here, but a further explanation will follow in chapter 5.

The chaotic configuration and the discontinuous reflections that much of the profile composes, indicates that much of the landform consists of diamict, as diamict typically is recognized by a dense distribution of diffractions, among other characteristics (Arcone *et al.,* 2014). The parallel reflections on the western ridge are regarded as stratified sandy sediments, and the curved lines at the crest implies that the deposits have undergone deformation. The eastern ridge has reflections resembling diamict, while the concave line and the lobate formed reflections between 400 and 435 meters on the profile (Figure 4.22c), may imply that some other kind of sediments are buried in the subsurface. Radar facies 4 in the center, presumably consists of the gravelly sand (K2-3) that was identified in the core. The stronger continuous reflections within facies 4 may represent organic layers, which were also found in the core. The organic layer at 150 centimeters corresponds with one of the stronger reflections, while the lower organic layer at 350, does not correspond with a reflector. Presumably, radar surface 1 originally continued across the moraine plateau, but has been crosscut by a later event, which makes radar surface 1 and 2 separate surfaces.
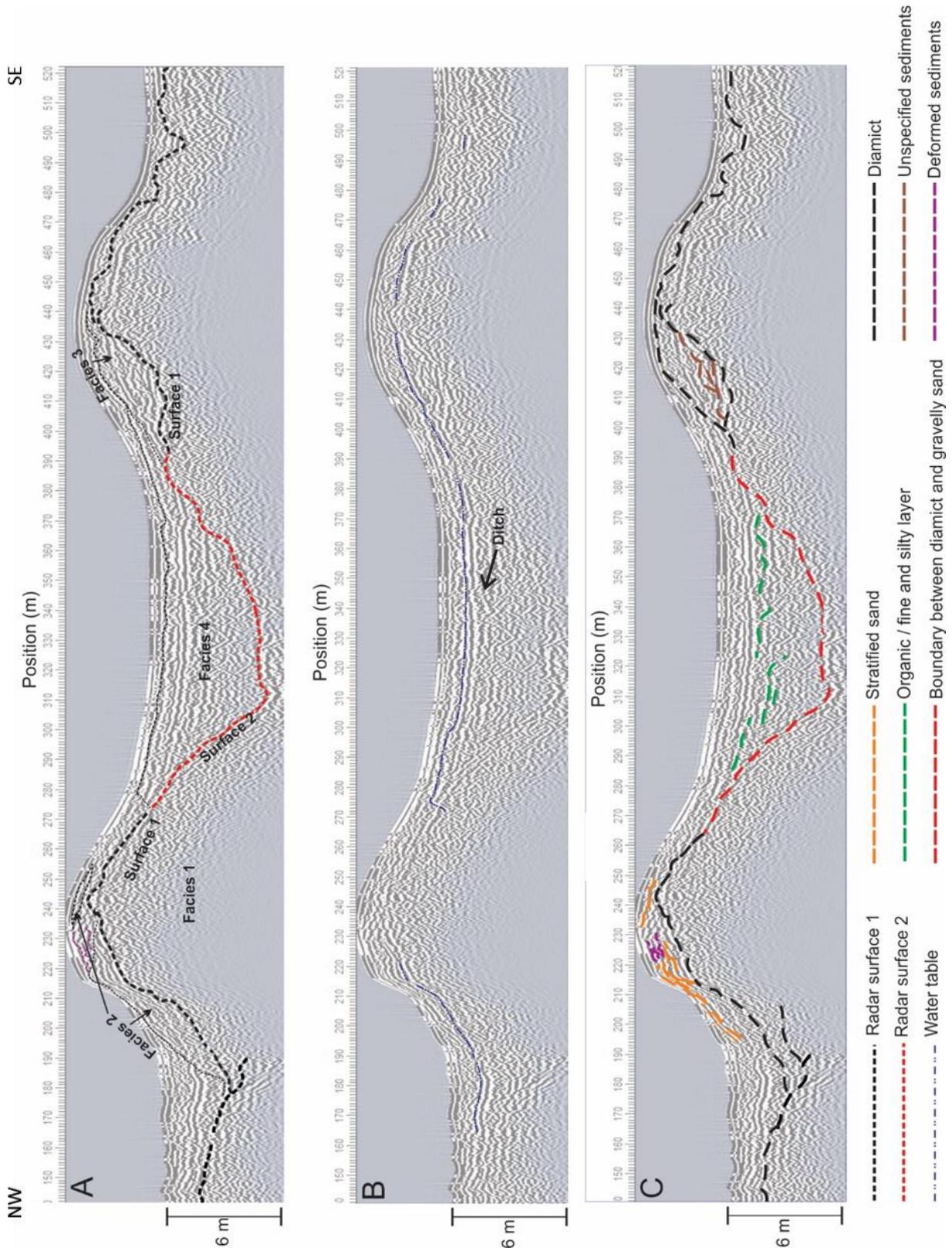
Figure 4.23. *All profiles processed as follows: Frequency 200 MHz Gain filter: dewow + AGC Gain (maximum gain: 50) Background subtraction. F-K migration. The profiles are cropped from the originally 520 meters long profile. See entire unprocessed profile in the Appendix 2.* **4.23a.** *Radar stratigraphy of Kortejärvi.* **4.23b.** *Artefacts identified in the profile.* **4.23c.** *Interpretations of the radar reflections.*

4.4 Luminescence dating

4.4.1 Equivalent dose

The number of accepted aliquots for each sample was determined by how well the aliquots of a sample passed the quality control criteria. Some aliquots showed a clear OSL signal with a rapidly decreasing signal, indicating quartz of good quality (Figure 4.24). If the OSL curve was lacking a clear peak signal (Figure 4.25), the aliquot was regarded less suitable for OSL analysis. The equivalent doses for each sample are presented in Table 4.1, together with other OSL data, including the obtained ages.
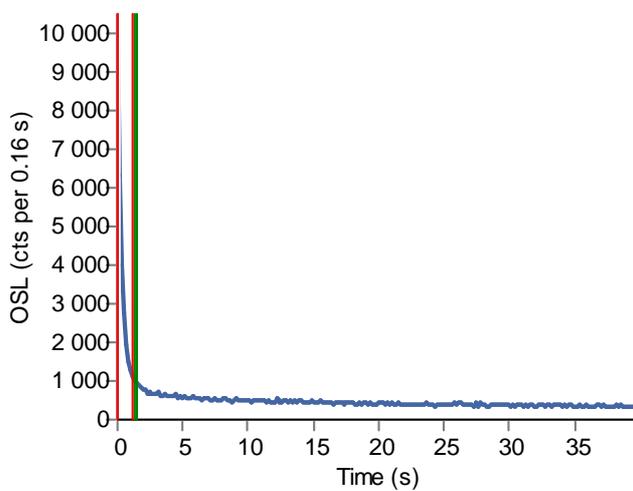
Figure 4.24. Clear OSL signal for one of the aliquots of OSL sample 19004. The red line marks the first 0.48 seconds which were integrated for the peak and the green line marks the following 0.48 seconds integrated for the background.
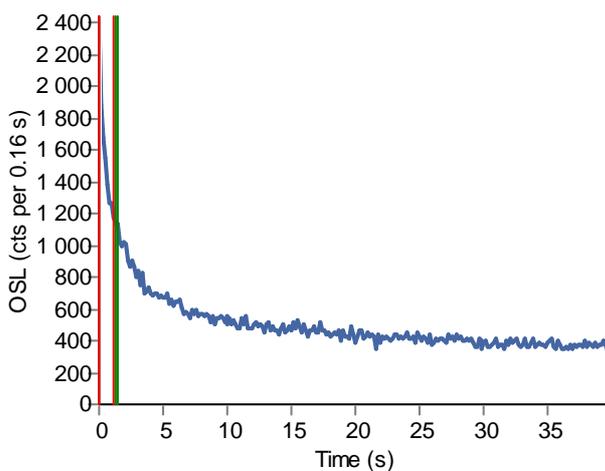
Figure 4.25. An aliquot of OSL sample 19003 showing a weak OSL signal. The red line marks the first 0.48 seconds which were integrated for the peak and the green line marks the following 0.48 seconds integrated for the background.

Table 4.1. *The table presents doses and errors, dose rates and errors, water contents and errors and the ages and errors for all nine samples. The number of accepted and measured aliquots are also presented, and yield information about how well the age is estimated.*

Lab number	Site	Unit	Depth (cm)	Dose (Gy)	Error dose (Gy)	Dose rate (Gy/ka)	Error dose rate (Gy/ka)	w.c. %	Error w.c. %	Number of aliquots (accepted/measured)	Age (ka)	Error age (ka)
18029	K3	K3-2	75	112	16	3.017	0.119	13	4	22/57	37.1	5.5
18030	K3	K3-2	48	183	25	3.138	0.184	13	4	13/48	58.3	8.7
18031	K3	K3-2	125	126	15	3.028	0.101	14	4	15/33	41.6	5.1
18032	K3	K3-2	55	64	8	1.671	0.057	15	4	15/63	38.3	5.0
19003	K2	K2-3	70-77	182	26	2.872	0.268	24	4	15/26	63.4	10.8
19004	K2	K2-3	153-163	31	3	3.383	0.279	26	4	29/45	9.2	1.2
19005	K2	K2-3	233-243	38	5	3.328	0.105	22	4	20/45	11.4	1.5
19006	K2	K2-3	339-347	75	12	3.303	0.105	20	4	18/40	22.7	3.7
19007	K2	K2-3	400-407	72	13	3.306	0.107	22	4	14/44	21.8	4.0

4.4.2 Dose rate

Water content, LOI, and bulk density (App. 1) were determined in the laboratory at UiT and together with the background radiation data obtained from Risø, the data was used in the DRAC v1.2 age calculations (App. 1) (Durcan *et al*., 2015). The dose rates are presented in Table 4.1.

The mean water content since time of deposition, was estimated from the field water content and the saturated water content. The geological setting of the site was accounted for in order to make an estimate of the time that the grains had been saturated contra drier (present day conditions in the end of a dry summer). The field water content, the saturated water content and the estimated average water content since time of deposition are presented in Table 4.2.

Considering that the core was retrieved from a topographic low and the area is covered in wetland today, it can be assumed that the water content has been close to saturation much of the time. The four OSL samples that were extracted from below 150 centimeters depth, are estimated to have been saturated 80% of the time, while values like the present-day water content were regarded likely 20% of the time. The topmost OSL sample, which was extracted just below the peat, has more likely been subjected to variable conditions due to proximity of the ground surface, and therefore the ratio between saturated- and the field water content was estimated as 70% /30%.

The water content in the outcrops was significantly lower at present day, compared to the core. A lower mean water content was selected for the outcrops, 60% of the time field water content and 40% of the time saturated, as they also stand elevated in the present day.

The LOI was below 2% for all samples and its impact for the dose rate estimations was insignificant.

The grain size in the beds sampled for OSL is fine to medium sand. For an unconsolidated sand or gravel, the density lies between 1.4 g/cm^3 and 2.3 g/cm^3, with sand having a density closer to 1.4 g/cm^3 and gravel closer to 2.3 g/cm^3 (Schön, 2015). The density of sand rarely exceeds 1.7 g/cm^3 (McKenzie *et al*., 2002). An average bulk density of $1.6 \pm 0.1 g/cm^3$ was used for the OSL samples from the core. The bulk densities for the samples from the outcrops was calculated with a known volume of undisturbed sediment and an average value of 1.3 ± 0.1 g/cm^3 was used.

Table 4.2 *Present day water content, saturated water content and the chosen value.*

Sample	In field (%)	Saturated (%)	Chosen value (%)
19003	22	25	24
19004	21	27	26
19005	17	23	22
19006	14	22	20
19007	19	23	22
18029	7	22	13
18030	8	21	13
18031	8	23	14
18032	10	22	15

4.4.3 OSL ages

The ages of the samples and their positions in the moraine are plotted in Figure 4.26. The ages were calculated following the central age model CAM (Galibraith *et al*. 1999). Samples 19003 and 18030 are less significant in the age interpretations due to the samples being less suitable for OSL. When determining the doses, a different protocol was used for the aliquots from the core and from the outcrops (Helena Alexanderson pers. comm.). This implies that the quartz has different characteristics and therefore could be of different origin. Further discussion will follow in the next chapter.
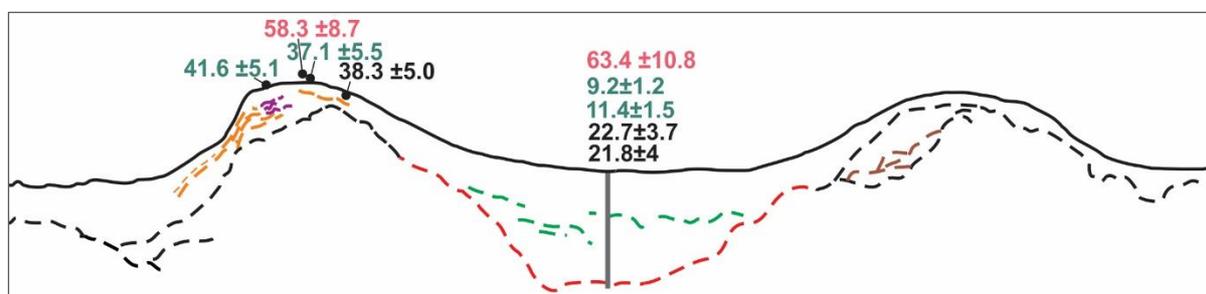
Figure 4.26. *The obtained ages for each OSL sample and their position in the core K2 in the center, and on the western ridge of the moraine plateau. The red color stands for a bad quality measurement, green stands for the good quality measurements and black for the ones in between. For legend of the dashed lines and scale, see Figure 4.23c.*

4.5 Radiocarbon dating

Three dated radiocarbon samples were obtained from 66 cm (unit K2-4), 135 cm (unit K2-3) and 399 cm (K2-3) depth of the core (Figure 4.5a). The species of the samples is somewhat uncertain, but suggestions state that C1 and C2 are from a type of *Carex*, while C3 is possibly a type of *Equisetum,* although the possibility of C3 being a modern rootlet cannot be fully rejected (Mats Rundgren pers. comm.). As seen in Table 4.3, all obtained results state an age younger than modern. Year zero for a radiocarbon age is considered AD 1950. In modern samples, very little decay has occurred in general, and therefore the error factor can be larger than the obtained date. Modern dates are hence not regarded very trustworthy and if samples have a younger age than 1950 AD, they are often presented as > modern. Reimer et al., 2004 have however, developed a post-bomb calibration program that is fractionation corrected. The modern radiocarbon ages in this program are stated as $F^{14}C$ (fraction modern). A regional, or even a local, atmospheric ^{14}C data set is the ideal for calibration of a post-bomb ^{14}C measurement. A number of post-bomb atmospheric ^{14}C records are available (Reimer *et al.*, 2004). The calibrated ages for the ^{14}C- samples range between 1990 and 2012.

Table 4.3 *Radiocarbon data and ages.*

Lab number	Depth (cm)	Material	Unit	$F^{14}C$	Age
LuS 14590 (C1)	65	*Carex*	K2-4	1.142±0.006	1990-1992
LuS 14591 (C2)	135	*Carex*	K2-3	1.125±0.006	1993-1995
LuS 14592 (C3)	399	*Equisetum*	K2-3	1.044±0.005	2009-2012

4.6 Pollen

The pollen samples were collected from the core from depths 67-68 cm (unit K2-4), 138-139 cm (K2-3) and 341-342 cm (K2-3) (Figure 4.5a). The labwork and pollen identification was performed by Martina Hättestrand, Stockholm University. The pollen samples were scanned and checked for most common pollen taxa (Table 4.4.), however a full pollen analysis was not performed.

Pollen 1 has a high representation of pine *(Pinus)* and spruce *(Picea)* and smaller amounts of birch *(Betula)*. Pollen 2 is dominated by birch but contains also smaller amounts of alder *(Alnus)*, pine and spruce. Pollen 3 consists mainly of pine and spruce with some birch and alder.

Overall the samples have a high represenation of conifers *(Pinophyta)* and seem to correspond with Holocene pollen assemblage (Martina Hättestrand pers. comm.).

Table 4.4 Pollen data and chronostratigraphical correlation of the results.

Sample	Depth (cm)	Unit	Pollen assemblage	Chronostratigraphic association
Pollen 1	67 - 68	K2-4	Mainly *Pinus* and *Picea,* some *Betula*	Holocene
Pollen 2	138 – 139	K2-3	Mainly *Betula,* some *Alnus, Pinus* and *Picea*	Holocene
Pollen 3	341 - 342	K2-3	Mainly *Pinus* and *Picea*, some *Betula* and *Alnus*	Holocene

4.7 X-ray fluorescence scanning

The reason why element ratios Zr/Rb and Zr/Ti were chosen as proxies will be clarified in the next chapter. The XRF element profiles are presented in Figure 4.27a. Especially the Zr/Rb profile is highly irregular, and no significant changes, which could represent a major change in the depositional conditions, are apparent in the data. However, at 250-300 centimeters depth, a correlation between a wide grain size distribution and an abundance of clasts > 1cm, and an increased peaking of both the Zr/Rb and Zr/Ti curves, can be noted (Figure 4.27a). In addition, a Zr/Rb peak seems to correlate with unit K2-2, as well as the organic layer at 130-150 cm depth and partly at 240 and 250 cm. The reliability of the results will be discussed further in chapter 5, but as the core composes mostly very coarse material (Figure 4.27b), it is doubtful if the obtained data can be trusted.
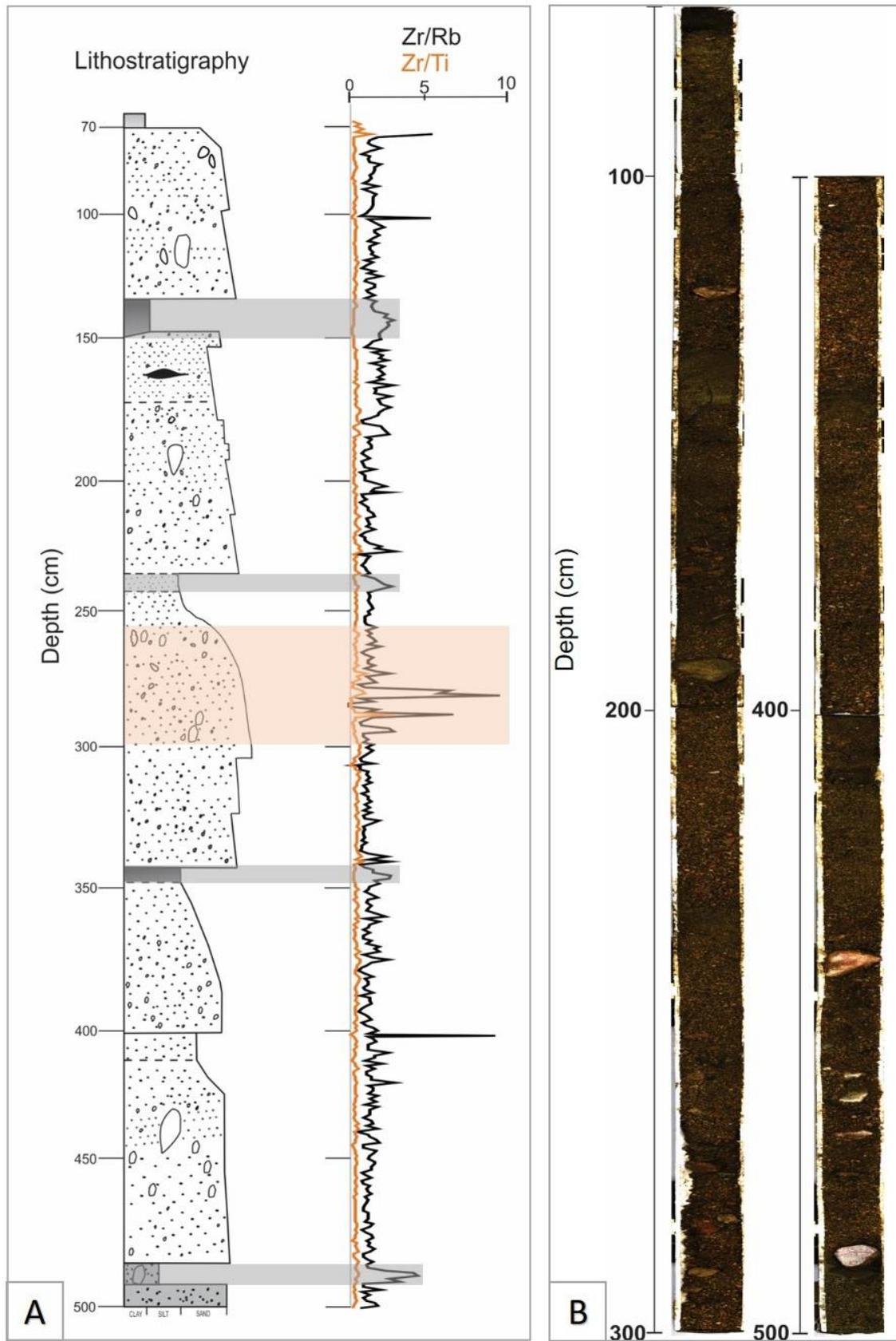
Figure 4.27a. *Element profiles Zr/Rb and Zr/Ti. The grey boxes mark the sections where finer grained sediment sections/ organic layers correlate with Zr/Rb peaks. The orange box marks the area where both element ratios are highly irregular, which correlates with an abundance of clasts > 1cm and large grain size distribution.* **4.27b.** *High-resolution line scan photograph of core K2 obtained from the Avaatech core scanner.*

5 Discussion

In this chapter the results will be discussed and a reconstruction model for Kortejärvi will be suggested. The order of presenting the data does not follow the order in the previous chapters. First the results will be discussed by method after which a formation process for Kortejärvi is presented. In the end of the chapter, the questions presented in chapter 1 function as an outline for the discussion of the outcomes of the study.

5.1 Interpreting core K2

It can be difficult to reconstruct the sedimentary history of a site with only one core, because when traced laterally, most Quaternary sedimentary sequences vary in thickness and composition (Lowe and Walker, 2015). At Kortejärvi, on the good side, investigations were carried out also on the ridges, and together with the GPR profiles, highly valuable information was gained regarding the continuity of the layers and the subsurface architecture. The core will be interpreted starting from the base and then continuing upwards.

Earlier studies suggest that much of the Veiki moraines consist of diamict with a glacial origin (Hoppe, 1952; Lagerbäck, 1988; Hättestrand and Robertsson, 2010; Sigfúsdóttir, 2013). The two grey base units of the core (K2-1 and K2-2) seemingly have a glacial origin as they consist of poorly sorted sediments (Figure 4.2a) characteristic of glacial diamicts (Krüger and Kjær, 1999). Structures, deformations and fabrics could not be determined from the core so the evaluation of how they were transported and deposited can solely be based on the grain size distribution and lithologies. The grain size distribution data for the core is only indicative and the lateral continuity of these layers is unknown, so only a vague interpretation can be performed for the diamicts. The two units have likely been emplaced in separate depositional processes as they are composed of different matrix material.

Sigfúsdóttir (2013) suggested that much of the center of the investigated moraine plateau ~16 kilometers north-northwest from Kortejärvi, consist of massive diamict deposited by mass flows prior to the lake formation. Moreover, the study does not exclude that subglacial till possibly lies closest to the bedrock. Having implemented more detailed clast and fabric analyses compared to what was performed in this study, we may assume that both subglacial and supraglacial diamict could in theory be found in the moraine plateau. If K2-1 and K2-2 were subglacial till, we could perhaps expect a laterally continuous radar reflection at that depth to mark the boundary between the layers. This is not the case. However, at about 16 meters depth,

in the 100 MHz GPR profile, stronger reflections appear (Figure 5.1) and may originate from a contact between supraglacial debris flow (layer 1) and subglacial till (layer 2) contact. Alternatively, it reflects the bedrock, which lies between 10- and 20-meters depth in the area (SGU, 2020c). Without a deeper ground truthing it is difficult to assess which one it is.

Figure 5.1. The 100 MHz GPR profile shows stronger reflections at ~ 16 meters depth in the center of the moraine. These reflections may come from the contact between subglacial till and debris flow deposits or alternatively it may be the reflection from the bedrock surface. Gain/filer: dewow + AGC gain.

The lithology distribution in diamict K2-1 and K2-2 is more varied than in the rest of the core (Figure 4.4.), implying that they have undergone a longer transport.

The characteristics of unit K2-3, including recurring fining upwards sequences (Figure 4.5a), sub rounded to sub angular clasts (Figure 4.3) and well sorted segments (Figure 4.5c), indicate deposition in an alluvial setting. The coarse sediment components of the entire unit suggest settling through bedload such as traction, saltation, rolling and sliding for most of the deposits. The aggradation was presumably rapid, since no overall fining upwards sequence can be distinguished from the base to the top of the core. The shape of the channel bed seen in the GPR profile, suggests that the water flow was violent in its initial phase and incised through five meters of the original sediments that had been deposited on the center of the moraine plateau. The channel bed cross cuts the underlying facies and is younger than the rest of the moraine, referring to the law of cross cutting relationships (Hutton, 1795).

The reoccurring poorly sorted gravelly sediments indicate that the sediments may have been deposited in a pro-glacial meltwater channel as they tend to be gravel-bedded (Nichols, 2009). The lack of pebbles, cobbles and boulders suggest deposition in a zone further downstream/ intermediate environment. The organic layers may document at the time abandoned stream channels or small mid-channel bars, implying that the channel was braided in its later phase. The strong but discontinuous radar reflections in radar facies 4, may represent these abandoned stream channels/ mid-channel bars (Figure 4.22d).

The study area is a relict glacial landscape (Lagerbäck, 1988; C. Hättestrand, 1998; Hoppe, 1952) and much of the former channels and alluvial deposits are remnants from the last deglaciation (Hättestrand, 1998). The sediments in K2-3 are therefore interpreted as a former branch in a network of braided rivers. This network of rivers likely was connected to the outwash plains that formed during and was active long after the last deglaciation. The age of the deposits will be discussed later in the chapter.

Aside from the channel, Kortejärvi moraine plateau seems to have been little affected by later glacial activity and there are not many outward signs of such. The basal till layer that has been described at many Veiki moraine plateaus was not found at Kortejärvi. Lagerbäck however, states that a layer of reworked sediments on top of some moraine plateaus also indicate post-formational glaciation. A thin layer at the top of the outcrops consisted of reworked sediments and soil, which perhaps were partly formed when the moraine was covered in cold based ice and permafrost. Only a few erratics were found on top of the ridges.

5.1.1 Element ratios of core K2

Within fluvial studies, XRF scanning has been used for identification of flood events. Coarse sediments are usually only mobile during flood flows, and hence a sudden increase in grain size normally points at a flooding event. Zr/Rb and Zr/Ti ratios are used as grain size proxies to reconstruct flood records. When Zr, Rb and Ti are transported by water or wind, they tend to concentrate in specific grain size fractions because the minerals, in which the elements commonly occur, differ in resistance. In general, Zr becomes concentrated in fine sand and coarse silt, Ti in slightly finer grains, while Rb concentrates in the finest silt and clay. Zr/Rb or Zr/Ti ratios increase as sediment grain size increases (Turner *et al.*, 2015).

The element ratios Zr/Rb and Zr/Ti were chosen not so much because of the interest in flooding events, but because an evaluation of the quality of the measurements was needed as the core consisted of coarser sediments than are common in XRF scanning. The measurements were hereby done mainly as an experiment to find out if XRF scanning on coarse sediments can give us trustworthy information.

The element profiles presented in Figure 4.27 show irregular curves with a few peak areas, but no overall increasing or decreasing trend was noted on the profiles. Flooding events should have, in an ideal case, been marked by peaks in both the Zr/Rb and Zr/Ti (Turner *et al.*, 2015). Both element ratios show more abundant peaks at the area between ~ 260 and 300 centimeters,

which correspond with a section of the core that has a relatively large abundance of coarse gravel. The organic layers and the silty layer at 240 centimeters depth, show a small peak in the Zr/Rb curve, which might imply that there were less air gaps and therefore, perhaps, resulted in more counts. A big clast was removed from unit K2-2 during the XRF scanning to avoid an uneven surface, leaving a small air gap instead. A peak in the Zr/Rb profile at this section of the core verifies that the data cannot be trusted, as an air gap in the sediments should not result in a peak in the element profiles. The obvious Zr/Rb peaks at 100 centimeter and 400 centimeters occur at the edges of the plastic tubes and hence do not represent elemental changes in the sediments.

Already medium size sediments has been proven to strongly influence XRF peak areas (Croudace *et al*., 2006). Another study regarding the reliability of XRF data by Bertrand *et al*., 2015 (in Croudace and Rothwell, 2015), concluded that grain sizes have a limited influence on XRF peak areas. However, the maximum grain size tested in their study was 200μm, so a comparison cannot be made since the grain-sizes represented in my core were much larger, most of it between coarse sand and gravel. Coarse and varying grain sizes in the core made the surfaces of the core uneven. Consequently, air gaps between the sediment surface and the measuring triangle could not be avoided, leading to debatable results. When accounting for the factors described above, XRF scanning is not an optimal method to use when addressing elemental ratios on cores composed of mainly sand and gravel. In such cases, a better way to determine flooding events in coarse grained alluvial sediments is perhaps, to assess the degree of sorting and the grain size distribution visually and in the laboratory.

In many rivers globally, gravel is deposited only as exceptions during flooding (Croudace and Rothwell, 2015). However, in outwash plains vast amounts of gravelly sediments are not exceptions, but typically occurring, especially during periods of high discharge (e.g. deglaciation, summer peak flow) or as a result of jökulhlaups. The coarsest sediments are typically deposited in the proximal environment while finer grain sizes are transported further away from the ice margin until they finally deposit in the ice distal environment.

Unit K2-3 does not comprise structures associated with sudden jökulhlaup events such as inverse-normal graded cobble and pebble gravel units overlain by thick laminated sands and silts (Maizels, 1993). The lithofacies profile of units K2-3 resembles more a non - jökulhlaup outwash plain, with repeated upward-fining cycles of heterogenous, clast supported subangular to subrounded gravels overlain by cross- and horizontally bedded gravels and sands (Maizels,

1993), although the latter structures cannot be confirmed from the core sediments. The grain sizes indicate deposition away from the ice proximal environment.

5.2 Interpretations of the outcrops K3 and K4

5.2.1 Diamict, unit K3-1 and K4-1

The outcrops in the ridges consist largely of diamict. The assessed diamict units are compact and have a fine massive matrix varying between silt, sandy silt and silty sand. Clasts up to cobble and pebble size are chaotically distributed. Such diamict composition could characterize both subaerial sediment gravity flows and subglacial tills (Benn and Evans, 2010). In this context however, it is more likely that the diamict is deposited in a glacigenic sediment gravity flow, as a number of factors speak against a subglacial formation of the Veiki moraine plateaus (Lagerbäck, 1988). Some differences were recognized between the diamicts, addressing the compactness, the color of the sediments and the size of the matrix material. The diamict in the western ridge is compact and has a light brownish grey color, while the diamict in the eastern ridge is composed of greyish less compact diamict. The size of the matrix material varies between the two ridges as the western ridge is dominated by sandy silt or silty sand, while the diamict in the eastern ridge is composed of a silty matrix. The clast shape and roundness were examined more closely on the western ridge. The bigger clasts are mostly subangular and subrounded and the overall shape is bladed or compact bladed (Figure 4.9). Cobble and pebble sized clasts were not as widely distributed in the eastern ridge compared to the western ridge.

Previous authors have suggested that the diamict within the Veiki moraines is a supra- and englacial till that has a subglacial origin, but has been thrusted to the supraglacial environment during a surge (Lagerbäck, 1988; Sigfúsdóttir, 2013). The examination of the diamicts in Kortejärvi supports the suggested theory from the previous studies, however keeping in mind that no in-detail description was done. At a lowland terrain ice margin the supraglacial till commonly has a subglacial or englacial origin, and therefore the supraglacial till often resemble the regional basal till (Johnson and Clayton, 2003), which can make identification challenging.

Thinking of the origin of the diamict in a large scale, we may assume that once the debris was on top of the ice, resedimentation of the uppermost surface of the debris occurred because of uneven downwasting processes, and perhaps also backwasting processes in a smaller scale. Hereby, the final deposits likely consist of sediments originating from many different sources,

with different transport paths within and on the surface of the ice sheet. Mass movements such as slumping, sliding and flowing of sediment-water mixtures were probably among the main transporting and depositing agents on top of the ice. These processes did perhaps not affect the entire debris cover, as it likely was very thick, referring to the thick accumulations of debris left behind after the ice melted. The deepest lying diamict could in theory have preserved the original englacial or subglacial sedimentary characteristics (Johnson *et al.*, 1995). The exposed outcrops at Kortejärvi are, however more likely composed of resedimented material as they are not deeply buried.

Variations in the composition of sediment gravity flows are closely related to differences in the water content during the flow and deposition (Benn and Evans, 2010). Flows with a low water content form clast-rich, poorly sorted deposits. Distinct structures are often missing (Benn and Evans, 2010). The higher the water content is in the flow, the lower is the shear strength and the less large clasts can be incorporated. Therefore, flows with high water content form deposits consisting of mainly silt and sand (Benn & Evans, 2010). Mass flow diamict deposits can, however, lose much of the finer matrix through rapid drainage (Lowe and Walker, 2015), which implies that deposits consisting of mainly coarse grain sizes might have undergone drainage. Having considered the above factors, the debris flow that deposited the diamicts in the western ridge at Kortejärvi likely had a low water content, perhaps somewhere between 8-14%, as it has formed clast rich, poorly sorted deposits (Benn and Evans, 2010). Larger clasts up to more than 30 centimeters in length were found at the top of the deposits, implying a shear strength strong enough to not lower the clasts to the bottom of the flow. The diamict in the eastern ridge was likely deposited in a flow with a slightly higher water content, as the biggest clasts are not as abundant as in the western ridge, and the matrix is, visually assessed, finer. A higher water content would result in finer-grained matrix material, which also gives the sediments a greyer color. The color difference between the ridges is additionally influenced by the present-day water content and soil processes, as the diamict in the eastern ridge seemingly had a higher water content compared to the western ridge. The finer sediments also have a lower permeability and are therefore capable of storing more water than coarser sediments like sand.

Examining fabrics in the ridges could have contributed with additional information on the diamict layers, such as flow direction. This aspect was not examined due to time restrictions in the field. Sigfúsdóttir (2013) and Hoppe (1952) have earlier suggested that a specific orientation can be noted in the diamicts in many of the Veiki moraines, which potentially verifies deposition by debris flows (Sigfúsdóttir, 2013). At first glance, sediment flow deposits may

appear chaotic, but a closer examination can reveal internal organization (Benn and Evans, 2010).

Due to insufficient data from the diamict layers in the core, it is hard to determine if it corresponds with the diamict in the ridges. The possible alternatives will be summarized here. As mentioned above, the diamicts in the ridges are interpreted as debris flows because of their composition, and position in the moraine plateau. It is possible that the diamict in the center of the plateau was deposited from debris slumping and flowing into the sinkhole from the surrounding ridges, which would mean that it was deposited by the same process as the diamict on the ridges. How do these diamicts correspond in terms of composition? The grain size distributions for K3-1 and K2-2 correspond, having the highest percentage of material > 63 µm (Figure 4.5b and 4.11b), while K2-1 is bimodal with also a high percentage of > 63 µm but a higher percentage of 1 mm clasts (Figure 4.5b). The fact that the bottom of the core is composed of two separate layers of diamict also speaks for them being deposited in separate events, which could imply separate debris flows. The lithologies of K2-1 and -2 correspond, implying that they are likely deposited in similar events that occurred close to each other in terms of time.

The lithologies of K3-1 diamict seem to have a slightly higher representation of red granite compared to the diamicts in the core (Figure 5.2). This could imply that K3-1 diamict was deposited at a different time, perhaps later, although still in a debris flow event related to the infill of the sinkhole.

Figure 5.2. The lithology distribution of the diamict K3-1 shows a higher distribution of red granite in comparison the diamicts K2-1 and K2-2.

The grain size distribution and lithologies of the diamict in the eastern ridge were not determined more closely. However, the visual appearance of the diamict and the position in the moraine plateau implies that it was emplaced in a debris flow from east. Consequently, the diamicts in the ridges and in the center of the moraine plateau are likely all deposited in separate

debris flow events, related to the infill of the water filled sinkhole that eventually formed the Kortejärvi Veiki moraine plateau. Therefore, the diamicts are older than the stratified sand superimposed on the diamict on the western ridge, and much older than the sediments in radar facies 4 or K2-3.

However, as mentioned earlier, the scarce data from K2-1 and -2 makes the interpretation somewhat uncertain. If we had obtained more of the diamict in the core, it would have been interesting to evaluate differences in more detail. An alternative interpretation is that the corer reached the subglacial till that presumably lies in the bottom of the moraine plateau. This is considered less likely, as there is no visible boundary between two separate diamict layers in the GPR profiles at this depth.

Assuming that the sediments are emplaced by debris flows, one could argue that they do not fulfill the description of till even though they have a glacial origin (Benn and Evans, 2010). The term 'glacigenic debris flow deposit' would perhaps be accepted by a wider audience of glaciologists and other geologists.

5.2.2 Stratified sand, unit K3-2

The sedimentary structures in outcrops A-E indicate an alluvial origin. Structures characteristic of different water flow regimes together with the gradational and erosional boundaries, point towards emplacement by water of changing flow regime. As the sediments today lie on a topographic high, we can assume that the water body likely has been ice-walled at the time of deposition. The sandy successions in outcrop A-E likely correspond with each other as a formerly laterally continuous succession, referring to their positions and a visual assessment regarding similarities in the grain size distributions and structures.

What kind of alluvium are the sediments? We can estimate the flow velocity, and to some extent the water depth of the former water flow, by looking at the bedforms in the western ridge. Bedforms are controlled mainly by sediment grain size, flow depth, and flow velocity (Miall, 2016). The size of a bedform depends on the depth of the water in which it forms and the amount of sediment available (Miall, 2016). The depth of the water will also influence the stability fields of the bedforms (Figure 5.3). Flow speed and water depth estimations are needed in the OSL measurements, to estimate how well the sediments have been bleached.

The lowermost layer of outcrop A unit K3-2 has faint lamination/trough cross lamination (3D-ripples) (Figure 4.11a), which in combination to the dominant grain sizes 0.125 mm and 0.250

mm (Gs 7, Figure 4.11b), imply a flow speed in the lower flow regime between 40 and 60 cm/s when estimating a water depth of 30 cm (Figure 5.3). The erosional contact on top of this lowermost layer indicates an increase in flow speed. From where Gs 8 was collected the particle sizes increase and there is an abundance of coarse sand and gravel lenses with particles up to 4- and 8 mm. In combination with parallel lamination, these are lower plane bed deposits, formed in a flow speed between 40-60 cm/s. The ripple cross laminated uppermost layer, which is separated from the underlying layer by a gradual boundary, has approximately the same grain size distribution as the lowermost layer, but includes randomly distributed larger clasts, implying a slightly lower flow speed, perhaps around 40 cm/s.

Since the outcrops in the western ridge likely have been a laterally continuous succession at the time of deposition, we may assume a similar flow velocity for the water flow as that of outcrop A, with a few exceptions. The parallel laminated layers between 60 and 70 cm depth in outcrop E in combination to an approximate mean grain size around 0.1 mm (Figure 4.18b), indicates that these are upper plain bed deposits deposited in the higher flow regime between 60 and 120 cm/s. Outcrops C and D (Figure 4.16) are composed of massive sand/very faint lamination, and the grain size is visually assessed close to that of Gs 7. The structures imply a flow speed in the higher flow regime, between 60 and 120 cm/s. The structures indicate emplacement by rapid deposition in a bedload transport or by gravity flow.
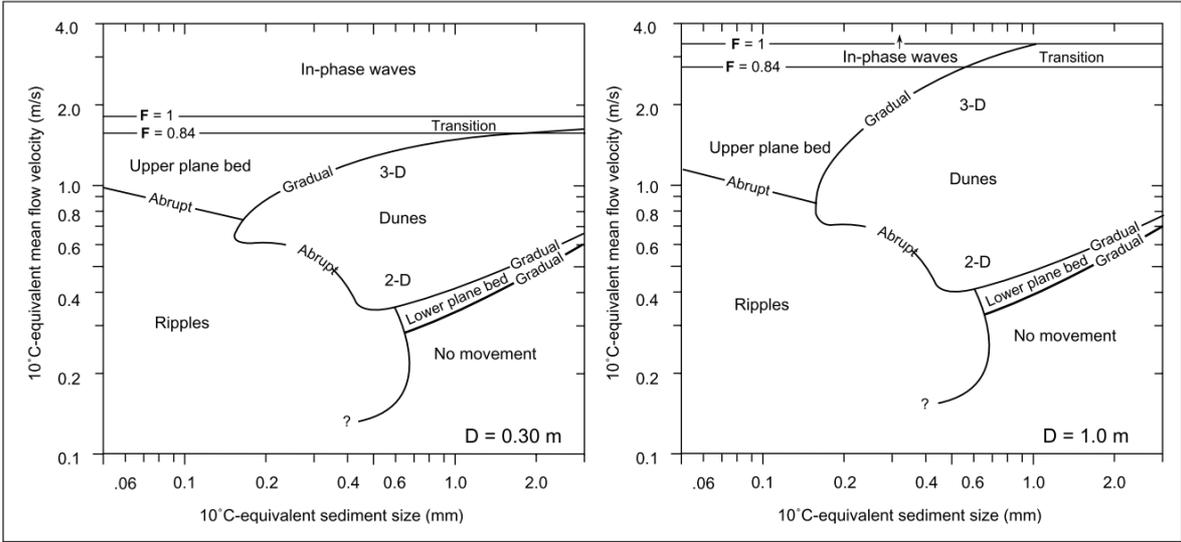
Figure 5.3. Stability fields of bedforms for two ranges of flow depth. 3D ripples form in the upper part of the stability field for ripples. After Southard and Boguchwal 1990 (Cheel, 2005).

The size of the bedform can be indicative of the depth of the channel. As an example, in large energetic channels that carry high amounts of sand, dunes >10 meters in height may form (Miall, 2016). In comparison, the greatest bedforms in the western ridge were only a few centimeters high and therefore a relatively shallow water depth can be assumed. The water depth was likely slightly deeper at outcrop E compared to the rest of the outcrops, due to an overall decrease in the grain size distribution. The stability fields for the bedforms were determined according to a flow depth of 30 cm.

Current ripples and cross-lamination have also been used to reconstruct paleo flow directions. The flow directions might be very local and should not be directly used as an indicator of the direction for the entire water flow. The trough cross laminae in outcrop A implies a local flow direction from north to south or south to north (Figure 4.7b). The dipping beds (Figure 4.10) indicate that the water was flowing downslope W - E, and if combined with the signal from the trough-cross lamination, we may assume a SW - NE flow direction.

At the dead-ice field of the modern day outlet glacier Kötlujökull in Iceland, a study by Krüger *et al*., (2010) concluded that changes in the sediment concentration of supraglacial streams fluctuates with changing weather. During days of heavy precipitation, streams were heavily loaded with sand and gravel while during sunny days, only small amounts of sediments are entrained in the stream (Krüger *et al*., 2010). The clear changes in the flow velocity seen in the stratified sands, might therefore indicate daily or weekly weather variations rather than seasonal or yearly variations, if assuming that similar processes prevailed in the ancient dead-ice field. It is also likely that much of the sediments are missing, indicated by the erosional contacts in the outcrops, which makes it even more complicated to assess for how long the water stream was active.

5.2.3 Secondary structures and deformations in the ridges

A few secondary structures and deformation structures were identified in the outcrops. Each of them is described separately below.

The sorted sand lens in outcrop G on the eastern ridge is likely a secondary dewatering structure, formed as a result of upward movement of confined pore fluids. In glacial environments pressurized groundwater is common (Benn and Evans, 2010)

The brownish diamict layer at the top of outcrop G is not interpreted as a separate diamict layer, but rather as a color change that is related to soil processes. Factors that strengthen this is that

it was only noted in one of the outcrops and its composition was otherwise the same as for the underlying grey diamict layer (Figure 4.20b). Lagerbäck (1988) also observed a brownish till layer at the top of Veiki moraines, interpreting it as a remnant from the Late Weichselian ice sheet. He did however not describe this brownish till in detail. It can be difficult to distinguish individual diamict units if they have a similar texture, however boundaries are commonly marked by, as an example basal concentration of clasts, upper washed horizons and interbeds of silt, sand and gravel (Benn and Evans, 2010). Such structures are absent in outcrop G and therefore it is likely not deposited by a separate event, such as an overriding ice sheet.

The small-scale faults in outcrops A (Figure 4.7d) and B are probably caused by a local collapse of the depositional floor. As the faults are not vertically continuous, they happened, not syn-sedimentary, but quite soon after deposition. The slightly loaded contact in outcrop E (Figure 4.18d) seems to be a density driven deformation. Both imply vertical deformation caused by gravity-driven processes, common in, for example, proglacial settings where buried ice is melting, and sediments have a high water content (Benn and Evans, 2010).

The heavily deformed sediments in outcrop B (Figure 4.14a) show structures implying a vertical deformation or collapse of the sediments. The laminated layers are not folded but either homogenized with the surrounding sediments or they appear randomly at inclined angles disconnected from each other. The "vein-like" sandy structure in the middle (Figure 4.14c) imply that the water content in the sediments was high and water intruded downwards. The deformations seem to continue in the subsurface (Figure 4.22b). One possible explanation is that when the supporting ice walls and underlying ice melted, the sediment sequence that was resting on it collapsed and subsided. Subsiding caused an over steepening of the surrounding ground. A part of the resulting mass movement is seen in outcrop B, where the nearly vertical boundary run throughout the outcrop (Figure 4.14a). The upper sandy sediments are heavily deformed while the lowest part of the sandy unit seems almost undisturbed. As this was happening in the melting phase, we can assume that the sediments were wet, which further contributed to an unstable ground and mixing of sediments. The later overriding ice sheet probably also contributed to reworking of the upper layer.

Different triggering agents can lead to the same deformation structures and potential triggering agents in the study area should be considered (Suter *et al.*, 2011). In glacial landscapes, it is common to find structures associated with hydrofractures, liquefaction and homogenization. As Kortejärvi lies in the Veiki moraine area, which presumably is a relict stagnant ice

environment (Lagerbäck, 1988; Hättestrand, 1998), downwasting of stagnant ice is a logical explanation for the deformations. Uneven downwasting of dead-ice blocks presumably lead to a highly unstable environment and water rich sediments, which resulted in homogenization, liquefaction and debris flows. The overriding Late Weichselian ice sheet likely caused some reworking in the upper sediment layer (Lagerbäck, 1988).

The observed deformations in Kortejärvi indicate that downwasting processes dominated during the melting phase of the ice, which further strengthens that there was a thick debris cover on the ice surface. In areas where backwasting is abundant, mass movement processes characterized by gravity sorted sediments are more common (Schomacker, 2008).

5.3 Age of the deposits

One of the aims of this study was to obtain absolute ages from a Veiki moraine plateau. Before going to conclusions, an evaluation on the reliability of the ages will be presented. The results of each dating method will be discussed separately.

5.3.1 OSL

The obtained ages can be divided into two age groups. These two generations can be regarded only if accounting for the ages from the good quality measurements, which excludes the samples of the poorest quality; sample 18030 and 19003 (Table 4.1).

The sediments in the western ridge K3 belong to the older group, in which the ages range between 37.1±5.5 ka and 41.6±5.1 ka (Table 4.1). The sediments from the core K2 belong to the younger group, with ages ranging between 9.2 ±1.2 ka and 22.7±3.7 ka (Table 4.1). Different protocols were used for age group 1 and -2 (Helena Alexanderson pers. con.), implying that the quartz have different characteristics and therefore likely a different origin. Some background information for OSL dating in Sweden will be presented before assessing the obtained ages.

Inconsistency in OSL-dates from Sweden have resulted in some skepticism towards the reliability of using the method for absolute dating in Sweden. Alexanderson & Murray (2012) have researched on the reasons behind the scattered ages that are often obtained. Two of the main problems seem to be related to incomplete bleaching of quartz and feldspar, and to dim or low-sensitivity quartz. Incomplete bleaching can lead to age overestimations, and therefore many of the OSL dates from Sweden are regarded as too old, while low sensitivity quartz has

led to practical problems when operating measurements and larger uncertainties in dose estimates (Alexanderson & Murray, 2012).

Incomplete bleaching is directly related to the depositional environment of the grains which have been dated. This problem is especially evident in ice-proximal environments and less so the further the distance to ice sheet becomes in both time and space. A distal sediment has higher chances of being zeroed. Scattered ages between and within samples is the result of poor luminescence characteristics of the material, meaning e.g. dim quartz with feldspar contamination. Better precision is obtained from clean luminescence sensitive quartz (Alexanderson & Murray, 2012). The luminescence sensitivity has been regarded as a factor that changes due to variations between geographical areas rather than the depositional environment (Alexanderson and Murray, 2012).

5.3.1.1 Age group 1

For reasons that have been explained earlier, the stratified sand unit is interpreted as supraglacial. Hence, we could generally speaking expect, that the quartz in our OSL samples from the ridge have been well bleached at the time of deposition, since supraglacial sediments ideally have good luminescence properties because of the dynamic environment in which they have been deposited and reworked (Thrasher *et al.*, 2009). The degree of bleaching also depends on the transport distance, water depth and turbidity of the flow.

The sedimentary structures in outcrops A and B imply deposition in relatively shallow waters in the lower flow regime. A shallow water depth enhances the likelihood of being well bleached. The water flow was likely turbulent, as most water flows that carry significant volumes of sediment are turbulent (Nichols, 2009). Additionally, as the debris cover on stagnant ice generally is well reworked, there is no reason to suspect that the ages are largely overestimated. The sediments in outcrop E have likely undergone the same transport path as the sediments in outcrops A and B and therefore we may assume that also these have been well bleached.

The dose measurements were regarded complicated when a relatively small number of aliquots were accepted in the quality controls and the ages between samples and within samples were scattered. This indicates that the luminescence characteristics are poor and result in less reliable age estimates and increasing errors.

Three of the ages in outcrops A, B and E yield similar ages ranging between 37.1 ± 5.5 ka and 41.6 ± 5.1 ka (Table 4.1). Only the second sample (18030) in outcrop A does not overlap and

is considerably older; 58.3± 8.7 ka (Table 4.1). This sample included many aliquots that did not pass the acceptance criteria and had a large skewness among the doses within the sample, and therefore the uncertainty of the age estimate rises. Hereby, the age of the sediments in the ridge probably lie closer to the ages obtained from the three other samples 18029, 18031 and 18032. These ages overlap with the OSL ages obtained by Sigfúsdóttir (2013) from another Veiki moraine plateau in the area, and can be correlated with the Middle Weichselian interstadials or Tärendö 2 (Hättestrand and Robertsson, 2010).

5.3.1.2 Age group 2

The OSL samples from the core were collected from unit K2-3 (Figure 4.5a), which is interpreted to be part of a former branch in a network of braided rivers related to the outwash plains from the last deglaciation. The coarse grain sizes indicate bedload transport of the sediments. The depth of the water has likely varied throughout the aggradation period, referring to the fining upwards sequences. These two factors raise the chances of being incompletely bleached. However, the relatively high amount of sorted material in the core indicates that the transport path has likely been of intermediate length and the coarse grain size distribution indicate deposition in the lower flow regime. These two factors could lead to a higher likelihood of being well bleached. After all, there is an uncertainty in the degree of bleaching of the sediments, however, bedload transport in a varying water depth may imply that the sediments are be poorly bleached.

The ages in group 2 range between 9.2 ± 1.2 ka and 63.4 ± 10.8 ka (Table 4.1). The samples with the best luminescence properties and therefore likely the best age estimates, are sample 19004 with age 9.2 ± 1.2 ka and sample 19005 with age 11.4 ± 1.5 ka (Table 4.1). How well these ages correspond to the local deglaciation will be discussed in subchapter 5.6.

5.3.1.3 Uncertainties

An evaluation regarding possible errors in the estimation of water content in the sediments and the bulk density should be made since the OSL ages can vary depending on the estimated mean water content and density.

If we had used the present-day water content as a long-term average, we would end up with slightly younger ages. The difference would be approximately 2000-3000 years for age group 1 and 1000-2000 years for age group 2. The uncertainty of 4% however covers the range from present day water conditions to the estimated water conditions in all samples. If we had

considered the saturated water content as a long-term average, we end up with older ages (2000-4000 years difference) for age group 1 and nearly the same ages for age group 2. In this case, too, the uncertainty of 4% covers the range from saturated- to the estimated conditions. Therefore, the estimated water contents do not affect the final ages by much. The significance of possible errors in the bulk density resulted in insignificant variations when including the error.

As mentioned earlier, the common uncertainty in OSL ages ranges between 5 and 10 %. In this study, the relative errors range between 12 – 18% and therefore we must assume a certain inaccuracy in the ages. The central age model is considered the best alternative for the age calculations as it enhances the significance of aliquots with smaller errors.

5.3.2 Radiocarbon ages and organic material

The modern radiocarbon ages caused the writer some confusion (Table 4.3). Even though it seems probable that the deposits in the center of the moraine plateau are younger than the ones in the ridges, a modern age seems highly unlikely, as there has not been any active river in modern times, verified by old areal images (Figure 5.4). Additionally, it seems unlikely that 4 meters of material have deposited in only 20-30 years in this environment.

A likely explanation for the modern age of sample C3, which was an unidentified piece of possibly *Equisetum*, is that the vibrocorer pushed surficial material deeper in the ground. This assumption is reinforced by the fact that the sample was found in between two separate core sections (399 cm depth). Another possibility is that the sample was a piece of a modern root. The second alternative cannot be rejected as the identification of the sample was somewhat uncertain. The same explanation is however less likely for sample C2 as the sample was a seed and was obtained from an organic layer that lie in between coarse grained units in the middle of one core section (135 cm depth), and hence should not have been pushed down by the corer. The possible explanations left are that the sample has been contaminated somehow, as an example by reworking due to freezing and thawing, bioturbation or a chemical reaction, or finally, by the scientist during sampling. The uppermost coarse sand and gravel layer that lies between the two top organic layers does not show distinct structures, indicating that it could be reworked.

Sample C1, which was a seed obtained from the base (between 66 -70 cm depth) of the top peat layer (unit K2-4), could in theory have been pushed down by the corer. In this process the layer

could have been compacted and mixed with seeds from the topmost organic layer. Other possibilities are as for sample C2, bioturbation, reworking due to freezing and thawing, chemical reactions or a mistake by the scientist during sampling. The fact that the uppermost sample has the oldest age out of the three ^{14}C samples indicates that the results are unreliable.

An additional explanation to the modern ages, although less likely, is that anthropogenic activities in the area has resulted in, for instance, a leakage of a substance of some kind, which affected the organic material in the moraine plateau. Areal images of Kortejärvi from 1962 and 2003 (Figure 5.4) by The Swedish National Land Survey (Lantmäteriet), document that the ridges have undergone extensive forestry, which seems to be ongoing. However, the central part of the moraine seems undisturbed by the forestry. Additionally, a road and a ditch have been constructed few meters off the core position sometime between 1962 and 2003 (Skogsstyrelsen, 2019).

As organic material was scattered throughout nearly the entire core, we may assume that vegetation had established in the nearby areas when the channel was aggrading.

Figure 5.4. *Areal images of Kortejärvi from 1962 (left) and 2003 (right). Between these years, the area has undergone forestry, roadwork and drainage. Background maps: Historiska ortofoto © Skogsstyrelsen (2019).*

5.3.3 Pollen

The pollen data (Table 4.4.) can be compared with previous palynological studies that have been performed just east of the Lainio arc (Hättestrand and Robertsson, 2010). The study reported local pollen assemblages from different times, such as Weichselian interstadial phases, different parts of the Holocene and present. The pollen assemblages from the present study correlate with Holocene pollen assemblages, since they have low amounts of pollen from grass and *Artemisia* and high percentages of conifers (Martina Hättestrand pers. comm.). The pollen analysis therefore reassures a Holocene age of the sediments in the two upper units of the core. Pollen assemblages from different parts of the Holocene are relatively similar to present day pollen deposition in the area so without a more detailed pollen analysis, the difference is difficult to assess. The pollen data does therefore not assure if the organic layers are of modern age, which is indicated by the radiocarbon results or if they are from an earlier phase of the Holocene, which would be the more likely alternative.

Möller *et al*., (2013) calibrated the ^{14}C ages obtained from Kangos by Östlund (2004), and suggests deglaciation sometime between 10.11 ka cal BP and 9.54 ka cal BP. The ^{14}C ages by Östlund (2004) were recalibrated again in the present study Using Oxcal v.4.3 (1 σ) (Ramsey, 2009), and resulted in a slightly younger age range between 9.73 ka cal BP and 9.51 ka cal BP. Studies by Stroeven *et al*. (2016) and Hughes *et al*., (2015) suggest deglaciation of the area between 10 ka cal BP and 9.9 ka cal BP or slightly later. By calculating a mean from the different ages presented above, we may assume a mean local deglaciation at 9.8 ka cal BP, but an error margin ± 0.2 ka should be incorporated.

At the time the channel was formed, pine, spruce and birch had most likely already established in the area. According to Möller *et al*., (2013), alder and pine tree expansion started 9.6 ka cal BP at Aareavaara. Comparing that with a deglaciation at 9.8 ± 0.2 ka cal BP, the pine and alder expansion started a few hundred years after the deglaciation. We may assume that same happened at Kangos; the alder and pine started to establish a few hundred years after the local deglaciation. However, pollen from spruce is rarely found in early-Holocene sediments (Giesecke, 2004). Spruce likely established sometime between 3000- and 4000-years BP in northeastern Sweden (Martina Hättestrand pers. comm.; Giesecke, 2004), and therefore, we may assume that the sediments are younger than that. At 4000 BP, Fennoscandia was already deglaciated (Östlund, 2004; Möller *et al*., 2013; Hughes *et al*., 2015; Stroeven *et al*., 2016).

Vast amounts of meltwater from the ice sheet persisted in the landscape for thousands of years after the deglaciation, during the post-glacial rebound.

5.4 Subsurface reflections

The radar facies were described and interpreted only briefly in chapter 4 so the discussion will continue in this subchapter. The radar reflections have been correlated with the field observations.

The parallel continuous to moderately continuous reflections within radar facies 2 (Figure 4.22b) lie deeper down than the stratified sandy sediments that constitute K3-2 on top of the western ridge. Presumably, these subsurface reflections come from stratified sand that was deposited by the same water body as the sediments on top of the ridge. Below the crest of the ridge, the reflections are deformed and the parallel continuous reflections dip down the outward slope (Figure 5.5). As indicated by the vertical diamict - sand contact across outcrop B (Figure 4.14a), a part of the ridge has subsided, probably after the supporting ice walls and underlying ice melted away. The reflections in the GPR profile are the subsided part of the sediments that belong to unit K3-2. The parallel reflections disappear almost completely on the inwards slope, suggesting that later processes, such as the younger alluvium in the center of the moraine plateau, have reworked much of the inner slopes.

The reflections of radar facies 3 (Figure 4.22c) together with field observations reinforce that the western ridge is composed mainly of diamict and there are no indications of a waterflow from east.

The GPR profile reinforce the assumption that a channel has crosscut the moraine. The strong reflection of radar surface 2 is defined by a channel shaped contour that is strongest at ~ five meters depth (Figure 4.23a). This is interpreted as the channel bed and the reflection likely originates from the contact between gravelly sand and silty diamict as seen in the base of the core at 4.8 m depth. Surface 2 becomes weaker eastward and therefore the lateral extent of the channel is difficult to define only by looking at the GPR profile. Observations from the field indicate that the width of the channel reached almost the crest of the western ridge, as the slope was partly covered in closely lying cobble and pebbles. The reflections within radar facies 4 are discontinuous and correspond with the coarse sediments examined from the core. The strong and continuous layers within the channel are likely organic layers with a higher water

concentration. The organic layer at 150 cm depth in the core corresponds with a radar reflection at the same depth.

The GPR profiles gave valauble information on the subsurface architecture, however, a more throughly field exploration would be desirable for a more confident evaluation of the subsurface. As an example, Lagerbäck (1988) carried out a study in which 18 cores were collected, at Outojärvi Veiki moraine plateau (~15 kilometers south of Kortejärvi). Sigfúsdóttir (2013) carried out excavations in different parts of two moraine plateaus. Both studies resulted in a more confident evaluation of the lateral continuity of the subsurface layers.
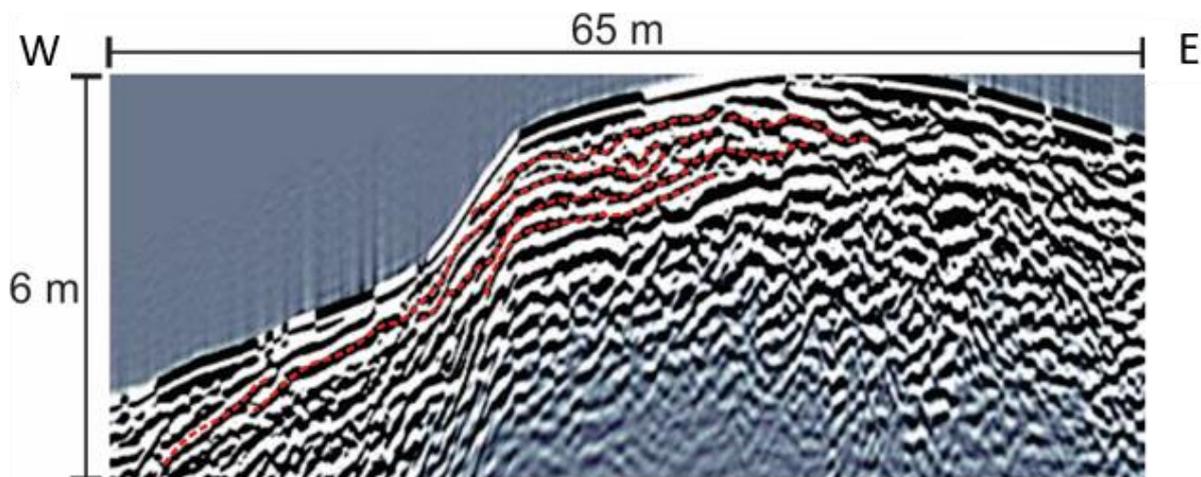
Figure 5.5. *The reflections within radar facies 2 in the western ridge indicate that the deformations in outcrop B continue in the subsurface. The red dashed lines make it easier to recognize the deformations at the crest. Radar facies 2 constitutes the collapsed part of the waterlaid sediments. The collapse occurred once the supporting ice had melted. The frequency of the profile is 200 MHz.*

5.5 Landform formation

By first glance, the explanation might seem quite simple; the moraine plateau is a former ice-walled lake plain that got crosscut by a channel. For several reasons however, it seems like the explanation is more complicated than this. I have looked for moraines like the one at Kortejärvi in the Lainio arc area using the elevation model over the area, but Kortejärvi seems to be unique among the Veiki moraines with two separate ridges. Therefore, the formation process for this moraine must continue from the presumed ice-walled lake phase. One main formation theory will be presented first, after which uncertainties and alternative theories will be presented briefly.

5.5.1 The theory of the merged ice-walled lakes

The inward bended western and eastern ridges imply that Kortejärvi started to form alike many Veiki moraine plateaus; as a water filled sink hole in the stagnant ice. The water laid deposits

on the western ridge were emplaced in a widespread water flow from southwest, perhaps due to the ice surface being subhorizontal in large-scale with a downslope towards E-NE. The bigger particles were deposited in the slope when the flow velocity of the water changed while the finest particles were deposited in the lake that formed in the center of the sinkhole.

A simple explanation to the younger fluvial sediments in the center would be that the moraine got cross cut by a channel, but this is contradicted by the fact that it seems highly unlikely that the channel would have followed a path straight through an elevated moraine instead of going around it. By looking at the surrounding Veiki moraines, none seems to be crosscut straight through the rim ridge and plateau. We can therefore assume that the center of the moraine was already lowered when the channel made its entrance.

When looking at the topography of Kortejärvi one observation should be pointed out from a morphological point of view; the southern limit of Kortejärvi is somewhat difficult to define (Figure 5.5). That is partly because later fluvial processes have reworked much of the area, but it also seems like some of the moraines have been connected to each other, which implies that
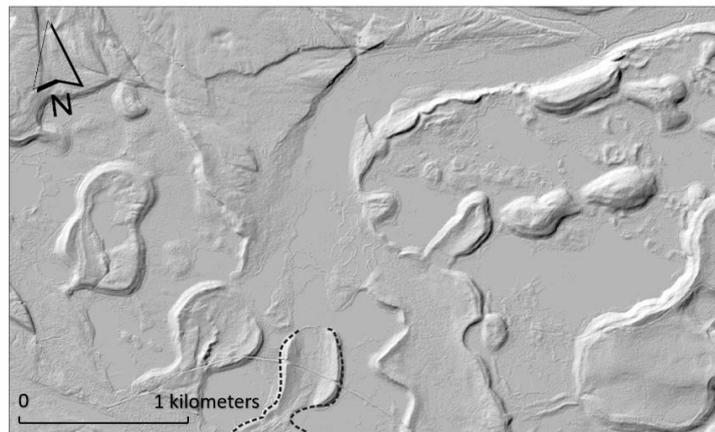
Figure 5.6. The black dashed line shows the clearly defined eastern and western ridges and the diffuse limit at the southern edge. Background map: Nationell höjdmodell © Lantmäteriet I2018/00104 (2011b).

adjacent lakes perhaps merged with one another. If Kortejärvi merged with adjacent lakes, it could explain why the southern part is lacking a ridge. In this scenario the process could have been much like the one explained by Benn and Evans, (2010) and Clayton *et al.,* (2006) in which ablation and calving on the steep nearly debris free ice-walls of the lakes cause lateral expansion of the lakes. Consequently, when the lakes merged with each other, some of the sediments within the lakes were removed during a high velocity sediment flow, as the water was reaching a new state of equilibrium. The "tail" in the southern part of Kortejärvi might hold some of the old lake sediments, but in a reworked state as they may originate from the center of the moraine plateau. Shortly after the integration of the lakes, the lakes probably drained, as drainage ways were formed because of faster melting.

North of the moraine, there are no distinct features suggesting that the same process caused the eroding, such as the "tail" in the southern edge. When looking at the two moraines on each side of Kortejärvi however (Figure 5.6), they lack a ridge in the northern part too. Perhaps the ridges were eroded in the same process.

By looking at the map, perhaps the first explanation that comes to mind is that a channel from north, branched into three channels, and eroded the northern parts of the moraine plateaus. Eroding a ridge would, however, require a water stream with a high velocity, and if that had been the case, we could assume that the esker seen on the moraine west of Kortejärvi (Figure 5.6) would have been eroded or affected somehow. Due to the good preservation of this esker, we may assume that a Late Weichselian vigorous channel did not crosscut the moraine west of Kortejärvi. If the northern part of the three adjacent moraines plateaus were eroded in the same process, we may consider some other process. Perhaps the lakes merged with adjacent lakes alike in the southern edge. A reconstruction model of what the lakes may have looked like prior to the merging is presented in Figure 5.7 and a reconstruction model of how the lakes may have merged is presented in Figure 5.8. Figure 5.9 presents a simple sketch of a 7-steps scenario, illustrating a formation theory for Kortejärvi moraine plateau,
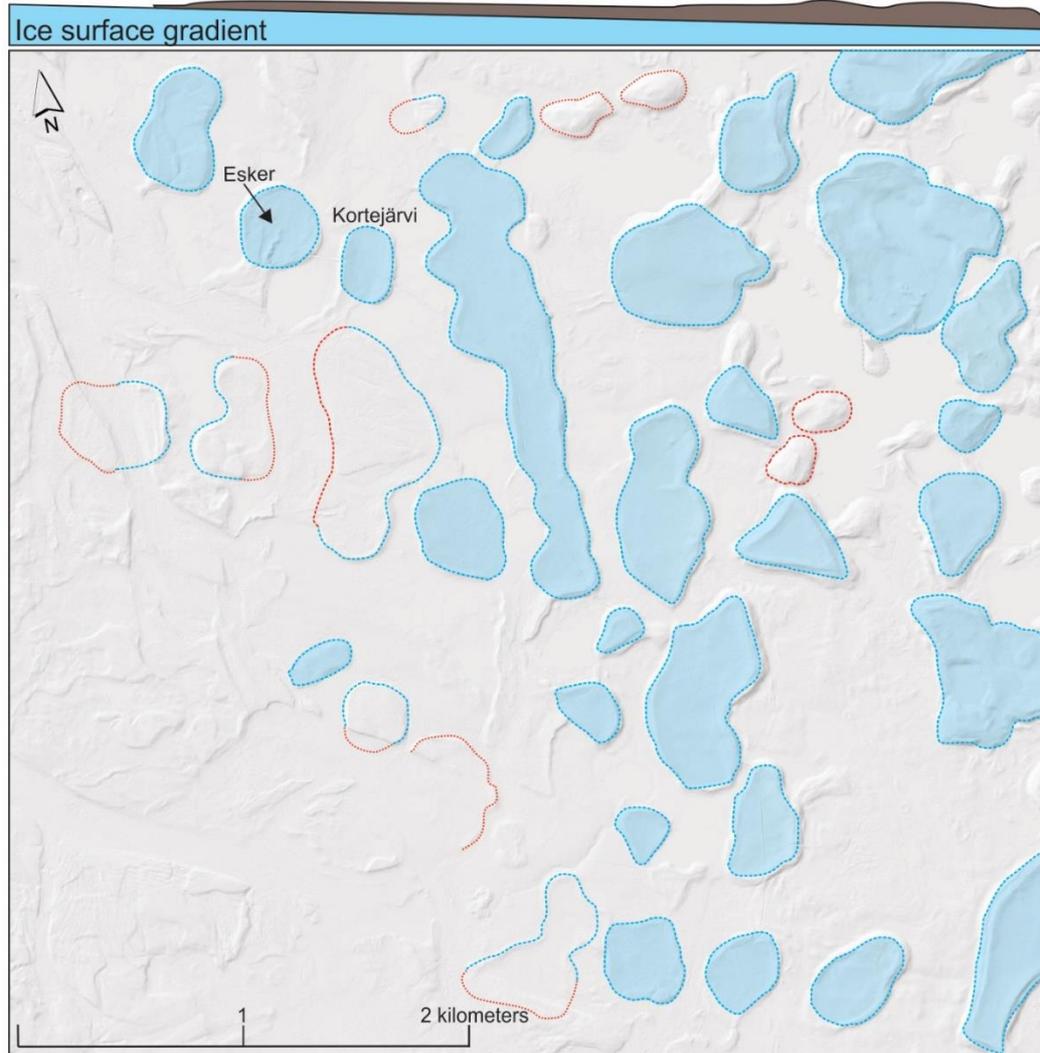
Figure 5.7. *Reconstruction of what the lakes may have looked like prior to the episode of merging lakes. The blue dashed lines mark the assumed ancient lake margins. The arrows show the similar direction for the collapsed parts of the lakes. The large-scale ice surface gradient is illustrated at the top together with the large-scale debris cover thickness. Background map: Nationell höjdmodell © Lantmäteriet (2011b).*
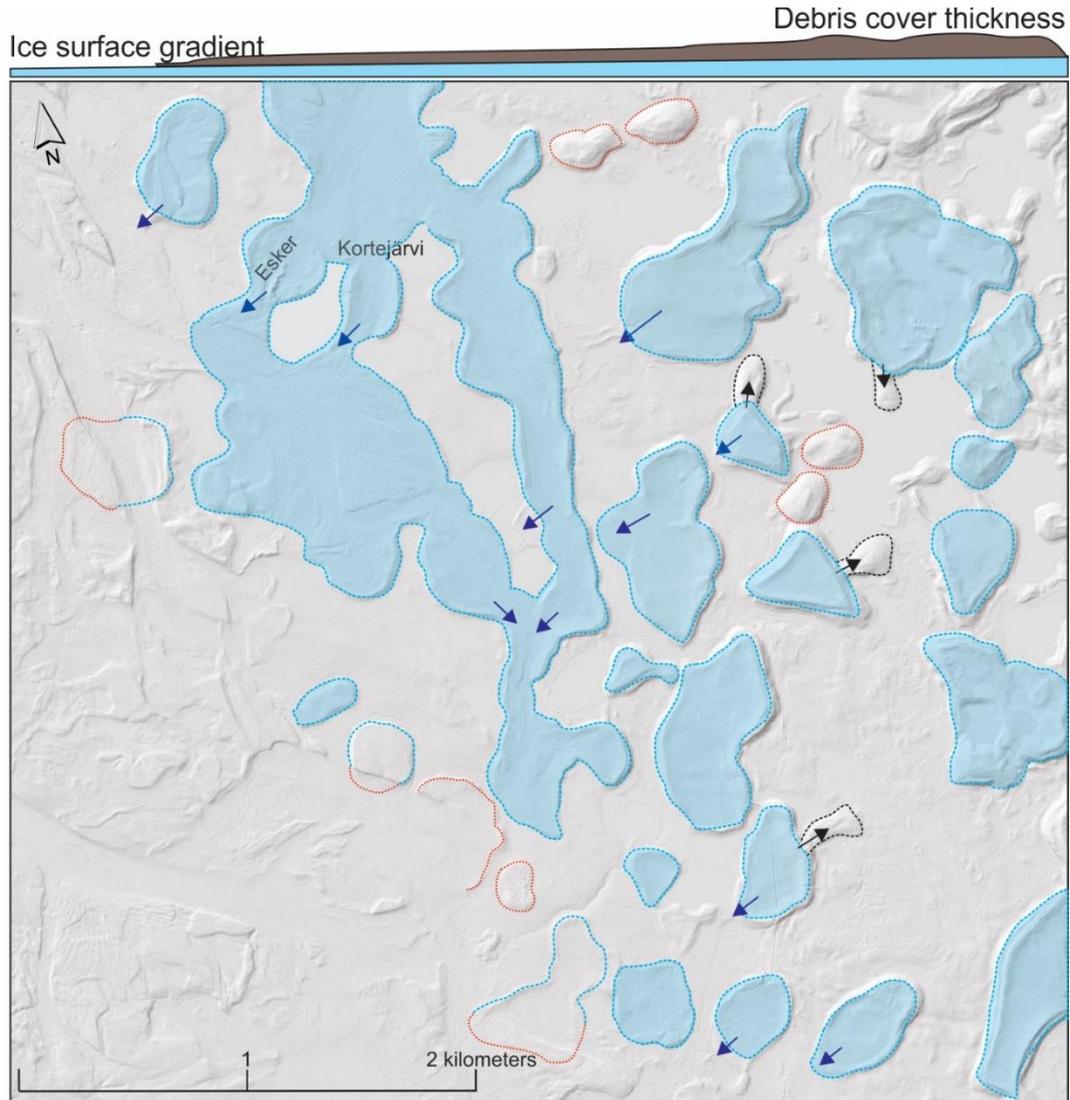
Figure 5.8. *Reconstruction of how the lakes may have merged with each other. Defining the limits is complicated as later fluvial reworking has remolded the area to some extent. The white patches demonstrate ice while grey areas demonstrate what the merged lakes could have looked like. The large-scale ice surface gradient is illustrated at the top together with the large-scale debris cover thickness. Background map: Nationell höjdmodell © Lantmäteriet (2011b).*
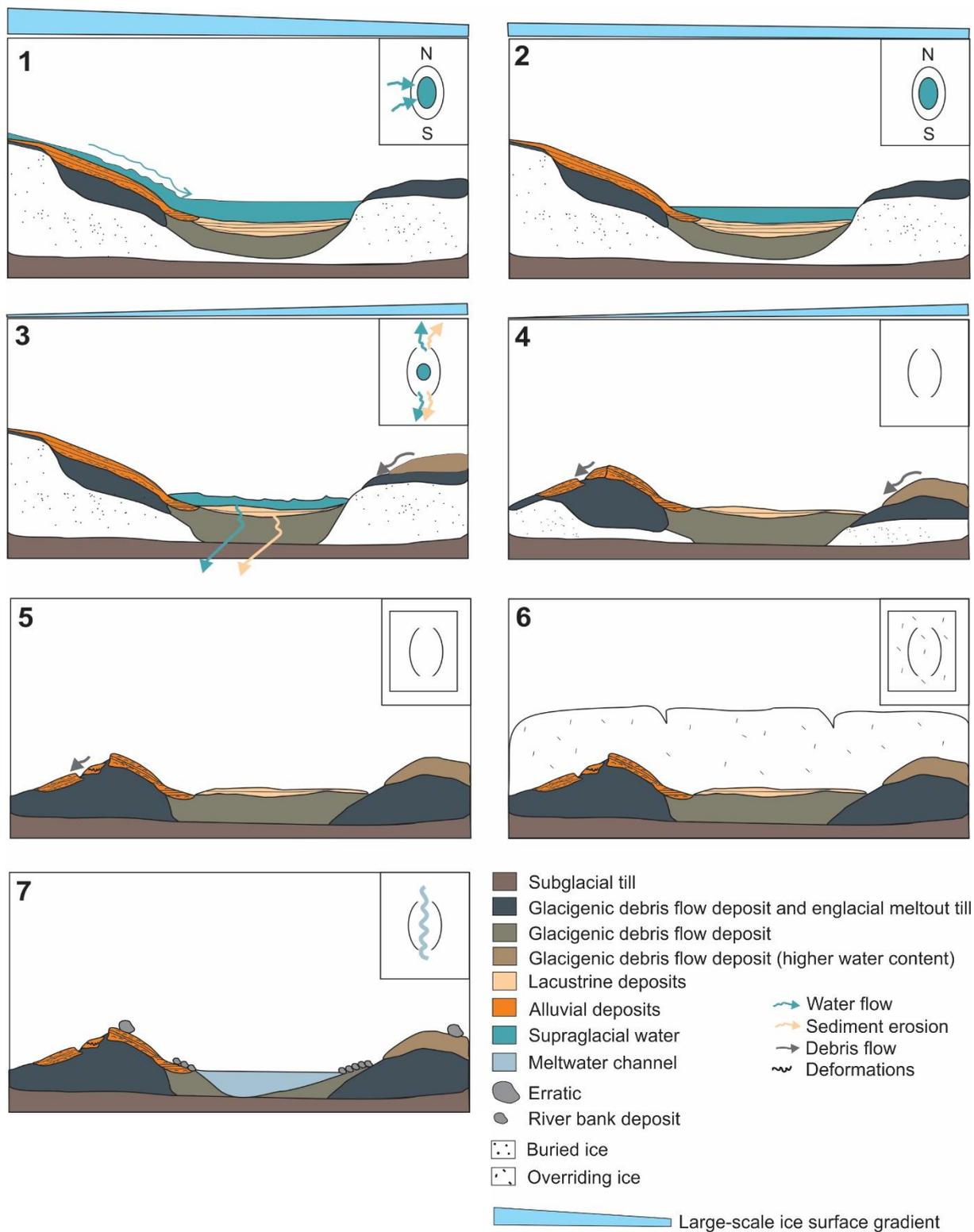
Figure 5.9. 7-step scenario showing different phases during the formation of Kortejärvi moraine plateau.

5.5.2 Alternative interpretations

Some of my data are inferences and have not been directly proven with own data, as an example the subsurface reflections and the origin of the diamict in the center. Therefore, alternative explanations cannot be ruled out. Lacustrine sediments were not observed in the field, so the existence of the former lake remains uncertain to some extent. As Lagerbäck (1988) states, some of the moraine plateaus were probably not water filled, but rather sinkholes that were filled with debris. The waterlaid sediments on the eastern ridge do however indicate that water was flowing towards the center of the sinkhole implying that a lake could have formed, unless there were open drainage ways. The water flow could also have been ongoing when the lakes merged, unlike what is illustrated in Figure 5.9.

An alternative explanation to why the northern and southern parts of the ridges are missing is that the younger channel eroded the ridges from either N-S or S-N direction. However, as explained earlier it is unlikely that it incised through an elevated ridge instead of going around it. Therefore, it is more reasonable that the ridges were already, at least partly eroded, when the channel cut across. The elevation model indicates that many of the lakes in this area have merged and collapsed, and therefore it does not seem like an unlikely scenario for Kortejärvi.

If attempting to connect my data with Hoppes (1952) theory, which states that the Veiki moraines were formed subglacially, there is a contradicting aspect. The stratified sand deposits on the western ridge were unlikely deposited subglacially, referring to the deformations that indicate downwasting and the fact that they are located on a topographic high, which implies that the sediment have been surrounded and perhaps also underlain by ice. Another aspect that makes me question the subglacial formation theory, but unrelated to my own data, are the second rim ridges that surround the inner rim ridges at many Veiki moraine plateaus. These are difficult to explain with a subglacial theory, as they are systematically aligned with the inner ridge and seemingly represent a widening of the former lakes.

5.6 Study outcomes

From a geomorphological point of view, a unique Veiki moraine plateau has been examined and new data has been obtained. To discuss the outcomes of the new data, let us return to the questions presented in chapter 1.

Which other processes had an impact on the irregular shapes?

The ablation and calving of the debris free steep ice slopes of the ice-walled lakes explain partly the irregular shapes of the moraines. Clayton *et al*., (2006) has described a similar process for ice-walled lake plains in North America. Expanding lakes have been described to be the most important ablation process on the terminus of some large debris-mantled glaciers (Benn and Evans, 2010) and this might have been the case for the stagnant ice which eventually formed the Veiki moraines, as rapid downwasting was prohibited by insulating debris.

Due to calving and ablation, some lakes merged, while others did not. This likely depended on several factors such as thickness of the surrounding debris cover, distance to the surrounding lakes, ice surface gradient differences and the height of the ice-walls of the lakes, out of which the latter may reflect melting rate and ice thickness. Merged lakes could also be an explanation to why lacustrine sediments in some moraines only occur in restricted parts of the moraines. When lakes merged, some of the sediments were likely displaced when the water mass in the lake strived a state of equilibrium in the new expanded lake, however, leaving some sediments on place. Another explanation to lake sediments occurring only in restricted parts of Veiki moraines, could be that some lakes were short lived and shallow and drained and were remolded before they grounded. This has been explained earlier by Clayton *et al*., (2006) and Ham and Attig (1996).

As explained by Johnson and Clayton (2003), the outer rim ridges of ice-walled lake plains are probably formed by progressive widening of the ice-walled lakes, such that each ridge or terrace represents a former position of the ice/sediment contact.

The shapes of the moraine plateaus have in varying degrees been eroded, smoothed and reworked by the Late-Weichselian ice sheet. Outwash plains that formed during the last deglaciation and were active long after, ran across a part of the Veiki moraine landscape, which is evident at Kortejärvi. The moraine plateau shows little signs of other type of later glacial activity, despite of a few erratics that were noted on top of the ridges and some reworked sediment layers close the ground surface, probably formed in the periglacial environment.

Does the gradual diminishment of Veiki moraines towards west signal of change in the ice sheet properties?

Under continental conditions, in general, the melting of a stagnant ice is slow because the exposed ice phases are short lived (Krüger *et al.*, 2010). Earlier studies suggest that the stagnant ice that formed the Veiki moraines was fairly thick and prevailed for at least 300-500 years, although 1000 and 2000 years have also been suggested (Lagerbäck, 1988). The gradual diminishment of the moraines towards the west likely indicates a change in the ice properties/ debris cover thickness.

The predominant evidence that indicates a thick ice, was obtained by counting silt layers, which were found in some of the prominent Veiki moraine plateaus and interpreted as lacustrine deposits (Lagerbäck, 1988). The thick lacustrine successions, out of which some were more than 10 meters thick, indicate that the lakes persisted for a long time, but also that the debris supply was high. A smaller debris supply on the ice surface would logically lead to a lower debris accumulation in the lakes. The fact that the landforms gradually become lower towards west therefore likely signals of a smaller debris supply into the lakes. Lagerbäck (1988) also mentioned a thinner debris cover as a possible explanation to the gradual diminishing towards west by stating that "the most spectacular parts of the Veiki moraine landscape often constitute areas with an excess of drift compared with their surroundings". According to literature, the thickest debris cover is commonly found at the ice margins (Benn and Evans, 2010), and hence it seems likely that this was also the case when the Veiki moraines were formed.

In the young stage of the stagnant ice, the ice surface gradient of the ice lobe was likely subhorizontal in large scale with a downslope towards E-NE. The lakes, which surroundings were poorly insulated, likely did not survive for as long as the lakes surrounded by well insulated ice. Poor insulation would have resulted in faster melting towards W-SW and this could have caused a change in the ice surface gradient, so that the downslope was towards the faster melting parts W-SW. A difference in the ice surface gradient would lead to an outburst of lakes and also trigger drainage (Benn and Evans, 2010). An ice surface gradient difference could therefore explain why many of the moraines that occur on the margin between the prominent moraines and the diminishing moraines have collapsed towards W-SW (Figure 5.8).

Ham and Attig, (1996) described a stable and an unstable phase of a stagnant ice, where at first the ice was not melting much, and the ice-walled lakes did not drain. The unstable phase naturally started when buried ice started to melt and drainage ways formed. Similarly, the

"Veiki lakes" on the ice margin likely formed all at the same time on a regionally stagnant ice, but the western parts melted faster due to a thinner debris cover and therefore a higher ablation rate, which led to a westward incline of the ice surface, more discharge and collapses and merging of lakes and finally drainage. The fossils found in other Veiki moraine plateaus reinforce a warmer climate during the formation of the lakes (Lagerbäck, 1988; Hättestrand and Robertsson, 2010).

As mentioned in chapter 1, the amount of climatic information that can be derived from ancient dead-ice deposits is limited since many of the processes that occur can take place in many different climatic settings. Paleoclimate parameters have been interpreted from proxies from lake sediments, but ice dynamics and melting rates are harder to establish (Johnson and Clayton 2003), since they are closely related to many other parameters like topography and debris-cover as mentioned earlier. By examining reoccurring orientations of collapsed lakes in a broader picture than in Figure 5.8, it might be possible to figure out ice surface gradient differences for the ice sheet.

A surge implies a change in the thermal regime within the ice; was the surge triggered by a climatic change?

The lobate formed end moraines that delimit the Veiki moraines eastward, and the large amount of debris that were left behind by the ice sheet, suggest that a surge occurred prior to the quiescent stagnant ice phase. The wide extent of the Veiki moraines presumably reflect a regional warming in the climate, which resulted in areal downwasting of the former ice sheet (Lagerbäck 1988). Lagerbäck (1988) suggested that the ice sheet had been very active, referring to the drumlinized terrain eastwards, which he assumed formed from the same ice sheet as the Veiki moraines. As I, together with Hättestrand (2007b) and Hättestrand and Robertsson (2010) and Sigfúsdóttir (2013) suggest that the Veiki moraines formed later, the thermal regime of the glacier, prior to the potential surge, is unknown. The thermal regime of a glacier depends on basal ice temperature, ice thickness and the substrate, which in order control the movement and flow. Because solely cold based ice sheets are unlikely to surge (Benn and Evans, 2010), we may assume that the ice was at least polythermal, if not warm based.

Warmer temperatures prevailed during the time when the Veiki lakes formed indicated by fossil pollen analyzed from the lake sediments (Hättestrand, 2007; Hättestrand and Robertsson, 2010) and by organic macrofossils including well-preserved aquatic mosses, twigs from juniper, willows, dwarf birch and blueberry (Lagerbäck, 1988). A warming climate prior to the surge

probably caused mass loss in the terminus of the ice while the accumulation area that was at a higher altitude (Hättestrand 1998) experienced an increase of mass. Therefore, the surge could have been climate triggered and corresponds to an interstadial as suggested by Lagerbäck (1988). After the surge, the ice contained significantly less debris upice, and hence melted more rapidly during the summer melt season, while the debris covered margin was better insulated. This led to a reversal of the ablation gradient and the ice became stagnant. Such scenarios have been explained by Ham and Attig (1996) and Benn and Evans (2010) among others.

In which ways have alluvial processes imprinted the landscape?

At least two generations of alluvial deposits can be found in the Veiki moraine landscape and as Lagerbäck (1988) stated, the findings reinforce that the landscape is composed of water laid sediments to a much larger extent than is visible from above; both lacustrine and fluvial. On stagnant ice snouts, supraglacial streams are not necessarily running in the direction of the terminus as is often the case on ice margins but are randomly oriented due to frequently occurring topographic inversion and changes in ice surface gradient. Therefore, all the alluvial deposits are not directly indicative of the direction of the former ice flow.

The traces of the old stagnant ice environment probably directed how the younger channels during and after the last deglaciation developed in the Veiki moraine landscape. The less prominent Veiki moraines towards west seem to have undergone more reworking by later alluvial processes, while this kind of disturbance is not visible or is completely absent closer to the demarcating terminal moraine eastward. This demonstrates how older landscapes act as an important base for landscape evolution and what we can see in the present-day landscape, is a window into past landscapes.

What is the absolute age of the landforms and how do they correlate to local interstadials?

Even though the obtained ages remain somewhat uncertain due to poor characteristics of the quartz and poorly bleached sediments, they give an estimation for the time of formation. The sediments in the ridges, which are a part of the original Veiki moraine landforms were emplaced during the Middle Weichselian interstadial or MIS 3 between 37.1±5.5 ka and 41.6±5.1 ka according to this study. Hereby, the study reinforces the Middle Weichselian age of the original Veiki moraine landforms and therefore corresponds better with the local interstadial Tärendö 2 (Hättestrand and Robertsson, 2010). Therefore, it seems likely that ice-free conditions prevailed

in parts of northern Fennoscandia during a MIS 3 interstadial, as has been suggested earlier by Hättestrand, (2007b), Hättestrand and Robertsson (2010) and Sigfúsdóttir (2013).

The sediments in the younger age group in the center of the moraine plateau were likely deposited in a branch within a network of braided rivers, which was formed during and active long after the deglaciation of the last Weichselian ice sheet in Fennoscandia during MIS 1.

The most reliable OSL ages obtained from core K2 are 11.4 ± 1.5 ka (sample 19005) and 9.2 ± 1.2 ka (sample 19004). At face value, the first mentioned appears overestimated, but it overlaps the local deglaciation age (Östlund, 2004; Möller *et al.* 2013; Stroeven *et al*. 2016; Hughes *et al*. 2015) within error. The younger age 9.2 ± 1.2, likewise, overlaps the local deglaciation within error. The pollen data, however, suggests an age no older than 4000 years BP for the organic bearing layers in the channel. Hereby, either the OSL ages are overestimated by a few thousand years, perhaps due to incomplete bleaching and/or dim quartz; or the organic layers have not been placed in situ and are misleading. The core is composed of four fining upwards sequences including a layer below the lowermost organic layer. These sequences indicate that at least the sediments below the middle organic layer, have not undergone post depositional mixing.

Hereby, the authors opinion is that the alluvial sequence likely deposited no later than 4000 years BP, and consequently that the OSL ages in age group 2 are overestimated, perhaps due to a combination of incomplete bleaching and dim quartz. As the sediments in age group 1 and 2 belong to different generations, we should not conclude that the same errors apply to age group 1.

6 Conclusions

- Kortejärvi Veiki moraine plateau formed during a Middle Weichselian interstadial, likely over a longer period, sometime between 37.1±5.5 ka and 41.6±5.1 ka according to the OSL ages obtained in this study. This time span corresponds to the local interstadial Tärendö 2 (as defined by Hättestrand and Robertsson, 2010). The D_e protocols indicate that the quartz was of poor quality and hence an uncertainty must be accounted for in the ages. It seems however likely that ice-free conditions prevailed in parts of northern Fennoscandia during a MIS 3 interstadial

- The sedimentological, stratigraphical and geomorphological analyses indicate that the studied moraine plateau is a former ice-walled lake that was crosscut by a channel, which eroded much of the sediments in the center of the plateau and deposited a ~5-meter-thick alluvial succession. This channel formed during the deglaciation of the last ice sheet and was still active thousands of years after the local deglaciation, which likely occurred at 9.8 ± 0.2 ka cal BP.

- During the LGM, the moraine was likely overridden by a cold based ice sheet alike the rest of the Veiki moraine landscape. The last ice sheet reworked a thin layer of the top sediments and left a few erratics on the ridges but left the landform nearly untouched otherwise.

- In the ice-walled lake stage, Kortejärvi lied in a less insulated area of the stagnant ice and underwent faster melting compared to the moraine plateaus in areas with thicker debris cover closer to the ice margin eastwards. The lake merged with surrounding lakes, as a result of ablation and melting on the debris free ice slopes. When the lakes merged, much of the lacustrine sediments within the lake were redeposited and, in this event, the northern and southern parts of the ridges were at least partly eroded.

- The western and eastern ridges mark the former ice-contact of the lake. A water flow, predominantly from southwest, deposited stratified sand on the western ridge. The deformation structures in the western ridge indicate that downwasting processes dominated during the melting phase of the ice. The diamict on the eastern ridge was emplaced by sediment gravity flows from the surrounding ice from east.

- As stratified sand was found solely on the western ridge, it could imply a large-scale ice surface gradient with a downslope eastward towards the terminus in its initial phase. Soon after the downwasting started, the thin debris covers east of the ice margin resulted in faster melting and to an ice surface gradient change with a downslope W-SW. This

change likely explains the collapsed Veiki moraine plateaus located in the "transition zone" between the prominent moraine plateaus and less prominent ones.

- In future studies it would be interesting to look more closely into the geomorphology of the moraine plateaus and to recognize patterns in collapsed Veiki moraine plateaus, which could reveal melting patterns of the ice. The distribution of moraines with second ridges contra moraines with one ridge could also be investigated, as it is still unclear why some moraine plateaus have them and others do not. The high-resolution LiDAR data set over Sweden is a very valuable tool for future studies, as it enables examination in remarkable detail. The original shapes of the moraine plateaus are in various degrees reworked by post depositional processes and this needs to be considered when attempting a reconstruction of the former ice-walled lakes.

7 References

Aitken, M.J. 1974. *Physics and Archaeology*. Second Edition. Oxford, England: Clarendon Press. First published by Interscience. 1961. New York, DOI 10.1017/S0003598X00070964.

Alexanderson, H. 2007. Residual OSL Signals from Modern Greenlandic River Sediments. *Geochronometria* 26 (1), pp. 1–9, DOI 10.2478/v10003-007-0001-6.

Alexanderson, H., Backman, J., M. Cronin, T., Funder, S., Ingólfsson O., Jakobsson, M., Landvik, J.Y., Löwemark, L., Mangerud, J., März, C., Möller, P., O'Regan, M., and Spielhagen, R.F. 2014. An Arctic Perspective on Dating Mid-Late Pleistocene Environmental History. *Quaternary Science Reviews.* 92, pp. 9–31, DOI 10.1016/j.quascirev.2013.09.023.

Alexanderson, H., and Murray, A.S. 2012. Problems and Potential of OSL Dating Weichselian and Holocene Sediments in Sweden. *Quaternary Science Reviews.* 44, pp. 37–50, DOI 10.1016/j.quascirev.2009.09.020.

Arcone, S., Campbell, S., and Pfeffer, W.T. 2014. GPR Profiles of Glacial till and Its Transition to Bedrock: Interpretation of Water Content, Depth and Signal Loss from Diffractions. *Journal of Environmental and Engineering Geophysics.* 19 (4), pp. 205–291, DOI 10.2113/JEEG19.4.207.

Benn, D. I., and Evans, D. J. A. 2010. *Glaciers and Glaciation*. Second Edition. London, England: Hodder Education, DOI 10.4324/9780203785010.

Bertrand, S., Hughen, K., and Giosan, L. 2015. Limited Influence of Sediment Grain Size on Elemental XRF Core Scanner Measurements in *Micro-XRF Studies of Sediment Cores*. Croudace, I.W., Rothwell, R.G. ed. pp. 473–490. London: Springer, DOI 10.1007/978-94-017-9849-5.

Boggs, S. Jr. 2009. *Petrology of Sedimentary Rocks*. Second Edition. Cambridge, England: Cambridge University Press, DOI 10.1017/CBO9780511626487.

Bowman, S. 1990. *Radiocarbon Dating (Interpreting the Past)*. London: University of California Press/ British Museum.

Brouwer, P. 2010. Theory of XRF, getting acquainted with the principles. Holland: PanAnalytical B.V.

Cheel, R. J. 2005. Introduction to Clastic Sedimentology. Department of Earth Sciences, Brock University, St. Catharines, Ontario, Canada.

Clayton, L., Attig, J.W., Ham, N.R., Johnson, M.D., Jennings, C.E., and Syverson, K. M., 2008. Ice-Walled-Lake Plains: Implications for the Origin of Hummocky Glacial Topography in Middle North America. *Geomorphology.* 97 (1–2), pp. 237–248, DOI 10.1016/j.geomorph.2007.02.045.

Cohen, K. M., and Gibbard, P. L. 2019. Global Chronostratigraphical Correlation Table for the Last 2.7 Million Years, version 2019 QI-500. *Quaternary International.* 500, pp. 20–31, DOI 10.1016/j.quaint.2019.03.009.

Collinson, J., Mountney, N., and Thompson, D. 2006. *Sedimentary Structures*. Third edition. Scotland: Terra Publishing.

Croudace, I. W., Rindby, A., and Rothwell, R. G. 2006. ITRAX: Description and Evaluation of a New Multi-Function X-Ray Core Scanner in *New techniques in sediment core analysis.* Rothwell, R.G. ed., 267 (1), pp. 51–63. London, UK: *Geological Society Special Publication*, DOI 10.1144/GSL.SP.2006.267.01.04.

Croudace, I. W., and R. G. Rothwell. 2015. *Micro-XRF Studies of Sediment Cores. Applications of a Non-Destructive Tool for the Environmental Sciences*. Volume 17. London, UK:Springer, DOI 10.1007/978-94-017-9849-5.

D'Agata, C., and Zanutta, A. 2007. Reconstruction of the Recent Changes of a Debris-Covered Glacier (Brenva Glacier, Mont Blanc Massif, Italy) Using Indirect Sources: Methods, Results and Validation. *Global and*

Planetary Change. 56 (1–2), pp. 57–68, DOI 10.1016/j.gloplacha.2006.07.021.

Duller, G. A. T. 2008. Luminescence Dating: Guidelines on Using Luminescence Dating in Archaeology. Swondon: English Heritage, DOI 10.1002/jqs.1328.

Durcan, J. A., King, G. E., and Duller, G. A. T. 2015. DRAC - Dose Rate and Age Calculator for Trapped Charge Dating. *Quaternary Geochronology.* 28, pp. 54–61, URL: https://www.aber.ac.uk/en/dges/research/quaternary/luminescence-research-laboratory/dose-rate-calculator/.

Gailbraith, R.F., Roberts, R.G., Laslett, G. M., Yoshida, H., and Olley, J. M. 1999. Optical Dating Of Single And Multiple Grains Of Quartz From Jinmium Rock Shelter, Northern Australia: Part I, Experimental Design And Statistical Models. *Archaeometry* 41 (2), pp. 339–64, DOI 10.1111/j.1475-4754.1999.tb00987.x.

Gehrig, M. D., Morris, D.V., and Bryant, J. T. 2004. Ground Penetrating Radar for Concrete Evaluation Studies. pp. 1–17.

Giesecke, T. 2004. The Holocene spread of spruce in Scandinavia. [Ph.D. Thesis]. Faculty of Science and Technology, Uppsala University, Uppsala, Sweden. pp, 46.

Graham, J.D., and Midgley, N. G. 2000. Graphical Representation of Particle Shape Using Triangular Diagrams: An Excel Spreadsheet Method. *Earth Surface Processes and Landforms.* 25 (13), pp. 1473–1477, DOI 10.1002/1096-9837(200012)25:13<1473::AID-ESP158>3.0.CO;2-C.

Ham, N. R., and Attig, J. W. 1996. Ice Wastage and Landscape Evolution along the Southern Margin of the Laurentide Ice Sheet, North-Central Wisconsin. *Boreas.* 25 (3), pp. 171–186, DOI 10.1111/j.1502-3885.1996.tb00846.x.

Helmens, K.F., Johansson, P.W., Räsänen, M. E., Alexanderson, H., and Eskola, K. O. 2007. Ice-free intervals continuing into Marine Isotope Stage 3 at Sokli in the central area of the Fennoscandian glaciations. *Bulletin of the Geological Society of Finland.* 79, pp. 17-39, DOI 10.17741/bgsf/79.1.002.

Hoare, P. G., and Gale, S. 1992. Bulk Sampling of Coarse Clastic Sediments for Particle-Size. *Earth Surface Processes and Landforms.* 17 (7), pp. 729–733, DOI 10.1002/esp.3290170709.

Hoppe, G. 1952. Hummocky Moraine Regions with Special Reference to the Interior of Norrbotten. *Geografiska Annaler.* 34 (1–2), pp. 1–72, DOI: 10.2307/520144.

Hughes, A. L.C., Gyllencreutz, R., Lohne, Ø. S., Mangerud, J., and Svendsen J.I. 2015. The last Eurasian ice sheets – a chronological database and time-slice reconstruction, DATED-1. *Boreas.* 45, pp. 1-45, DOI 10.1111/ bor.12142.

Huntley, D. J., Godfrey-Smith, D. I., and Thewalt, M. L. W. 1985. Optical Dating of Sediments. *Nature.* 313 (5998), pp. 105–107, DOI 10.1038/313105a0.

Hutton, J. 1795. *The Theory of Earth*. Edinburgh, Scotland: Royal Society of Edinburgh.

Hättestrand, C. 1998. The Glacial Geomorphology of Central and Northern Sweden. *Sveriges Geologiska Undersökning* Ca 85, pp. 47.

Hättestrand, M. 2007a. Vegetation and Climate during Weichselian Ice Free Intervals in Northern Sweden – Interpretations from Fossil and Modern Pollen Records. [Doctoral Thesis]. Department of Physical Geography and Quaternary Geology, Stockholm University, Stockholm, Sweden.

——— 2007b. Weichselian Interstadial Pollen Stratigraphy from a Veiki Plateau at Rissejauratj in Norrbotten, Northern Sweden. *Gff.* 129 (4), pp. 287–94, DOI 10.1080/11035890701294287.

Hättestrand, M., and Robertsson, A. M. 2010. Weichselian Interstadials at Riipiharju, Northern Sweden - Interpretation of Vegetation and Climate from Fossil and Modern Pollen Records. *Boreas* 39 (2), pp. 296–

311, DOI 10.1111/j.1502-3885.2009.00129.x.

Imbrie, J., Berger, A., Boyle, E. A., Clemens, S. C., Duffy, A., Howard, W. R., Kukla, G., Kutzbac, C. J., Martinson, D. J., Mcintyr, A., Mix, A.C., Molfino, B., Morley, J.J., Peterson, L.C., Pisias, N. G., Prell, W.L., Raymo, M. E., Shackleton, N. J., and Toggweiler, J.R. 1993. Milankovitch Theory , the Two Shorter Cycles Can Be Explained Radiation Cycle. *Paleoceanography and Paleoclimatology*. 8 (6) pp. 699–735, DOI 10.1029/93PA02751.

IPCC. 2001. *Climate Change 2001: The Scientific Basis*. Contribution of Working Group I to the Third Assessment Report of the Intergovernmental Panel on Climate Change [Houghton, J.T., Y. Ding, D.J. Griggs, M. Noguer, P.J. van der Linden, X. Dai, K. Maskell, and C.A. Johnson (ed.). Cambridge, United Kingdom and New York, NY, USA: Cambridge University Press, pp. 881, URL: https://www.ipcc.ch/site/assets/uploads/2018/07/WG1_TAR_FM.pdf.

Jensen, J.L., Schj, P., Watts, C. V., Christensen, B. T., and Munkholm, L.J. 2017. Soil Texture Analysis Revisited: Removal of Organic Matter Matters More than Ever. *PLoS ONE*. 12(5): e0178039. DOI 10.1371/journal. pone.0178039.

Johnson, M. D., Mickelson, D.M. Clayton, L. and Attig, J. W. 1995. Composition and genesis of glacial hummocks, western Wisconsin, USA. *Boreas*. 24(2), pp. 97-116, DOI 10.1111/j.1502-3885.1995.tb00630.x.

Johnson, M. D., and Clayton, L. 2003. Supraglacial landsystems in lowlandterrain. In: Evans, D.J.A. (Ed.), *Glacial Landsystems*. Arnold, London, pp. 228–258.

Johnsson, A., Reiss, D., Conway, S., Hauber, E., Johnson, M.D., Olvmo, M., and Hiesinger, H. 2017. Veiki-Moraine-like Landforms on Mars: Insights from Analogues in Northern Sweden. *EPSC Abstracts*. 11 (October): EPSC2017-918.

Johnsson, A., Reiss, D., Conway, S., Hauber, E., Johnson, M.D., Olvmo, M., and Hiesinger, H. 2016. *Veiki-moraine-like Landforms in the Nereidum Montes Region on Mars: Insights from Analogues in Northern Sweden*. 47th Lunar and Planetary Science Conference.

Kovin, O. N. 2016. Ground Penetrating Radar Investigations in Upper Kama Potash Mines. no. LAP Lambert Acad. Publ. November, pp. 1–181.

Krüger, J., and Kjær, K. H. 2000. De-Icing Progression of Ice-Cored Moraines in a Humid, Subpolar Climate, Kötlujökull, Iceland. *The Holocene*. 10 (6), pp. 737–47, DOI 10.1191/09596830094980.

Krüger, J., and Kjær, K. H. 1999. A Data Chart for Field Description and Genetic Interpretation of Glacial Diamicts and Associated Sediments - with Examples from Greenland, Iceland, and Denmark. *Boreas*. 28 (3), pp. 386–402. DOI: 10.1111/j.1502-3885.1999.tb00228.x.

Krüger, J., Kjær, K. H., and Schomacker, A. 2010. 7 Dead-Ice Environments: A Landsystems Model for a Debris-Charged, Stagnant Lowland Glacier Margin, Kötlujökull. *Developments in Quaternary Science*. 13, pp. 105–26, DOI 10.1016/S1571-0866(09)01307-4.

Krumbein, W. C. 1941. Measurement and Geological Significance of Shape and Roundness of Sedimentary Particles. *Journal of Sedimentary Pertology*. 11 (2), pp. 64–72.

Lagerbäck, R. 1988. The Veiki Moraines in Northern Sweden - Widespread Evidence of an Early Weichselian Deglaciation. *Boreas*. 17 (4), pp. 469–86, DOI 10.1111/j.1502-3885.1988.tb00562.x.

Lantmäteriet. 2015. GSD-Vägkartan. Scale 1:100 000. Licensavtal I2018/00104 för forskning, utbildning och kulturverksamhet.

Lantmäteriet. 2011a. Geodata GSD-Höjddata, grid 2+. Licensavtal I2018/00104 för forskning, utbildning och kulturverksamhet.

——— 2011b. Nationell höjdmodell. Scale 1:100 000. Licensavtal I2018/00104 för forskning, utbildning och

kulturverksamhet.

Libby, W. F. 1946. Atmospheric Helium Three and Radiocarbon from Cosmic Radiation [8]. *Physical Review.* 69 (11–12), pp. 671–72, DOI 10.1103/PhysRev.69.671.2.

Lowe, J., and Walker, M. 2015. *Reconstructing Quaternary Environments.* Third Edition. Oxon and New York: Routledge.

Magnusson, N. H., Granlund, E., and Lundqvist, G. 1949. Sveriges geologi.

Maizels, J. 1993. Lithofacies variations within sandur deposits: the role of runoff regime, flow dynamics and sediment supply characteristics. *Sedimentary geology.* 85 (1-4), pp. 299-325, DOI 10.1016/0037-0738(93)90090-R.

Mangerud, J. 1991. The Scandinavian Ice Sheet through the Last Interglacial/Glacial Cycle. *Paleoklimaforschung.* 1 (March), pp. 307–330.

Mangerud, J., Gyllencreutz, R., Lohne, Ø., and Svendsen, J. I. 2011. Chapter 22: Glacial History of Norway. *Developments in Quaternary Sciences.* 15, pp. 279–298, DOI 10.1016/B978-0-444-53447-7.00022-2.

McKenzie, N., Coughlan, K., and Cresswell, H. 2002. *Soil Physical Measurement and Interpretation for Land Evaluation.*

Medialdea, A., Thomsen, K.J., Murray, A. S., and Benito, G. 2014. Reliability of Equivalent-Dose Determination and Age-Models in the OSL Dating of Historical and Modern Palaeoflood Sediments. *Quaternary Geochronology.* 22, pp. 11–24, DOI 10.1016/j.quageo.2014.01.004.

Miall, A. 1996. *The Geology of Fluvial Deposits, Sedimentary Facies, Basin Analysis and Petroleum Geology.* Berlin, Heidelberg: Springer, DOI 10.1007/978-3-662-03237-4.

Miall, A. 2016. *Stratigraphy: A Modern Synthesis.* First Edition. Cham, Switzerland: Springer, DOI 10.1007/978-3-319-24304-7.

Murray, A. S., and Roberts, R.G. 1998. Measurement of the Equivalent Dose in Quartz Using a Regenerative-Dose Single-Aliquot Protocol. *Radiation Measurements.* 29 (5), pp. 503–515, DOI 10.1016/S1350-4487(98)00044-4.

Murray, A. S., and Wintle, A. G. 2000. Luminescence Dating of Quartz Using an Improved Single-Aliquot Regenerative-Dose Protocol. *Radiation Measurements.* 32 (1), pp. 57–73. DOI 10.1016/S1350-4487(99)00253-X.

Murray, A.S., Marten, R., Johnston, A., and Martin, P. 1987. Analysis for Naturally Occuring Radionuclides at Environmental Concentrations by Gamma Spectrometry. *Journal of Radioanalytical and Nuclear Chemistry.* 115 (2), pp. 263–288, DOI 10.1007/BF02037443.

Möller, P., Östlund, O., Barnekow, L., Sandgren, P., Palmbo, F., and Willerslev, E. 2013. Living at the Margin of the Retreating Fennoscandian Ice Sheet: The Early Mesolithic Sites at Aareavaara, Northernmost Sweden. *The Holocene.* 23 (1), pp. 104–116, DOI 10.1177/0959683612455546.

Neal, A. 2004. Ground-Penetrating Radar and Its Use in Sedimentology: Principles, Problems and Progress. *Earth-Science Reviews.* 66 (3–4), pp. 261–330, DOI 10.1016/j.earscirev.2004.01.004.

Nichols, G. 2009. *Sedimentology and Stratigraphy.* Second Edition. Wiley-Blackwell.

Oerlemans, J. 2005. Atmospheric Science: Extracting a Climate Signal from 169 Glacier Records. *Science.* 308 (5722), pp. 675–677, DOI 10.1126/science.1107046.

Oerlemans, J., Anderson, B., Hubbard, A., Huybrechts, P., Johannesson, T., Knap, W.H., Schmeits, M., Stroeven, A. P., van de Wal, R. S. V., Wallinga, J., and Zuo, Z. 1998. Modelling the response of glaciers to climate warming. *Climate Dynamics.* 14, pp. 267-274, DOI 10.1007/s003820050222.

Pillans, B., and Naish, T. 2004. Defining the Quaternary. *Quaternary Science Reviews.* 23 (23-24), pp. 2271-2282, DOI 10.1016/j.quascirev.2004.07.006.

Povinec, P. P., Litherland, A. E., and von Reden, K.F. 2009. Developments in Radiocarbon Technologies: From the Libby Counter to Compound-Specific Ams Analyses. *Radiocarbon.* 51 (1), pp. 45–78, DOI 10.1017/S0033822200033701.

Powers, M. C. 1953. A New Roundness Scale for Sedimentary Particles. *Journal of Sedimentary Petroleum.* 23 (2), pp. 117–119.

Raymond, B. S. 2015. *Paleoclimatology: Reconstructing Climates of the Quaternary*. Third Edition. Elsevier. DOI 10.1016/C2009-0-18310-1.

Ramsey, C. B. 2009. Bayesian analysis of radiocarbon dates. *Radiocarbon.* 51 (1), pp. 337-360, DOI 10.1017/S0033822200033865.

Reimer, P., Brown, J., Reimer, T.A., and Ron, W. 2004. Discussion: reporting and calibration of post-bomb 14c data. *Radiocarbon.* 46 (3), pp 1299–1304, DOI 10.1017/S0033822200033154.

Rhodes, E. J. 2011. Optically Stimulated Luminescence Dating of Sediments over the Past 200,000 Years. *Annual Review of Earth and Planetary Sciences.* 39 (1), pp. 461–488, DOI 10.1146/annurev-earth-040610-133425.

Richter, T. O., Van der Gaast, S., Koster, B., Vaars, A., Gieles, R., De Stigter, H.C., De Haas, H., and Van Weering, T. C. E. 2006. The Avaatech XRF Core Scanner: Technical Description and Applications to NE Atlantic Sediments. *Geological Society of London Publications*, Special Publications. 267 (1), pp. 39–50, DOI 10.1144/GSL.SP.2006.267.01.03.

Rodnight, H. 2008. How Many Equivalent Dose Values Are Needed to Obtain a Reproducible Distribution ? *Ancient TL.* 26 (1), pp. 3–10.

RStudio Team. 2015. RStudio. URL: http://www.rstudio.com/.

Schomacker, A. 2008. What Controls Dead-Ice Melting under Different Climate Conditions? A Discussion. *Earth-Science Reviews*. 90 (3–4), pp. 103–113, DOI 10.1016/j.earscirev.2008.08.003.

Schön, J. H. 2015. *Physical Properties of Rocks: Fundamentals and principles of Petrophysics*. Second Edition. Developments in Petroleum Science. 65, pp. 109-114. Elsevier.

SGU 2020a. Jordarter nordligaste Sverige 1: 250 000. Geological Survey of Sweden Kartvisare. URL: https://apps.sgu.se/kartvisare/kartvisare-jordarter-norra-sverige-250-tusen.html. [Retrieved: 13.02.2020].

——— b. Berggrund 50 000-250 000. Geological Survey of Sweden Kartvisare. URL: https://apps.sgu.se/kartvisare/kartvisare-berg-50-250-tusen.html. [Retrieved: November, 2019].

——— c. Jorddjup 1:1250-1:9 000 000. Geological Survey of Sweden Kartvisare. URL: https://apps.sgu.se/kartvisare/kartvisare-jorddjup.html. [Retrieved: November, 2019].

Sigfúsdóttir, T. 2013. A Sedimentological and Stratigraphical Study of Veiki Moraine in Northernmost Sweden.[M. Sc Thesis]. Department of Geology, Lund University, Lund, Sweden.

Skogsstyrelsen. 2019. Historiska flygfoto. Kartorapp. URL: https://kartor.skogsstyrelsen.se/kartorapp/. [Retrieved: November, 2019].

Smitha, N., Ullas Bharadwaj, D.R., Abilash, S., Sridhara, S. N., and Singh, V. 2016. Kirchhoff and F-K Migration to Focus Ground Penetrating Radar Images. *International Journal of Geo-Engineering*. 7 (4). DOI 10.1186/s40703-016-0019-6.

Sneed, E. D., and Folk, R. L. 2009. Pebbles in the Lower Colorado River, Texas a Study in Particle

Morphogenesis. *The Journal of Geology*. 66 (2), pp. 114–50, DOI 10.1086/626490.

Southard, J. B., and Boguchwal, L. A. 1990. Bed configuration in steady unidirectional water flows; Part 2, Synthesis of flume data. Journal of Sedimentary Research. 60 (5), pp. 658-679, DOI 10.1306/212F9241-2B24-11D7.

Stål, T. 1972. Kornfördelning, förslag till geotekniska laboratorieanvisningar, del 4. Byggforskningens informationsblad B2, Statens institution för byggnadsforskning, Stockholm.

Stroeven, A. P., Hättestrand, C., Kleman, J., Heyman, J., Fabel, D., Fredin, O., Goodfellow, B. W. Harbor, J. M., Jansen, J.D., Olsen, L., Caffee, M.W., Fink, D., Lundqvist, J., Rosqvist, G.C., Strömberg, G.,and Jansson, K. N. 2016. Deglaciation of Fennoscandia. *Quaternary Science Reviews*. 147, pp. 91-121, DOI 10.1016/j.quascirev.2015.09.016.

Suter, F., Martínez, J. I., and Vélez, M. I. 2011. Holocene Soft-Sediment Deformation of the Santa Fe-Sopetrán Basin, Northern Colombian Andes: Evidence for Pre-Hispanic Seismic Activity? *Sedimentary Geology*. 235 (3–4), pp. 188–99, DOI 10.1016/j.sedgeo.2010.09.018.

Svendsen, J. I., Alexanderson, H., Astakhov, V. I., Demidov, I., Dowdeswell, J.A., Funder, S., Gataullin, V., *et al*. 2004. Late Quaternary Ice Sheet History of Northern Eurasia. *Quaternary Science Reviews*. 23 (11–13), pp. 1229–1271, DOI 10.1016/j.quascirev.2003.12.008.

Thrasher, I. M., Mauz, B., Chiverrell, R. C. and Lang, A. 2009. Luminescence Dating of Glaciofluvial Deposits: A Review. *Earth-Science Reviews*. 97 (1–4), pp. 133–146, DOI 10.1016/j.earscirev.2009.09.001.

Truelsen, J. L., and Wallinga, J. 2003. Zeroing of the OSL Signal as a Function of Grain Size: Investigating Bleaching and Thermal Transfer for a Young Fluvial Sample. *Geochronometria*. 22 (January), pp. 1–8.

Turner, J. N., Jones, A. F., Brewer, P. A., Macklin, M. G., and Rassner, S. M. 2015. Micro-XRF Applications in *Fluvial Sedimentary Environments of Britain and Ireland: Progress and Prospects in Micro-XRF Studies of Sediment Cores: Applications of a Non-Destructive Tool for the Environmental Sciences*. Pp. 227–265.

Wadell, H. 1932. Volume, shape, and roundness of rock particles. *The Journal of Geology*. 40 (5), pp. 443-451, DOI 10.1086/623964.

Wallinga, J. 2002. Optically Stimulated Luminescence Dating of fluvail deposits: A Review. *Boreas*. 31(4), pp. 303–322, DOI 10.1111/j.1502-3885.2002.tb01076.x.

Winters, H. A. 1961. Landforms Associated with Stagnant Glacial Ice. *Professional Geographer*. 13 (4), pp. 19–23, DOI 10.1111/j.0033-0124.1961.134_19.x.

Östlund, O. 2004. *Rapport Arkeologisk Förundersökning Stenåldersboplats Samt Skärvstensförekomst Raä 22 Samt Raä 98, Junosuando Socken Norrbottens Län, Västerbotten*, Dnr 442-2004. Norrbottens Museum, Luleå.

Appendix 1

Input data for DRAC.

Project ID	Sample ID	Mineral	External U (ppm)	errExternal U (ppm)	External Th (ppm)	errExternal Th (ppm)	External K (%)	errExternal K (%)	Grain size min (microns)	Grain size max (microns)	Etch depth min (microns)	Etch depth max (microns)	Water content %	errWater content %	Depth (m)	errDepth (m)	Overburden density (g cm-3)	errOverburden density (g cm-3)	Latitude	Longitude	Altitude (m)	De (Gy)	errDe (Gy)
Kortejarvi	18029	Q	2.12	0.48	6.95	0.13	2.33	0.04	180	250	8	10	13	4	0.75	0.05	1.3	0.1	67.521	22.568	245	112	16
Kortejarvi	18030	Q	2.55	1.06	6.45	0.20	2.38	0.07	180	250	8	10	13	4	0.48	0.05	1.3	0.1	67.521	22.568	241	183	25
Kortejarvi	18031	Q	2.10	0.21	5.64	0.08	2.50	0.03	180	250	8	10	14	4	1.25	0.05	1.3	0.1	67.521	22.568	240	126	15
Kortejarvi	18032	Q	1.91	0.18	6.09	0.07	0.87	0.02	180	250	8	10	15	4	0.55	0.05	1.3	0.1	67.521	22.569	239	64	8
Kortejarvi	19003	Q	9.03	1.77	2.88	0.11	1.22	0.22	180	250	8	10	24	4	0.735	0.035	1.6	0.1	67.521	22.571	236	182	26
Kortejarvi	19004	Q	4.17	2.04	5.78	0.36	2.90	0.12	180	250	8	10	26	4	1.58	0.05	1.6	0.1	67.521	22.571	236	31	3
Kortejarvi	19005	Q	1.65	0.21	5.84	0.08	3.29	0.03	180	250	8	10	22	4	2.38	0.05	1.6	0.1	67.521	22.571	234	38	5
Kortejarvi	19006	Q	1.76	0.21	6.12	0.08	3.17	0.03	180	250	8	10	20	4	3.43	0.04	1.6	0.1	67.521	22.571	233	75	12
Kortejarvi	19007	Q	2.28	0.27	6.27	0.11	3.13	0.04	180	250	8	10	22	4	4.375	0.375	1.6	0.1	67.521	22.571	232	72	13

Appendix 2

GPR profiles before processing but including "standard processing" dewow + AGC gain.

Frequency of the upper profile: 100 MHz, freq. of lower profile 200 MHz.